UNIVERSITY OF CALIFORNIA, SAN DIEGO

Investigating the Role of AMPA Receptors in Learning and Memory

A Dissertation submitted in partial satisfaction of the
requirements for the degree

Doctor of Philosophy

in

Biology

by

Yvonne Pao

Committee in charge:

Roberto Malinow, Chair
Professor Darwin Berg
Professor Edward Koo
Professor Gentry Patrick
Professor Steven Wagner

2017

The Dissertation of Yvonne Pao is approved, and it is acceptable in quality and form for publication on microfilm and electronically:

_____

_____

_____

_____

_____

Chair

University of California, San Diego

2017

DEDICATION

For my mother.

EPIGRAPH

"What do you do when it rains?"

The captain answered frankly. "I get wet."

—Joseph Heller, *Catch-22*

TABLE OF CONTENTS

LIST OF FIGURES

ACKNOWLEDGEMENTS

I would like to express my profound gratitude to Dr. Roberto Malinow, whose support has been essential to my development as a scientist during my graduate career. My research experience prior to graduate school was largely in the field of developmental biology, and his patience and guidance has enabled me to gain expertise in the field of molecular and cellular neuroscience. I feel privileged to have worked with him over the past five years. I would also like to thank my committee: Dr. Edward Koo, Dr. Darwin Berg, Dr. Steven Wagner, and Dr. Gentry Patrick. They have provided direction to my research and supported my many thesis projects.

I would also like to thank Dr. Christophe Proulx, Dr. Sadegh Nabavi, Dr. Steven Shabel, Dr. Stephanie Alfonso, and Dr. Jonathan (Shao) Aow, who trained me in electrophysiology and behavioral assays, helped me troubleshoot experiments, and shared laughs with me when I most needed them. Most importantly, they prevented me from taking hedge clippers to my rig when I was most frustrated with fixing it (just kidding).

I would also like to thank the many friends I have made in San Diego: Leilani, James, Zohreh, Hannah, Suneer, and Eunice. Without their friendship and kindness during graduate school, the work presented in this dissertation would not have been possible. Finally, and most importantly, I would like to thank my partner, Georg. His scientific prowess and passion for research has always inspired me to become a better scientist myself, and always encouraged me to stick with it when the obstacles of graduate school seemed too large to overcome.

Chapter 2, in full, is a reprint of the material as it occurs in *Proceedings of the National Academy of Sciences*, Reinders NR, Pao Y, Renner MC, da Silva-Matos

CM, Malinow R, and Kessels HW, "AMPA-receptor subunit GluA3 makes synapses susceptible to amyloid-beta," *Proceedings of the National Academy of Science*, 113(42):e6526-6534, 2016. I was one of two primary authors, and I produced Figures 2.4 and 2.9.

Chapter 3 is a description of the work I did examining AAV-introduced expression of amyloid-β and the effect of γ-secretase modulators (GSM). I would like to thank Dr. Maria Kounnas (Neurogenetics Pharmaceuticals) and Dr. Steve Wagner for providing the GSM NGP-555. Phuong Nguyen, from Dr. Steve Wagner's laboratory, contributed to Figure 3.2A and Stephanie Alfonso, from Dr. Roberto Malinow's laboratory, contributed to Figure 3.3B.

Chapter 4, titled "SYNPLA: a new method for detecting recently potentiated synapses," was produced in collaboration with Justus Kebschull and Dr. Anthony M. Zador, from Cold Spring Harbor Laboratory. Justus Kebschull and I were the primary researchers for this project. Justus Kebschull produced Figures 4.1, 4.2, and 4.3.

VITA

2009	Bachelor of Science, Biology, California Institute of Technology, Pasadena, CA
2009-2010	Science Teacher, New York City Department of Education, New York, NY
2010-2011	Research Technician, Memorial Sloan-Kettering Cancer Center, New York, NY
2012-2015	Cellular and Molecular Genetics Training Grant Fellow, University of California, San Diego
2012-2015	Biology Peer Mentor, University of California, San Diego
2012-2015	Graduate Instructional Assistant, University of California, San Diego
2014-2015	Marketing and Technology Manager, Advanced Professional Degree Consulting Club, University of California, San Diego
2017	Ph. D. in Biology, University of California, San Diego

PUBLICATIONS

Reinders NR, **Pao Y**, Renner MC, da Silva-Matos CM, Lodder TR, Malinow R, Kessels HW, "AMPA-receptor subunit GluA3 makes synapses susceptible to amyloid-beta," *Proceedings of the National Academy of Science*, 113(42):e6526-6534, 2016.

Page DM, Wittamer V, Bertrand JY, Lewis KL, Pratt DN, Delgado N, Schale SE, McGue C, Jacobsen BH, Doty A, **Pao Y**, Yang H, Chi NC, Magor BG, Traver D, “An evolutionarily conserved program of B-cell development and activation in zebrafish", *Blood*, 122(8):e1-11, 2013.

ABSTRACT OF THE DISSERTATION

Investigating the Role of AMPA Receptors in Learning and Memory

by

Yvonne Pao

Doctor of Philosophy in Biology

University of California, San Diego, 2017

Roberto Malinow, Chair

Excitatory synapses possess a vast array of proteins, including glutamate receptors such as α-amino-3-hydroxy-5-methyl-4-isoxazolepropionic acid (AMPA) receptors, which mediate fast synaptic transmission. There are four different AMPA receptor subunits: GluA1, GluA2, GluA3, and GluA4). AMPA receptors are generally found in the adult rodent brain in two heteromeric forms: GluA1/GluA2 receptors and GluA3/GluA2 receptors. Trafficking of GluA1/GluA2 receptors is activity-dependent, while GluA3/GluA2 heteromers are constitutively cycling and replacing synaptic GluA1/GluA2 and GluA3/GluA2 receptors. It has largely been thought that the GluA1

subunit is critical to plasticity, but that GluA3 has little impact on the induction and expression of synaptic plasticity. Because of this, GluA3 has not been well studied. As it turns out, GluA3 is required for the expression of the synaptic dysfunction caused by amyloid-β (Aβ), a small peptide thought to be responsible for the pathogenesis of Alzheimer's disease. In the absence of GluA3, Aβ does not cause synaptic depression, memory deficits, or block long-term potentiation (LTP). These results will be described in Chapter 2.

Studies have demonstrated that Aβ causes synaptic dysfunction by activating signaling pathways involved in long-term depression (LTD). Previous studies from our lab established successfully engineered associative fear memories by pairing optogenetic activation of the auditory cortex (AuC) and medial geniculate nucleus (MGN) with footshock in cued fear conditioning. Replacing the traditional conditioned stimulus (CS) with an optogenetically-delivered input (ODI) allowed us to utilize LTP and LTD protocols to activate and inactivate memories. To examine if Aβ in Alzheimer's disease behaves as LTD *in vivo*, Aβ and a blue-shifted form of channelrhodopsin (ChR), known as oChIEF, were co-expressed in the AuC and MGN. A class of Alzheimer's disease therapeutics known as γ-secretase modulators (GSMs) were used to control Aβ levels, and a behaviorial paradigm was established to determine whether Aβ could remove inactivate memories like LTD, and later be recovered with LTP in the presence of GSMs. This study will be described in Chapter 3.

Lastly, given the importance of LTP in learning and memory, a new method for identifying recently potentiated synapses was investigated. One existing strategy for assessing learning-induced plasticity involves the use of two-photon laser scanning

microscopy (TPLSM) *in vivo*, which can provide high visual and temporal resolution on synapses undergoing potentiation. However, a caveat to this technique is that TPLSM techniques are labor intensive and thus low throughput. Another strategy for brain regions involved in a learning task is examining the localization of immediate-early gene (IEG) transcripts and proteins. Despite this method being relatively high throughput, the correlation between synaptic strength and IEG expression is poorly understood. Thus, we established a new technique, which we call SYNaptic Proximity Ligation Assay. SYNPLA applies the antibody-based methodology of PLA to the diversity of transsynaptic proteins to label synapses. In Chapter 4, SYNPLA's labeling of all synapses or recently potentiated synapses will be described.

Chapter 1

Introduction

1.1 AMPA receptors in learning and memory

Excitatory synapses possess a complex array of proteins, including AMPA and NMDA ionotropic receptors, along with metabotropic-type glutamate receptors (mGluRs). AMPA receptors mediate basal synaptic transmission, while NMDA receptors mediate long-term changes in synaptic transmission.

AMPA receptors comprise four different subunits: GluA1, GluA2, GluA3, and GluA4. In the adult rodent brain, AMPA receptors at glutamatergic synapses primarily comprise GluA1/GluA2 and GluA2/GluA3 heteromers (Wenthold et al., 1996). AMPA receptor trafficking to synapses is dependent on the carboxy-terminal tails (c-tails): short-tailed subunits (GluA2, GluA3, and GluA4c, a short-tailed variant of GluA4) are trafficked to the synapse constitutively, while the insertion of long-tailed subunits (GluA1, GluA4, and GluA2L, a long splice variant of GluA2) is activity-dependent (Hayashi, 2000; Shi et al., 2001).

NMDA receptors are known as a “molecular coincidence detectors" because

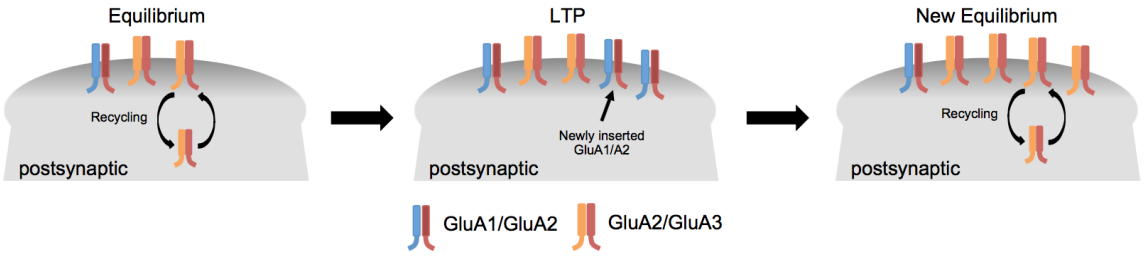

Figure 1.1: A prevailing model for AMPA receptor trafficking, described in Section 1.1.

they require both ligand binding and membrane depolarization to conduct calcium (Mayer and Armstrong, 2004). Tetanic stimulation causes NMDA receptors to open, allowing calcium influx and subsequently activating a variety of kinases, such as protein kinase A (PKA), Ca^{2+}/calmoldulin-dependent protein kinase II (CaMKII), and protein kinase C (PKC). These kinases phosphorylate the AMPAR subunit GluA1 at various sites on its c-tail, causing increased GluA1 insertion into synapses in long-term potentiation (LTP) (Shi, 1999; Hayashi, 2000). Low frequency stimulation (LFS) has long been thought to activate NMDA receptors, causing them to conduct low levels of calcium that will activate phosphatases, such as calcineurin, and result in the internalization of AMPA receptors in NMDA receptor-dependent long-term depression (LTD) (Malenka and Bear, 2004). Recent work from our lab has shown that antagonists of the NMDA receptor glutamate-binding site prevents the induction of LTD, while application of antagonists specific to the NMDA receptor ion channel or glycine-binding site do not affect LTD (Nabavi et al., 2013; Dore et al., 2015; Aow et al., 2015). These results suggest that LTD may be occurring through an Ca^{2+}-independent mechanism, instead requiring conformational changes in the cytoplasmic domain of NMDA receptors.

While NMDA receptors are critical for NMDAR-dependent LTP and LTD,

studies have elucidated an important role for AMPA receptors in LTP. AMPA receptors comprise four different subunits: GluA1, GluA2, GluA3, and GluA4. In the adult rodent brain, AMPA receptors at glutamatergic synapses primarily comprise GluA1/GluA2 and GluA2/GluA3 heteromers (Wenthold et al., 1996). Previous work in our lab has demonstrated that GluA1/GluA2 heteromers are only trafficked to the synapse during LTP, while GluA2/GluA3 heteromers are constantly trafficked to the synapse and play a role in the maintenance of LTP (Fig. 1.1 (Shi, 1999; Hayashi, 2000; Malinow et al., 2000). Electrophysiology experiments have also shown that GluA1 KO tissue does not undergo LTP when high frequency stimulation is delivered to the Schaffer collaterals, whereas LTP appears to be enhanced in GluA3 KO tissue (Zamanillo, 1999; Meng et al., 2003).

1.2 The role of amyloid-β in Alzheimer's disease

Alzheimer's disease is a neurodegenerative disease that is initially characterized by mild memory loss and eventually progresses into severe memory deficits and dementia (Selkoe and Schenk, 2003). Pathologically, Alzheimer's disease is characterized by amyloid plaques, neurofibrillary tangles containing hyperphosphorylated tau, and neuronal death. As a common cause of dementia among the elderly, Alzheimer's disease is projected to affect 1 in 85 persons worldwide by the year 2050, unless therapeutic advances that delay onset and progression are discovered (Brookmeyer et al., 2007).

Amyloid plaques are a classic diagnostic hallmark of Alzheimer's disease, but plaque burden does not correlate well with memory loss. These plaques comprise

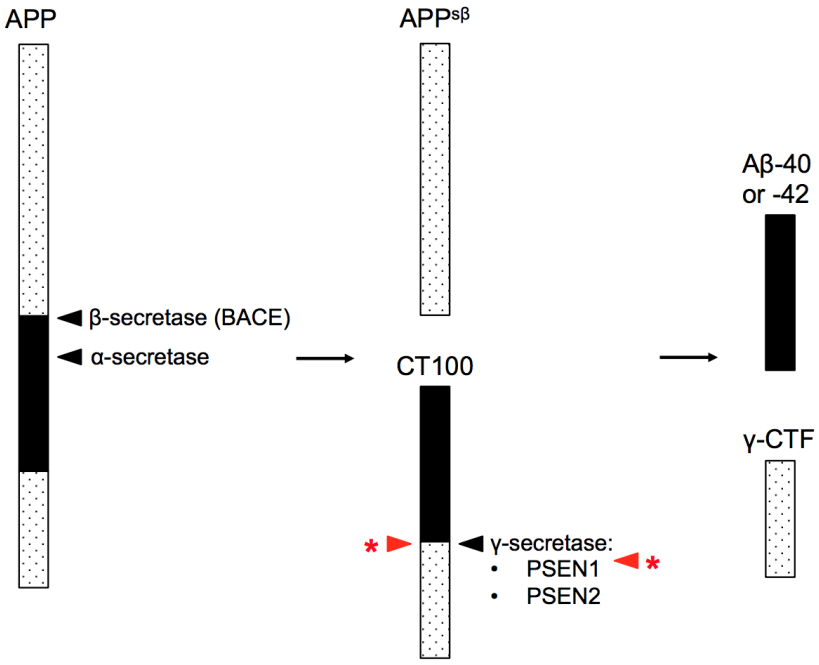

Figure 1.2: Sequential cleavage of the amyloid precursor protein (APP). APP is cleaved by β-secretase and γ-secretase to generate $A\beta_{40}$ or $A\beta_{42}$. Red arrows indicate some sites where mutations are often found in familial Alzheimer's disease.

the small peptide Aβ, which is the product of sequential cleavage of the amyloid precursor protein (APP) (Fig. 1.2). APP is first cleaved by β-secretase, leading to the production of a large, soluble ectodomain ($APP^{S\beta}$) and a membrane-associated fragment called CT100. CT100 is then cleaved by γ-secretase to form $A\beta_{40}$ or $A\beta_{42}$ (Vassar, 1999).

The amyloid cascade hypothesis suggests that reduced Aβ clearance, increases in the ratio of $A\beta_{42}$ to $A\beta_{40}$, and/or increased total Aβ production will first lead to the formation of soluble Aβ oligomers, followed by eventual deposition of amyloid plaques. While fibrillar amyloid deposition might lead to neuronal damage (Tsai et al., 2004), there is a growing consensus that soluble, oligomeric Aβ species are responsible for the synapse loss and memory impairment seen in Alzheimer's disease (Haass and Selkoe, 2007). Soluble Aβ oligomers are found in APP transgenic mice, which express human familial mutations of APP and possess learning deficits resembling those of Alzheimer's disease patients (Haass and Selkoe, 2007). More importantly, oligomeric species of Aβ are also found in Alzheimer's disease patients (Lesné et al., 2006).

What are the molecular mechanisms underlying Aβ-mediated synaptotoxicity? A brief literature search would demonstrate that Aβ could be acting through a variety of mechanisms, including N-methyl-D-aspartate (NMDA) receptors, α7-nicotinic acetylcholine receptors (nAcChR), GSK-3β, cellular prion protein, and so on (Liu et al., 2001, 2013; Jo et al., 2011; Collingridge, 2012; Laurén et al., 2009). What is very clear is that Aβ dysregulates plasticity by impairing long-term potentiation (LTP) and facilitating long-term depression (LTD), thereby demonstrating its impact on signaling cascades that affect the downstream trafficking of α-amino-3-hydroxy-

5-methyl-4-isoxazolepropionic acid (AMPA) receptors (Walsh et al., 2002; Li et al., 2009).

Studies have shown that Aβ-overexpression in rodent organotypic slices leads to synaptic depression similar to LTD. Viral overexpression of CT100, the precursor to Aβ, partially occludes the expression of LTD, and requires p38 MAPK and calcineurin activity to induce synaptic depression (Wang, 2004; Hsieh et al., 2006). This synaptic depression occurs in a non-cell-autonomous manner, and drives the endocytosis of AMPA and NMDA receptors (Hsieh et al., 2006). Other studies have shown that the exogenous application of Aβ-derived diffusible ligands (ADDLs) prepared synthetically, from cell lines, and from Alzheimer's disease brains, blocks LTP *in vivo* and *in vitro*, demonstrating that Aβ has an acute effect on synaptic transmission (Walsh et al., 2002).

Although significant advances have been made in understanding how Aβ leads to synaptic deficits, one area of great interest is determining the receptor target for Aβ. Several potential receptors have been identified, including the α7-nicotinic receptor (Snyder et al., 2005; Wang et al., 2000; Liu et al., 2001), RAGE (Du Yan et al., 1997; Sturchler et al., 2008), cellular prion protein (Laurén et al., 2009; Kessels et al., 2010; Balducci et al., 2010), and APP (Lorenzo et al., 2000). Interestingly, the application of NMDA receptor antagonists in the presence of Aβ prevents the blockade of LTP (Shankar et al., 2007, 2008; Hu et al., 2009). The receptor tyrosine kinase EphB2 has also been implicated as a target for Aβ (Cissé et al., 2010). Knockdown of EphB2 in wild-type mice leads to decreased NMDA receptor currents and impaired LTP, whereas overexpression of EphB2 in APP transgenic mice rescued LTP and behavioral memory deficits. These experiments

suggest that NMDA receptors play a crucial role in Aβ-induced synaptic depression and memory loss.

While it is not surprising that Aβ may target NMDA receptors, AMPA receptors are critical for mediating basal synaptic transmission and may also be affected by Aβ. Our lab has found that Aβ-induced synaptic depression is absent in tissue obtained from GluA3 KO mice, whereas Aβ-induced synaptic depression is normal in tissue obtained from GluA1 KO mice. The absence of synaptic depression in GluA3 KO mice suggests that GluA3 is required for mediating the effects of Aβ, which will be discussed in Chapter 2.

1.3 Alzheimer's disease therapeutics targeting γ-secretase

Identifying treatments that will slow or prevent the progression of Alzheimer's disease is important because of the disease's growing prevalence (Brookmeyer et al., 2007). Generally, there are several approaches to treating Alzheimer's, including treating the disease symptomatically, preventing the production of Aβ, and clearing Aβ oligomers and plaques from the brain by using antibodies targeting Aβ. In the interest of brevity, I will limit my discussion on Alzheimer's disease therapeutics to pharmacological treatments that aim to reduce the production of Aβ.

As described in the previous section, Aβ is produced when APP is sequentially cleaved by β-secretase (BACE) and γ-secretase. BACE1 cleavage of APP is the initiating factor involved in Aβ production, and is therefore an attractive target for Alzheimer's disease therapeutics. Studies of BACE1 knockout mice have shown

that these mice completely lack Aβ, without any gross developmental and behavioral abnormalities (Roberds et al., 2001; Luo et al., 2001), although subsequent studies showed that BACE knockout mice have more subtle neuronal abnormalities, such as reduced myelination (Willem et al., 2006; Hu et al., 2008) and reduced spine density (Savonenko et al., 2008). Since BACE has been established as the initial protease involved in Aβ production, there have been extensive efforts to develop BACE inhibitors. However, there has been limited success in identifying drugs that penetrate the blood-brain barrier (BBB) and sufficiently inhibit BACE, as reviewed in Vassar (2014).

Another attractive target for preventing Aβ production is γ-secretase, which is a multi-protein aspartic protease complex, comprising presenilin-1 or presenilin-2, nicastrin, anterior pharynx-defective 1 (APH-1), and presenilin enhancer 2 (PEN-2) (Kaether et al., 2006). Presenilins are the catalytic domains of γ-secretases, and are responsible for the transmembrane cleavage of the CT100 fragment to yield $A\beta_{40}$ or $A\beta_{42}$ and γ-CTF. Large-scale screens aimed at identifying compounds that would reduce Aβ cleavage in cell lines led to the identification of γ-secretase inhibitors (GSIs) such as semagacestat. Given the need for identifying drugs that would slow the onset of Alzheimer's, Eli Lilly moved forward with phase III clinical trials (Doody et al., 2013) despite the lack of evidence indicating the efficacy of semagacestat at lowering levels of Aβ levels (Karran et al., 2011). More interestingly, all patients receiving the GSI semagacestat worsened according to the Alzheimer's Disease Assessment Scale for cognition (ADAS-cog) and Alzheimer's Disease Cooperative Study-Activities of Daily Living (ADCS-ADL) scale after the clinical trial, as well as having more skin cancers and infections compared with the placebo group (Doody

et al., 2013).

Given that γ-secretase is required for Notch signaling, it is likely that the failure of GSIs to improve patient outcomes in clinical trials was caused by unforeseen impacts of GSIs on Notch signaling (Doody et al., 2013). Another possibility is that GSIs lead to the accumulation of β-CTFs, which may also have synaptotoxic effects resembling those of Aβ (Mitani et al., 2012). Whatever the case, the Eli Lilly clinical trials demonstrated that the complete inhibition of γ-secretase is not a suitable therapeutic strategy for slowing the onset of Alzheimer's disease.

Although complete inhibition of γ-secretase was revealed to be a poor therapy for Alzheimer's, other studies have characterized a new class of drugs described as γ-secretase modulators (GSMs). GSMs are compounds that reduce $A\beta_{40}$ and $A\beta_{42}$ levels without inhibiting affecting γ-secretase cleavage of Notch (Kounnas et al., 2010). GSMs reduce levels of $A\beta_{40}$ and $A\beta_{42}$, while increasing the levels of non-pathogenic $A\beta_{38}$ *in vitro* and *in vivo*, while GSIs lead to a decrease in $A\beta_{38}$, $A\beta_{40}$, and $A\beta_{42}$ (Kounnas et al., 2010). Chronic administration of GSMs, such as NGP-555, referred to as compound 4 in Kounnas et al. (2010), reduces plaque formation in the APP transgenic model, Tg 2576. Furthermore, Tg 2576 mice receiving GSIs showed reduced cognitive function in the Y maze 8 days after treatment, whereas Tg 2576 mice receiving GSMs show no apparent cognitive deficits in the Y maze (Mitani et al., 2012)

These studies have demonstrated the potential of γ-secretase modulators as a treatment for Alzheimer's disease. To further examine the therapeutic potential of these drugs, our lab embarked upon a study in which we utilized GSMs on rats acutely overexpressing CT100 in the auditory cortex (AuC) and medial geniculate

nucleus (MGN). In these experiments, a few preliminary findings demonstrated the promise of GSMs in ameliorating the effects of Aβ, which will be described in Chapter 3.

1.4 Methods for assessing synaptic plasticity

Learning and memory are impacted during the course of Alzheimer's disease, and it is well established that changes in synaptic strength are the basis of learning and memory (Kandel, 2001). Long-term potentiation (LTP) is a form of synaptic plasticity that involves synaptic strengthening, and has been well-characterized in *in vitro* and *in vivo* mammalian systems, as reviewed by Malenka (2003).

There are currently two widely used strategies for assessing learning-induced plasticity. One strategy relies on physiology and imaging techniques, which can be applied *in vivo* and *in vitro*. Two-photon excitation microscopy allows us to identify changes in spine growth and density during plasticity (Grutzendler and Gan, 2006). However, the caveat is that these techniques are labor intensive and require costly equipment, making the acquisition of data a very low throughput process.

Another strategy involves examining changes in the expression of immediate early genes (IEGs), like *c-fos*, *arc*, and *zif268*. Applying immunohistochemistry or *in situ* hybridization to whole-mount brain slices to examine protein or transcript localization has identified brain regions involved in learning and memory (Okuno, 2011). However, IEG expression is mostly prominently detected at the cell soma, and thus provides poor resolution of the synapses involved in plasticity. The correlation between IEGs and synaptic plasticity is also poorly understood, further complicating

the interpretation of IEG screens (Madison et al., 1991).

Although these techniques make it possible to identify synaptic changes and brain regions that undergo plasticity during various learning tasks, an ideal technique would combine a high throughput process that yields high resolution information. Chapter 4 will describe a new technique, called the SYNaptic Proximity Ligation Assay (SYNPLA). SYNPLA combines the methodology of the proximity ligation assay (PLA) and AMPA receptor trafficking at excitatory synapses during LTP.

PLA is an antibody-based method that can be used to detect protein complexes, or simply proteins in close proximity. Like immunohistochemistry, two primary antibodies are initially used to detect two antigens that are in proximity (<40 nm). Subsequently, secondary antibodies that are conjugated to oligonucleotides are used to detect the primary antibodies (Söderberg et al., 2006, 2008). When two antigens are sufficiently close, the complementary oligonucleotides can be ligated and amplified to create a “rolony,” which can then be detected as a fluorescent dot. PLA has been used reliably to detect protein complexes in cultured cells and in the mouse striatum (Söderberg et al., 2006; Trifilieff et al., 2011).

Chapter 2

AMPA-receptor subunit GluA3 makes synapses susceptible to amyloid-β

2.1 Abstract

Amyloid-β (Aβ) is a prime suspect to cause cognitive deficits during the early phases of Alzheimer's disease (AD). Experiments in AD-mouse models have shown that soluble oligomeric clusters of Aβ degrade synapses and impair memory formation. We show that all Aβ-driven effects measured in these mice depend on AMPA-receptor subunit GluA3. Hippocampal neurons that lack GluA3 were resistant against Aβ-mediated synaptic depression and spine loss. In addition, Aβ oligomers only blocked long-term synaptic potentiation in neurons that expressed GluA3. Furthermore, whereas Aβ-overproducing mice showed significant memory impairment, memories in GluA3-deficient congenics remained unaffected. These

experiments indicate that the presence of GluA3-containing AMPA-receptors is critical for Aβ-mediated synaptic and cognitive deficits.

2.2 Introduction

At the early stages of Alzheimers disease (AD), synaptic perturbations are strongly linked to cognitive decline and memory impairment in AD patients (Brown et al., 1998; Scheff et al., 2006). The accumulation of soluble oligomeric clusters of amyloid-β (Aβ), a secreted proteolytic derivative of the amyloid precursor protein (APP), may be important for the early synaptic failure that is seen in AD pathogenesis (Lambert et al., 1998; Lesné et al., 2006; McLean et al., 1999; Shankar et al., 2008). Neurons that overexpress APP or are exposed to Aβ-oligomers show synaptic depression, a loss of dendritic spines and a reduced capacity for synaptic plasticity (Kamenetz et al., 2003; Lacor et al., 2007; Walsh et al., 2002; Mucke and Selkoe, 2012). For all these effects to occur NMDA-receptor (NMDAR) activity is required (Kamenetz et al., 2003; Kessels et al., 2013; Shankar et al., 2007; Wei et al., 2009). Aβ-oligomers trigger an NMDAR-dependent signaling pathway that leads to synaptic depression through the removal of AMPA-receptors (AMPARs) and NMDARs from synapses (Kamenetz et al., 2003; Kessels et al., 2013; Snyder et al., 2005). Interestingly, a blockade of AMPAR endocytosis prevents the depletion of NMDARs and a loss of spines (Hsieh et al., 2006; Miyamoto et al., 2016), suggesting that the removal of AMPARs from synapses is critical for this pathway to induce synaptic failure.

Excitatory neurons of the mature hippocampus predominantly contain two

types of AMPARs in approximately equivalent amounts (Kessels et al., 2009): those consisting of subunits GluA1 and GluA2 (GluA1/2s), and those consisting of GluA2 and GluA3 (GluA2/3s) (Wenthold et al., 1996). GluA1-containing AMPARs are inserted into synapses upon the induction of long-term potentiation (LTP) in brain slices (Hayashi, 2000) and play a prominent role in memory formation (Mitsushima et al., 2011; Rumpel, 2005). In contrast, GluA2/3s contribute relatively little to synaptic currents, LTP or memory formation (Adamczyk et al., 2012; Humeau et al., 2007; Meng et al., 2003) and have been implicated to participate in homeostatic scaling of synapse strength (Makino and Malinow, 2011; Rial Verde et al., 2006). We here demonstrate that the AMPAR subunit GluA3 plays a major role in AD pathology by showing that mice lacking GluA3 are protected against Aβ-driven synaptic deficits, spine loss and memory impairment.

2.3 Results

2.3.1 GluA3-deficient neurons are resistant against Aβ-mediated synaptic depression

To assess whether the removal of AMPARs from synapses by Aβ depends on AMPAR subunit composition, organotypic hippocampal slice cultures were prepared from GluA1-deficient or GluA3-deficient mice and their wild-type littermates. CA1 neurons were sparsely (<10%) infected with Sindbis virus expressing APP_{CT100}, the β-secretase product of APP and precursor to Aβ, together with tdTomato under control of a second subgenomic promoter. 20-30 hrs after viral infection, synaptic currents evoked by electrical stimulation of Schaffer collateral inputs were mea-

sured on tdTomato-expressing and neighboring uninfected pyramidal CA1 neurons simultaneously.

We ascertained that the majority of tdTomato expressing neurons produced APP_{CT100} without affecting their membrane resistance (Fig. 2.7), supporting previous demonstrations that in these conditions the health of the neurons is not affected by Sindbis infection (Hayashi, 2000; Kamenetz et al., 2003; Kessels et al., 2013). Wild-type neurons that expressed APP_{CT100} showed decreased AMPAR currents ($p<0.01$; Fig. 2.1A) and reduced AMPA/NMDA ratios ($p=0.03$; Fig. 2.1C), which has been shown to be caused by increased neuronal production of Aβ (Kessels et al., 2013; Kamenetz et al., 2003). In CA1 neurons of GluA3-deficient organotypic slices the AMPA/NMDA ratios were on average 35% reduced compared with wild-type neurons CA1 neurons ($p=0.05$; Fig. 2.1C) and APP_{CT100} expression failed to decrease synaptic AMPAR currents ($p=0.6$; Fig. 2.1A and B) or AMPA/NMDA ratios ($p=0.6$; Fig. 2.1C and D). However, GluA1-deficient neurons had a more reduced AMPA/NMDA ratio (55%; Fig. 2.1C), yet still show APP_{CT100}-induced synaptic AMPAR depression ($p=0.01$; Fig. 2.1A) that was a similar depression as in wild-type neurons ($p=0.2$; Fig. 1B). These data indicate that the presence of GluA3-containing AMPARs, but not of those containing GluA1, is crucial for Aβ to trigger synaptic AMPAR depression.

Figure 2.1: GluA3-deficient neurons are resistant against Aβ-mediated synaptic AMPAR depression. (A-D) Dual whole-cell recordings of APP_{CT100} infected and neighboring uninfected CA1 neurons from organotypic slices of wt mice (black), GluA3-KO littermate mice (blue), or GluA1-KO littermate mice (red). (A) Example traces (top) and dot plots (bottom) of paired EPSC recordings (open dots) with averages denoted as filled dots (wt: n=27; GluA3-KO: n=27; GluA1-KO: n=31). Genotype x APP_{CT100}: $p<0.01$ (two-way ANOVA). Scale bars: 20 ms and 50pA. (B) Fold change in AMPAR currents upon APP_{CT100} expression, calculated as the average log2-transformed ratio of EPSC recorded from APP_{CT100}-infected over EPSC from neighboring uninfected neuron. (C) AMPA/NMDA ratios of uninfected and APP_{CT100} infected neurons (wt: n=18; GluA3-KO: n=18; GluA1-KO: n=20); Genotype x APP_{CT100}: $p=0.3$ (two-way ANOVA). (D) Fold change in AMPA/NMDA ratios upon APP_{CT100} expression, calculated as in (B). Data are mean ±SEM. Statistics: 2-tailed paired (A,C) or unpaired (B-D) t test. * indicates $p<0.05$.

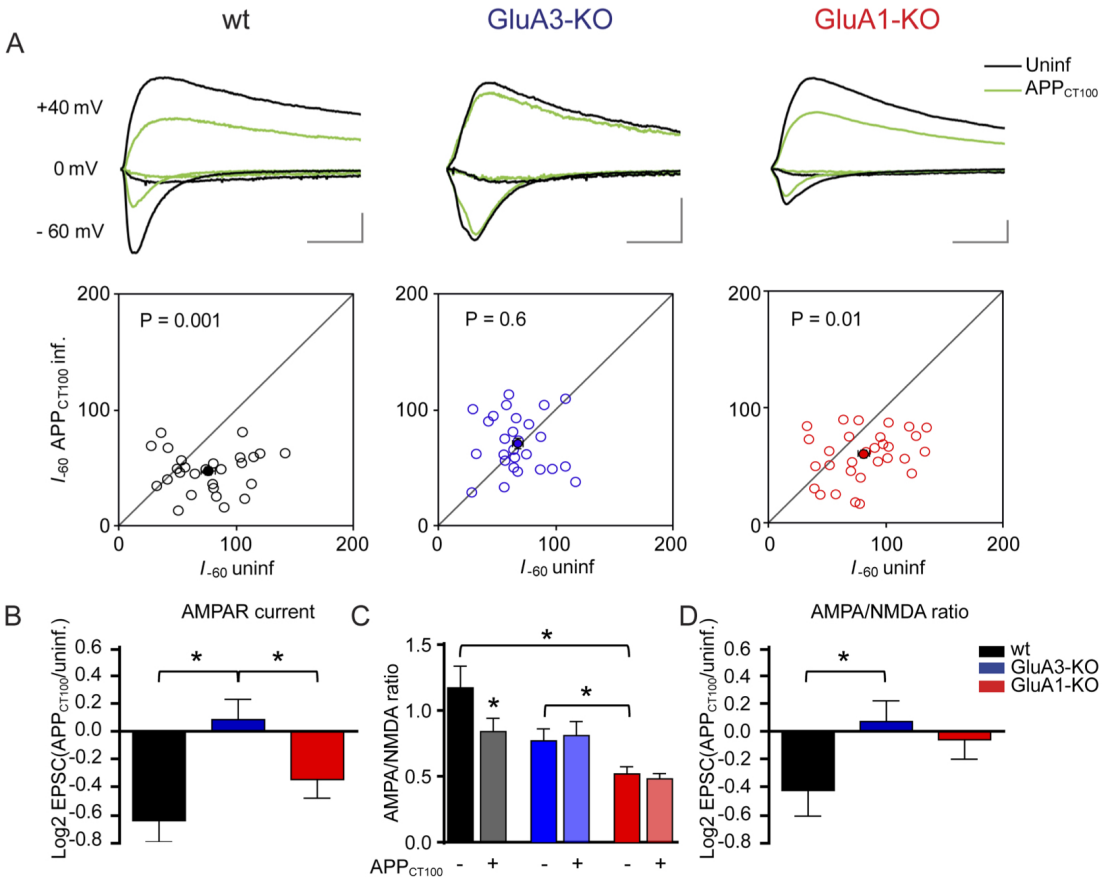
A
wt
GluA3-KO
GluA1-KO
Uninf
APP$_{CT100}$
+40 mV
0 mV
- 60 mV
P = 0.001
P = 0.6
P = 0.01
I_{-60} APP$_{CT100}$ inf.
I_{-60} uninf
B
AMPAR current
Log2 EPSC(APP$_{CT100}$/uninf.)
C
AMPA/NMDA ratio
APP$_{CT100}$
D
AMPA/NMDA ratio
wt
GluA3-KO
GluA1-KO

Figure 2.2: GluA3-deficient neurons are resistant against Aβ-mediated synaptic NMDAR depression. (A-E) Dual whole-cell recordings of APP infected and neighboring uninfected CA1 neurons from organotypic slices of wt mice (black), GluA3-KO littermate mice (blue), or GluA1-KO littermate mice (red). (A) Example traces (top) and dot plots (bottom) of paired NMDAR EPSC recordings (open dots) with average denoted as filled dot (wt: n=17; GluA3-KO: n=16; GluA1-KO: n=17). Genotype x APP_{CT100}: p=0.05 (two-way ANOVA). Scale bars: 20 ms and 50 pA. (B) Example traces (top) and average EPSC currents normalized to the average of the uninfected neurons (bottom) before and after Ro 25-6981 wash-in to reveal GluN2A and GluN2B contributing NMDAR currents. Scale bars: 20 ms and 50pA. (C) Fold change in total NMDAR, (D) GluN2A and (E) GluN2B currents upon APP_{CT100} expression, calculated as the average log2-transformed ratio of EPSC recorded from APP_{CT100}-infected over EPSC from neighboring uninfected neuron. Data are mean ±SEM. Statistics: 2-tailed paired (A,B) or unpaired (C-E) t test. * indicates $p<0.05$.

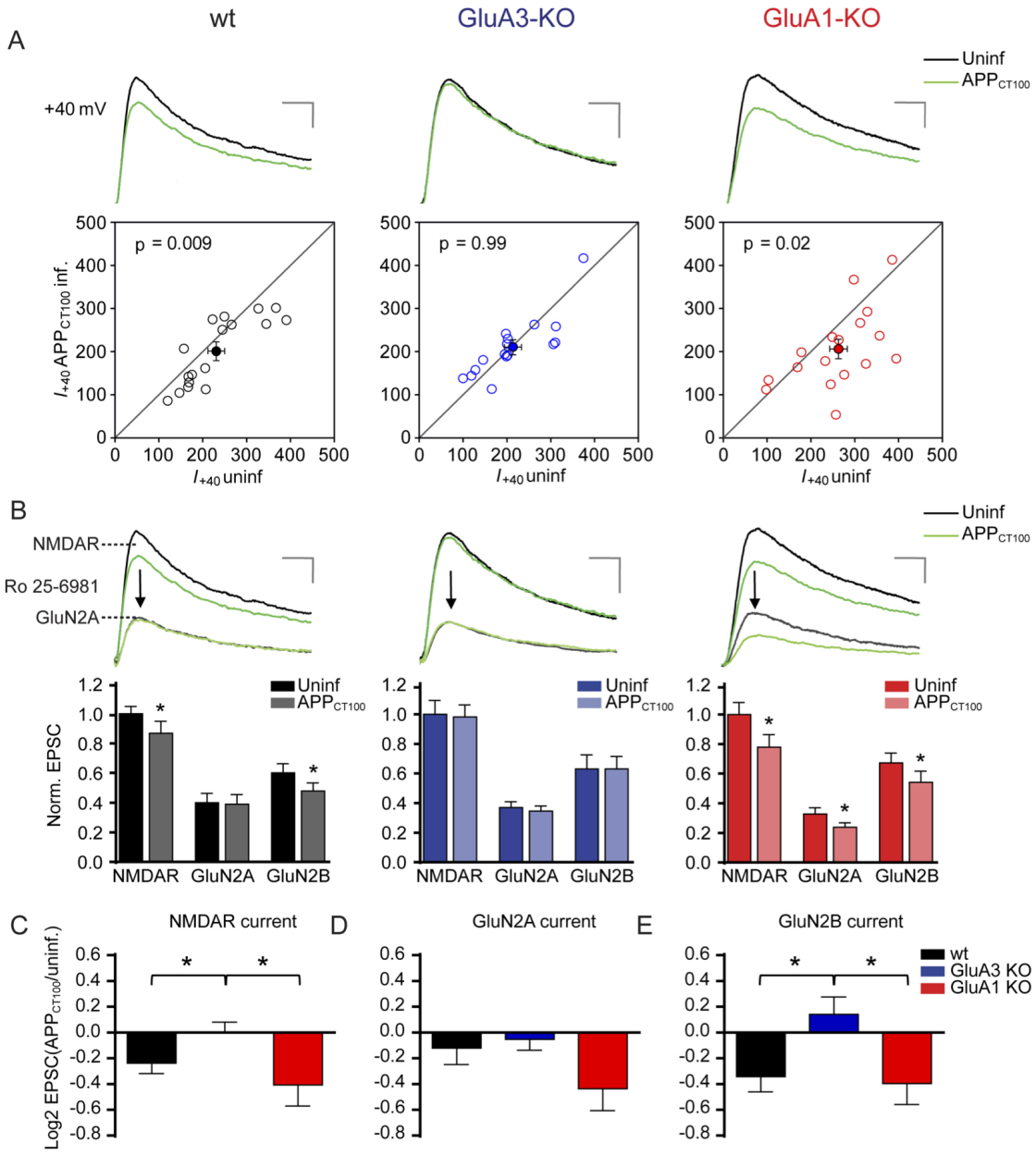
wt
GluA3-KO
GluA1-KO
A
+40 mV
Uninf
APP$_{CT100}$
p = 0.009
p = 0.99
p = 0.02
I_{+40} APP$_{CT100}$ inf.
I_{+40} uninf
B
NMDAR
Ro 25-6981
GluN2A
Norm. EPSC
NMDAR
GluN2A
GluN2B
C
NMDAR current
D
GluN2A current
E
GluN2B current
Log2 EPSC(APP$_{CT100}$/uninf.)
wt
GluA3 KO
GluA1 KO

To assess the effect of Aβ on NMDARs, we compared synaptic NMDAR currents between pairs of APP_{CT100} infected and nearby uninfected neurons (Fig. 2.2). APP_{CT100} expression led to a significant decrease in synaptic NMDAR currents in wild-type CA1 neurons ($p<0.01$; Fig. 2.2A) and in GluA1-deficient CA1 neurons ($p=0.02$), but not in those lacking GluA3 ($p>0.9$; Fig. 2.2A and C). These data indicate that neurons are only susceptible to Aβ-mediated NMDAR depression when they express AMPAR subunit GluA3. Digital subtraction of currents before and after wash-in of the specific GluN2B blocker Ro 25-6981 permitted measurement of the relative contribution of GluN2A and GluN2B to the NMDAR currents. The relative contribution of GluN2A and GluN2B to total NMDAR currents was not altered by the absence of GluA1 or GluA3 (Fig. 2.2B). As previously shown (Kessels et al., 2013), APP_{CT100} expression in wild-type neurons selectively affected NMDAR currents mediated by GluN2B ($p=0.01$; Fig. 2.2B and E) and not those mediated by GluN2A ($p=0.4$; Fig. 2.2B and D). APP_{CT100} expression in GluA3-deficient neurons failed to reduce NMDAR currents independently of whether they contained GluN2A ($p=0.6$; Fig. 2.2B and D) or GluN2B ($p=0.3$; Fig. 2.2B and E). In GluA1-deficient neurons both GluN2A ($p=0.02$) and GluN2B ($p=0.03$) NMDAR currents were significantly reduced upon APP_{CT100}-expression (Fig. 2.2B to E), suggesting that the presence of GluA1 protects synapses from an Aβ -mediated reduction in synaptic GluN2A currents. A proportional decrease in AMPAR (Fig. 2.1B) and NMDAR (Fig. 2.2C) currents in APP_{CT100}-expressing GluA1-deficient neurons corresponds with their unchanged AMPA/NMDA ratio (Fig. 2.1D).

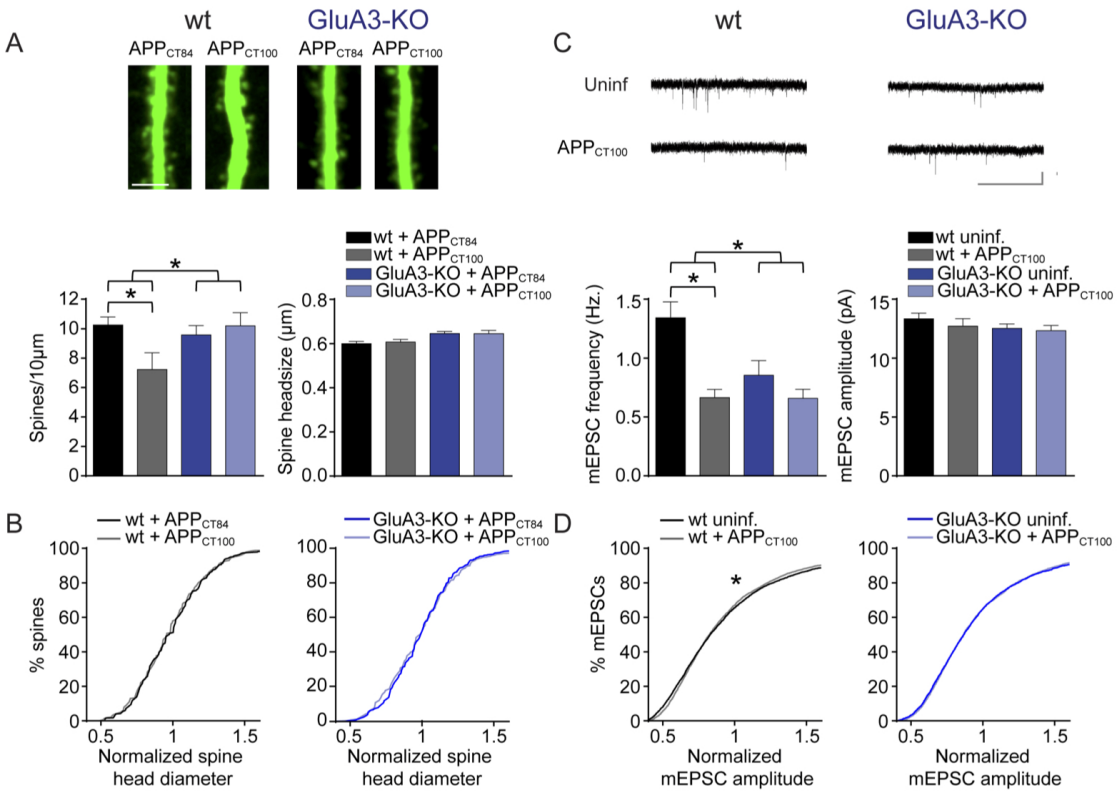

Figure 2.3: GluA3-deficient neurons are resistant against Aβ-mediated spine loss. (A-D) Spine and mEPSC analysis of CA1 neurons in organotypic slices from wild-type (black) or GluA3-KO mice (blue). (A, top) Example images of wt and GluA3-KO dendrites expressing APP$_{CT84}$ or APP$_{CT100}$. Scale bar: 5 μm. (A, bottom) APP$_{CT100}$ expression reduced spine density in wild-type but not GluA3-KO neurons without changing the average spine head diameter. (wt, APP$_{CT84}$: n=20 and APP$_{CT100}$: n=13; GluA3-KO, APP$_{CT84}$: n=26; APP$_{CT100}$: n=19). (B) Distribution of spine head diameters in APP$_{CT100}$ versus APP$_{CT84}$ expressing wt or GluA3-KO neurons. (C, top) Example mEPSC traces of wt and GluA3-KO neurons with or without APP$_{CT100}$-expression. Scale bar: 3 sec, 10 pA. (C, bottom) APP$_{CT100}$ expression reduced mEPSC frequency in wild-type but not GluA3-KO neurons without changing average mEPSC amplitude. (wt, APP$_{CT100}$: n=24 and uninf: n=25; GluA3-KO, APP$_{CT100}$: n=21 and uninf: n=22). (D) APP$_{CT100}$ changed the normalized distribution of mEPSC amplitudes of wt but not of GluA3-KO neurons. Data are mean ± SEM. Statistics: two-way ANOVA with post-hoc Sidak (A,C) or K-S test (B,D). * indicates $p < 0.05$.

2.3.2 Aβ-mediated synapse loss depends on the presence of GluA3

The number of AMPARs at a synapse correlates well with the synapse size and the spine size (Matsuzaki et al., 2001). To examine whether Aβ selectively targets a specific subtype of synapses harboring GluA3-containing AMPARs, we analyzed spine densities, spine size and miniature EPSC (mEPSC) events in Aβ-overproducing neurons. We assessed Aβ-induced spine loss by expressing APP_{CT100} together with the cytosolic marker tdTomato in CA1 neurons of organotypic slices. As a control we expressed APP_{CT84}, the α-secretase product of APP, which does not produce Aβ, and did not affect spine density, mEPSC frequency or mEPSC amplitude (Fig. 2.8). The spine density at apical dendrites was significantly lower in APP_{CT100}-expressing wild-type CA1 neurons compared to APP_{CT84} infected ones ($p=0.01$; Fig. 2.3A). The loss of spines in APP_{CT100}-expressing CA1 neurons occurred without a change in the average spine head diameter ($p=0.6$; Fig. 2.3A) or in the distribution of spine head sizes (Fig. 2.3B). Correspondingly, CA1 neurons expressing APP_{CT100} showed a decrease in mEPSC frequency ($p<0.01$; Fig. 2.3C) but not in average mEPSC amplitude ($p=0.9$; Fig. 2.3C). A minor change in the distribution of mEPSC amplitudes ($p=0.02$; Fig. 2.3D) indicates that APP_{CT100}-expressing neurons have a slightly smaller proportion of synapses with large AMPAR current amplitudes.

GluA3-deficient CA1 neurons have a similar spine density as wild-type neurons ($p=0.6$) with on average slightly larger spine heads ($p=0.02$; Fig. 2.3A). APP_{CT100} expression in these GluA3-deficient neurons did not lead to a reduced spine density ($p>0.9$) or spine head size ($p>0.9$; Fig. 2.3A). The average mEPSC

amplitude and was also similar between GluA3-deficient neurons and wild-type neurons ($p=0.2$), and was not altered upon APP_{CT100}-expression in GluA3-deficient neurons ($p=0.7$; Fig. 2.3C, $p=0.6$; Fig. 2.3D). Notably, the mEPSC frequency was significantly lower in GluA3-deficient neurons ($p<0.01$; Fig. 2.3C) to a size similar to APP_{CT100}-expressing wild-type neurons ($p=0.2$), and did not change upon APP_{CT100} expression ($p=0.2$; Fig. 2.3C). These findings indicate that Aβ triggers a reduction in synaptic AMPAR currents and a loss of spines, only when GluA3 is present. Combined with previous reports that show that AMPAR endocytosis is required for the synaptotoxic effects of Aβ (Hsieh et al., 2006; Miyamoto et al., 2016), our data imply that the active removal of GluA3-containing AMPARs by Aβ (but not the genetic deficiency of GluA3) leads to a loss of spines.

Figure 2.4: GluA3-deficient neurons are resistant against the Aβ-mediated block in LTP. (A,B) Example traces (top) and average peak field potential responses recorded at the CA1 stratum radiatum before and after theta burst stimulation (TBS). Scale bars: 10 ms, 0.2 mV. (A) LTP was inhibited in wild-type neurons by Aβ-containing medium (gray: n=11) compared with control medium (black; n=6). (B) In GluA3-KO slices LTP was not inhibited by Aβ-medium (light blue; n=8) in comparison to control medium (dark blue; n=8). (C) In the presence of Aβ-medium, the fold change in AMPAR currents upon TBS, calculated as log2-transformed ratio of the fEPSP 50-60 min after TBS (70-80 min) over the fEPSP during baseline (0-20 min), was larger in LTP pathway of GluA3-KO slices compared to wt slices and control pathways. Data are mean ±SEM. Statistics: 2-tailed unpaired t test over the last 10 minutes of the recording (A,B) and two-way ANOVA with post-hoc Sidak (C). * indicates $p<0.05$.

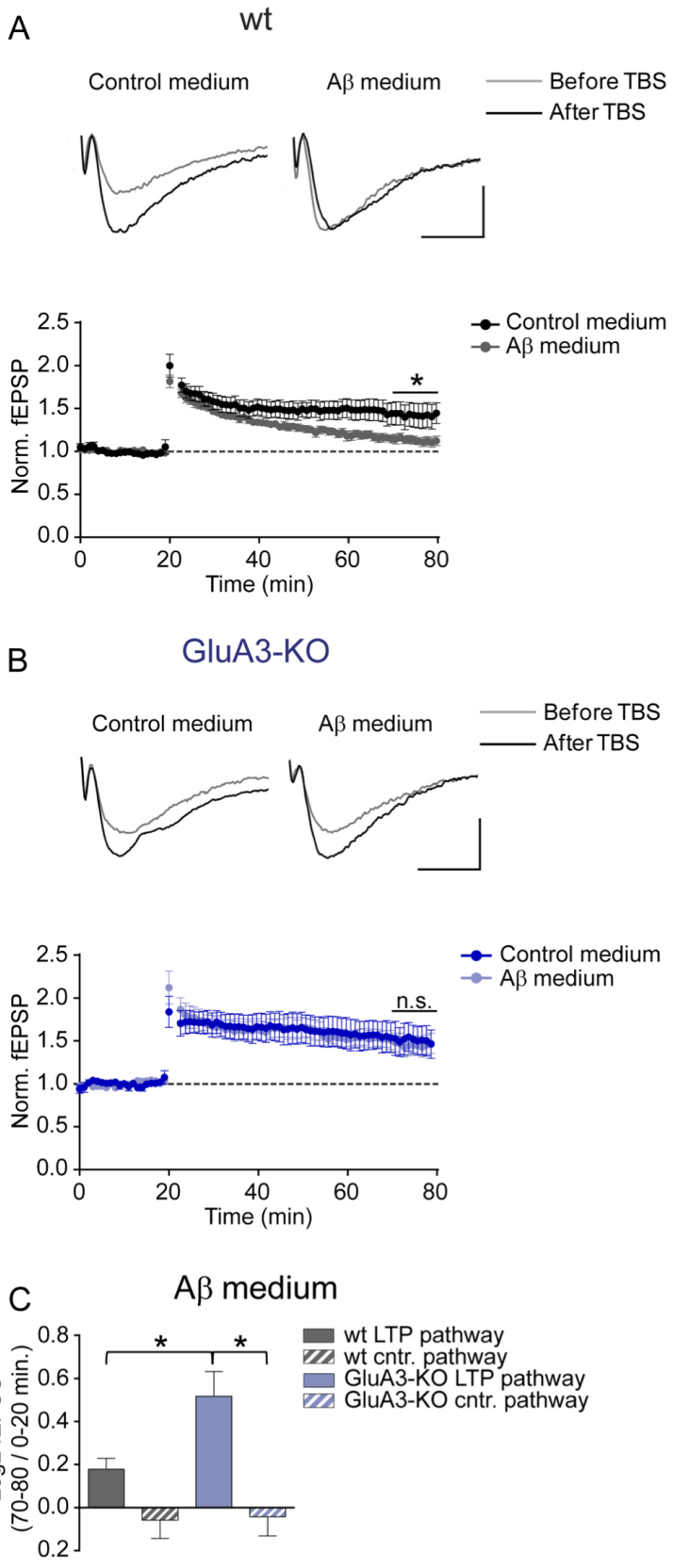
A
wt
Control medium
Aβ medium
Before TBS
After TBS
Control medium
Aβ medium
Norm. fEPSP
Time (min)
*
B
GluA3-KO
Control medium
Aβ medium
Before TBS
After TBS
Control medium
Aβ medium
Norm. fEPSP
Time (min)
n.s.
C
Aβ medium
Log2 fEPSC (70-80 / 0-20 min.)
wt LTP pathway
wt cntr. pathway
GluA3-KO LTP pathway
GluA3-KO cntr. pathway
*
*

2.3.3 GluA3-deficient neurons are insensitive to the Aβ-mediated blockade of LTP

Aβ-oligomers are capable of blocking NMDAR-dependent LTP (Walsh et al., 2002). To assess whether GluA3-deficient neurons are susceptible to the Aβ-mediated blockade of LTP, we performed extracellular local field potential recordings in brain slices acutely isolated from wild-type mice and GluA3-deficient littermates. Previous studies have shown that LTP induction in GluA3-deficient brain slices produces a level of potentiation that is similar (Humeau et al., 2007) or larger (Meng et al., 2003) than in wild-type neurons. We observed that a theta-burst stimulation onto CA3-CA1 synapses produced stable, pathway-specific LTP of similar magnitude in wild-type and GluA3-deficient slices (Fig. 2.9). This experiment was repeated in slices incubated with cell culture medium from a cell line that produces Aβ in oligomeric form, or with control medium (Podlisny et al., 1995). The incubation of slices with 1 nM of oligomeric Aβ blocked LTP in wild-type slices ($p=0.03$; Fig. 2.4A), but failed to block LTP in GluA3-deficient slices ($p=0.8$; Fig. 2.4B). In the presence of Aβ-oligomers LTP was significantly smaller in wild-type slices compared to GluA3-deficient slices ($p=0.04$; Fig. 2.4C). Thus, GluA3-expression was critical for Aβ-oligomers to block LTP.

2.3.4 GluA3-deficient APP/PS1 transgenic mice do not display spine loss or memory impairment

Mice that express human APP (APPswe) and mutant presenilin 1 (PS1dE9) transgenes produce high levels of $A\beta_{42}$ and are used as a mouse model for familial

AD (Savonenko et al., 2005). An immunostaining for Aβ shows that these APP/PS1-transgenic mice started to develop plaques in the CA1 region of the hippocampus at the age of 6 months, with more plaques situated in the stratum lacunosum-moleculare (SLM) than in the stratum radiatum (SR) (Fig. 2.5A and Fig. 2.10A). To assess whether these local differences in Aβ-load correspond with location-specific patterns of spine loss (Šišková et al., 2014), spine analysis was performed on oblique CA1 dendrites in both SR and SLM. Indeed, whereas the spine density remained unaffected in the SR ($p=0.6$; Fig. 2.5C and D and Fig. 2.10B), we did observe a reduced spine density in the SLM ($p<0.01$; Fig. 2.5E and F). Although in 12-month old mice the plaque load had approximately quadrupled in both the SR and the SLM (Fig. 2.5B), the spine loss in the CA1 had not aggravated (Fig. 2.5D and F). The observed spine loss in the SLM of APP/PS1-transgenic mice was not accompanied by a change in the average diameter of spine heads (Fig. 2.5G and J) or the distribution of spine head sizes (Fig. 2.5I and J). In APP/PS1 mice that were GluA3-deficient the development of plaque formation was similar compared to GluA3-expressing APP/PS1 littermates ($p>0.9$; Fig. 2.5A and B), suggesting that the level of Aβ accumulation was unaffected in the absence of GluA3. As we observed in organotypic slice cultures, GluA3-deficient CA1 neurons have on average a similar spine density (Fig. 2.5C to F) and larger spine heads (Fig. 2.5G and H; and Fig. 2.11) compared with age-matched wild-type littermates. Notably, in GluA3-deficient mice the APP/PS1 transgenes did not cause a reduced spine density in the SLM at both 6 and 12 months of age (Fig. 2.5E and F), indicating that APP/PS1 mice are only susceptible to spine loss when they express AMPAR subunit GluA3.

Figure 2.5: APP/PS1 mice that lack GluA3 develop Aβ plaques but do not show spine loss. (A,B) Examples of 6E10 staining (left) and average mean plaque load of 6 month (A) and 12 month (B) APP/PS1 mice (n=4 mice for all groups) demonstrate that more Aβ plaques were formed in the stratum lacunosum-moleculare (SLM) than in the stratum radiatum (SR). PCL, pyramidal cell layer; MO, molecular layer of the dendate gyrus. (C,D) Example images (left) and average spine density (right) of CA1 dendrites in the SR was similar in dendrites of 6 month (C, wt=18; APP/PS1=24; GluA3-KO=18; APP/PS1/GluA3-KO=18) and 12 month old APP/PS1 mice (D, wt=24; APP/PS1=24; GluA3-KO=12; APP/PS1/GluA3-KO=18) Scale bar: 2 μm. (E,F) Example images (left) and average spine density (right) was lower in APP/PS1-expressing SLM dendrites provided that they expressed GluA3 for both 6 month (E, wt=18; APP/PS1=24; GluA3-KO=18; APP/PS1/GluA3-KO=18) and 12 month (F, wt=24; APP/PS1=24; GluA3-KO=12; APP/PS1/GluA3-KO=18) old mice. Scale bar: 2 μm. (G,H) Mean spine head diameter was unaffected in 6 month (G) and 12 month (H) old APP/PS1 mice. (I,J) Spine head size normalized distribution was unaffected in 6 month (I) and 12 month (J) old APP/PS1 mice. Data are mean ±SEM. Statistics: two-way ANOVA with post-hoc Sidak test (A-H), or K-S test (I,J). * indicates $p<0.05$.

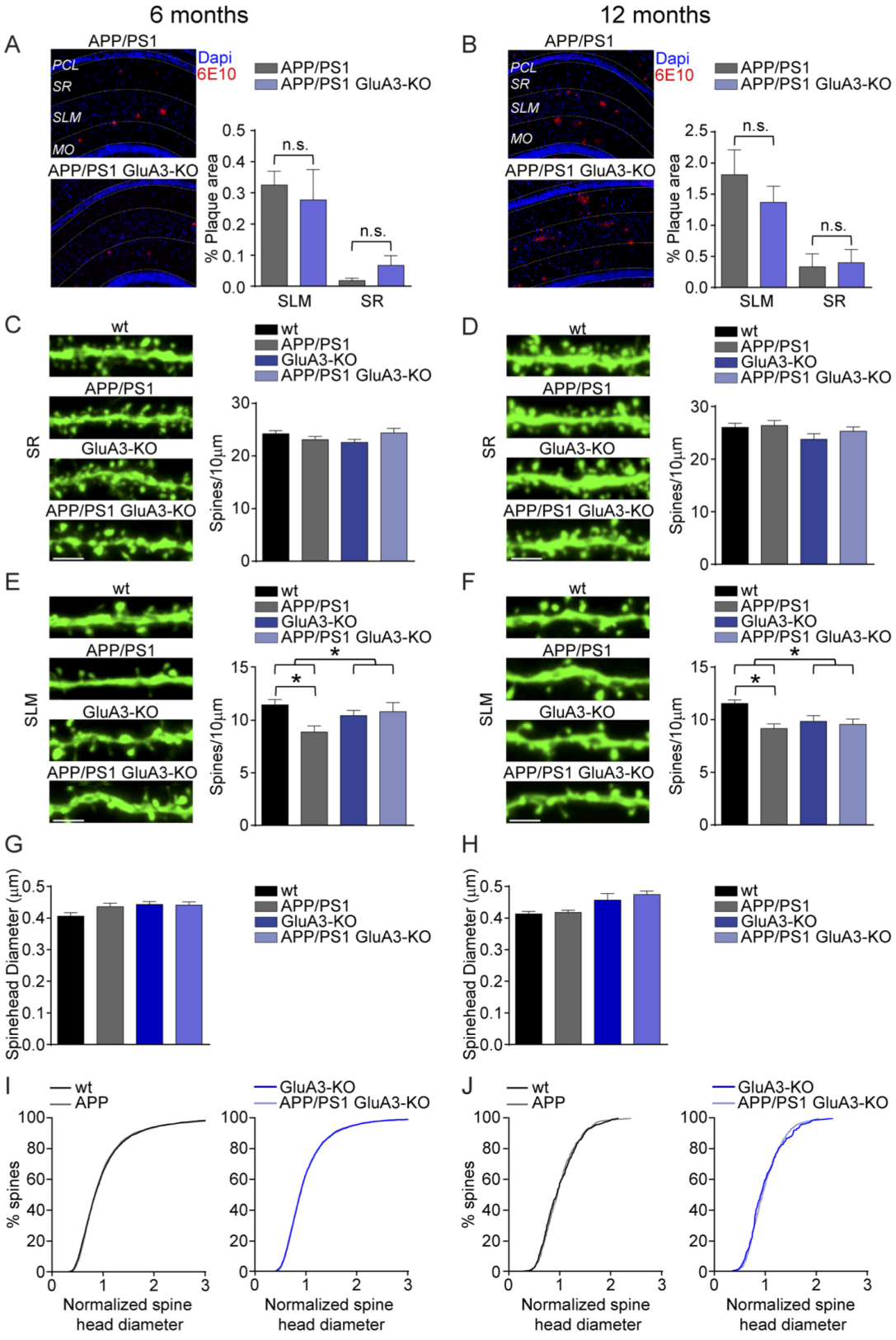
6 months
12 months
A
B
APP/PS1
PCL
SR
SLM
MO
Dapi
6E10
APP/PS1 GluA3-KO
APP/PS1
APP/PS1 GluA3-KO
% Plaque area
n.s.
SLM
SR
C
D
wt
APP/PS1
GluA3-KO
APP/PS1 GluA3-KO
SR
Spines/10µm
E
F
SLM
*
G
H
Spinehead Diameter (µm)
I
J
wt
APP
GluA3-KO
APP/PS1 GluA3-KO
% spines
Normalized spine head diameter

In addition to Aβ plaque and spine pathology, APP/PS1 mice show cognitive deficits and premature mortality. In our colony the survival rate of APP/PS1 mice was reduced compared with wild-type littermates ($p<0.01$). APP/PS1 mice did not show premature mortality when they were GluA3-deficient ($p=0.2$, Fig. 2.6A). We tested the ability to form hippocampus- and amygdala-dependent memories by submitting either 6 or 12-month old mice to a contextual fear-conditioning paradigm. Upon exposure to the shock cage, the mice with different genotypes displayed a similar locomotor activity in a novel environment and a similar startle response to a mild foot shock (Fig. 2.6B and C). When re-exposed to the shock cage 24 hours after conditioning, APP/PS1 mice showed impaired fear memories as expressed by a lower level of freezing behavior compared with wild-type littermates ($p=0.01$; Fig. 2.6D and $p=0.03$; Fig. 2.6E). For GluA3-deficient mice, the freezing response to the fearful context were equal irrespectively of having APP/PS1 transgenes ($p>0.9$; Fig. 2.6D and $p>0.9$; Fig. 2.6E). Similar results were obtained when another group of 6-month old mice was tested 7 days after conditioning (Fig. 2.6F and G), indicating that also the long-term stability of contextual fear memories remained unaffected by APP/PS1 transgenes in the absence of GluA3. GluA3-deficient mice consistently displayed a lower (non-significant) memory performance compared to their wild-type littermate controls at both 6 ($p=0.7$; Fig. 2.6D) and 12 months of age ($p=0.6$; Fig. 7E). In 3-month old mice this was not observed (Fig. 2.12). Combined, these findings indicate that GluA3 renders APP/PS1 mice susceptible to memory impairment.

Figure 2.6: APP/PS1 mice do not show increased mortality or memory deficits when they lack GluA3. (A) Kaplan Meier curves demonstrating that APP/PS1 but not APP/PS1/GluA3-KO mice have increased mortality rates (n=780 at 1 month, n=127 at 12 months). (B,C) Locomotion is similar before and during (startle response) the foot-shock in the conditioning trial, in both 6 month old (B) and 12 month old (C) mice. Automated quantification of motion as the number of Significant Motion Pixels (SMP) as described previously (49). (D,E) Freezing levels during fear-memory retrieval 24 hrs after conditioning in 6-month old littermates (D, wt n=13; APP/PS1 n=13; GluA3-KO n=11; APP/PS1/GluA3-KO n=15) and 12-month old littermates (E, wt n=13; APP/PS1 n=20; GluA3-KO n=12; APP/PS1/GluA3-KO n=19). (F) Freezing responses to the fear context at 24 hrs (same as in D) and a different group of mice tested 7 days after conditioning (wt n=14; APP/PS1 n=13; GluA3-KO n=16; APP/PS1/GluA3-KO n=19) showed that long-term stability of contextual fear memories is unaffected in APP/PS1/GluA3-KO mice. Data are mean ±SEM. Statistics: Mantel-Cox test with Bonferroni correction (A), two-way ANOVA with post-hoc Sidak test (D,E), and unpaired t test (F,G). * indicates $p<0.05$.

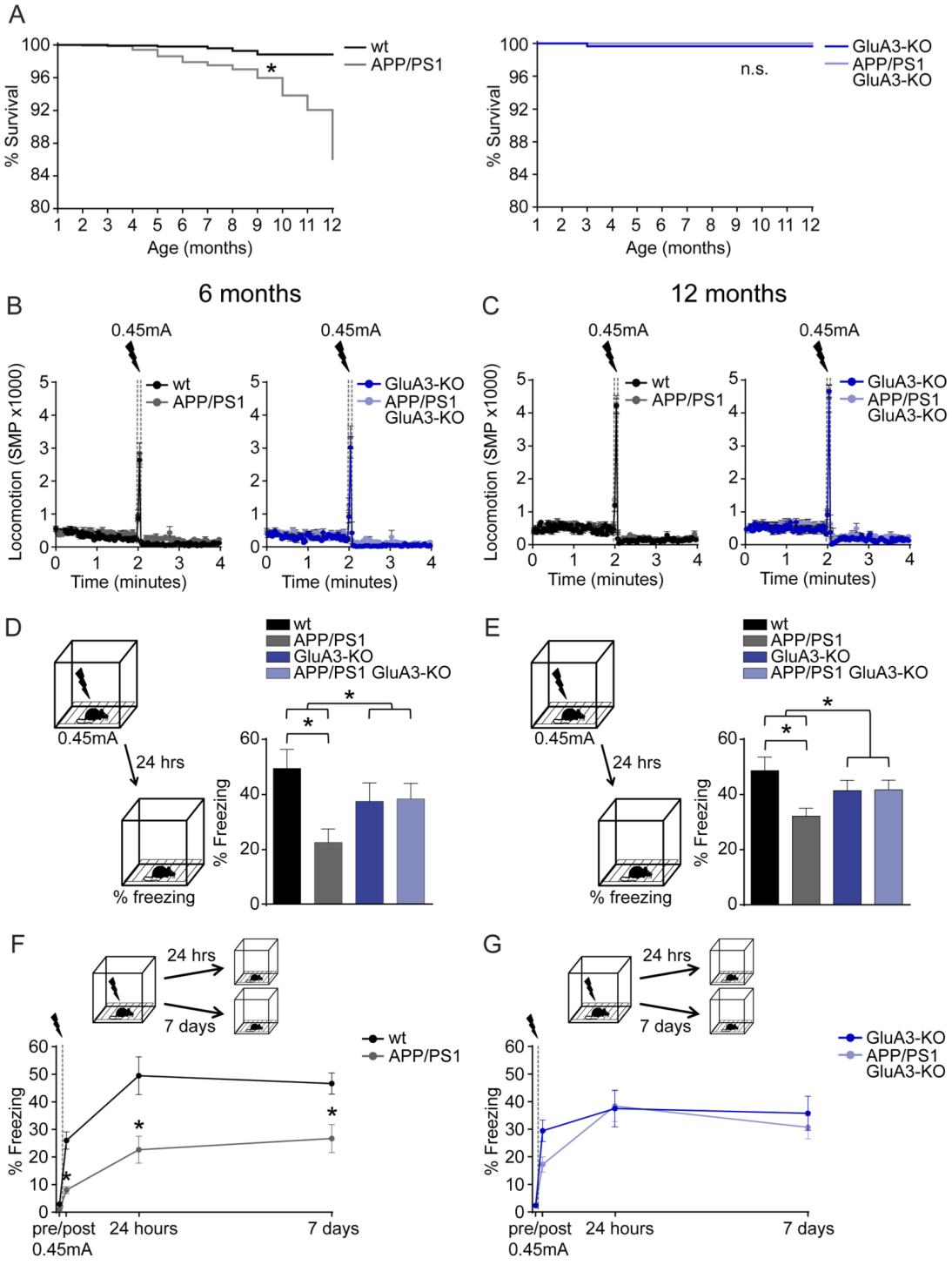
A
% Survival
Age (months)
wt
APP/PS1
*
GluA3-KO
APP/PS1 GluA3-KO
n.s.
B
6 months
0.45mA
Locomotion (SMP x1000)
Time (minutes)
C
12 months
D
0.45mA
24 hrs
% freezing
% Freezing
E
F
7 days
pre/post 0.45mA
24 hours
7 days
G

2.4 Discussion

We studied the influence of AMPAR subunit composition on Aβ-mediated synapto-toxicity in three different model systems. Firstly we showed that synaptic depression and spine loss in APP_{CT100}-overexpressing CA1 neurons of organotypic slices require GluA3 expression. Secondly, exogenously added Aβ-oligomers block LTP in acutely isolated brain slices of wild-type mice, but not of GluA3-deficient mice. Finally, increased mortality, contextual fear memory deficits and spine loss in APP/PS1-transgenic mice are absent when they lack GluA3. Our data indicate that GluA3-containing AMPARs play a central role in these Aβ-mediated deficits. The increased mortality of APP/PS1 transgenic mice appears related to the occurrence of epileptic seizures and not to neurodegeneration (Scharfman, 2012). It will be interesting to assess whether GluA3 is also required for seizure generation in APP/PS1 mice.

How Aβ-oligomers initiate synaptic deficits remains largely unclear. Aβ-oligomers have a broad range of binding partners at the surface of neurons (Rahman et al., 2015), and a number of these partners have been proposed to be necessary for inducing pathological effects (Benilova et al., 2012; Mucke and Selkoe, 2012). Although GluA3 may be another candidate Aβ receptor, we consider the possibility that GluA3 is not so much responsible for the induction, but rather for the expression of Aβ-driven synaptic deficits. We propose a model where Aβ-oligomers bind one (or a combination) of surface receptors, thereby hijacking or facilitating an endogenous NMDAR-dependent signaling cascade that ultimately leads to the selective removal of GluA3-containing AMPAR from synapses. A factor that potentially mediates the depletion of GluA2/3 AMPARs from synapses is PICK1, an adaptor protein that

selectively interacts with GluA2 and GluA3. The phosphorylation of the GluA2 or GluA3 c-tail by protein kinase Cα (PKCα) permits PICK1 to bind, leading to AMPAR endocytosis (Kim et al., 2001; Terashima et al., 2008). Notably, PICK1 as well as PKCα are necessary for Aβ-mediated synaptic depression to take place (Alfonso et al., 2014, 2016). The PICK1-dependent removal of AMPARs from the surface by Aβ was shown to be more prominent for GluA2 than for GluA1 (Alfonso et al., 2014), suggesting that Aβ-oligomers particularly trigger the endocytosis of GluA2/3s. The removal of GluA3-containing receptors by Aβ as a mechanism of action is supported by our finding that AMPAR currents are similarly reduced in neurons lacking GluA3 as in wild-type neurons expressing APP_{CT100}. (i.e. similar mini EPSC frequency and AMPAR/NMDAR ratio). Other effects of Aβ, including synaptic NMDAR depression, spine loss, LTP blockade, memory impairment and premature mortality did not fully mimic the lack of GluA3, possibly because these effects require the active removal of GluA3-containing AMPARs and/or because GluA3-deficiency is chronic and could allow compensatory mechanisms to ameliorate some of the deficits. Regardless of the mechanisms underlying the partial mimicry, our experiments indicate that the presence of GluA3 is required for these effects to occur.

GluA3-containing AMPARs have been proposed to be involved in the homeostatic scaling of synapse strength (Makino and Malinow, 2011; Rial Verde et al., 2006). In such a scenario, neurons that are deprived of synaptic input increase their synaptic GluA2/3 levels, and conversely neurons that are hyperactive counteract by lowering the number of GluA2/3s at synapses. It has recently been suggested that AD-related synaptic and memory deficits may arise from defects in homeostatic plasticity (Megill et al., 2015; Jang and Chung, 2016). Possibly Aβ-oligomers

mediate a persistent synaptic downscaling by reducing the levels of GluA2/3s at synapses irrespective of the history of neuronal activity. Alternatively, Aβ-oligomers may trigger an increased neuronal network activity (Verret et al., 2012) to which neurons respond by lowering synaptic GluA2/3 levels. However, the consequences of an excess deposition of Aβ are not limited to the loss of synaptic AMPAR levels. Our observation that other Aβ-driven effects are not observed in GluA3-deficient mice is consistent with the notion that the removal of AMPARs from synapses is one of the first critical steps in Aβ pathogenesis (Hsieh et al., 2006; Miyamoto et al., 2016), followed or accompanied by the collateral removal of GluA1/2s and GluN2B-containing NMDARs and the disintegration of the synapse. Possibly GluA2/3s play a role in the stabilization of spine structures, for instance through their interaction with N-cadherins at synapses (43, 44)(Saglietti et al., 2007; Silverman et al., 2007). Alternatively, the endocytosis of GluA3-containing AMPARs may trigger a cellular signal that leads to the dismantling of spine structures. We propose that an intervention in the signaling pathway that is used by Aβ to remove GluA2/3s from synapses may be an attractive approach to prevent all Aβ-driven synaptic and memory deficits.

Lowering the neuronal or synaptic levels of GluA3-containing AMPARs may reduce the vulnerability of neurons for the detrimental effects of oligomeric Aβ. Interestingly, a recent study that screened for gene expression profiles associated with mild cognitive impairment (MCI), a clinical transition stage between aging and AD dementia (Boyle et al., 2006), found that among the genes that showed a strong negative correlation with cognitive performance were genes encoding glutamate receptors GluA3 and GluN2B (Berchtold et al., 2014). It is tempting to speculate that people with relatively low levels of GluA3 and GluN2B expression are less

likely to develop MCI despite the presence of Aβ-oligomers. Along these lines, a mentally active brain would theoretically provide a reduced susceptibility for MCI, since learning behavior and sensory experiences trigger the delivery of GluA1-containing AMPARs to synapses (Mitsushima et al., 2011; Rumpel, 2005) and the subsequent homeostatic removal of synaptic GluA2/3s (Makino and Malinow, 2011; Rial Verde et al., 2006). Future experiments may reveal under which physiological conditions the levels of GluA3 change in neurons, and whether differences in the expression levels of GluA3 determine the severity of AD-symptoms.

2.5 Experimental Procedures

Mice

GluA3-deficient (Gria3tm1Dgen/Mmnc; MMRRC, Davis, CA), APP-swe/PS1dE9 mice (Savonenko et al., 2005) (kindly provided by Dr. Elly Hol), and Thy1-eYFP mice (B6.Cg-Tg(Thy1-YFP)HJrs/J; Jackson, Bar Harbor, USA) were at least 6 times backcrossed to c57bl6 mice. GluA1-deficient mice were in a c57bl6/129 hybrid background and were a kind gift from Dr. R. Huganir (Kim et al., 2005). GluA3 is an X-linked gene; for behavioral experiments only male GluA3-/Y and littermate GluA3+/Y were used. For electrophysiology both male $GluA3^{-/Y}$ and $GluA3^{+/Y}$ and female $GluA3^{-/-}$ and $GluA3^{+/+}$ littermates were used; female $GluA3^{+/-}$ were excluded from this study. Mice were kept on a 12-hours day-night cycle and had ad libitum access to food and water. All experiments were were approved by the Institutional Animal Care and Use Committee of the Royal Netherlands Academy of Arts and Sciences (KNAW) or the University of San Diego, California.

Organotypic and acute hippocampal slices

Organotypic hippocampal slices were prepared from P7-8 mice as described previously (Stoppini et al., 1991) and used after 7-12 days in culture for electrophysiology or after 13-15 days in culture for spine analysis. Constructs of APP-CT100+tdTomato, APP-CT84+tdTomato, GFP-GluA3(i) and GFP-GluA3(i)+APP-CT100 were cloned into a pSinRep5 shuttle vector and infective Sindbis pseudo viruses were produced according to the manufacturer's protocol (Invitrogen BV, Leek, Netherlands). Acute hippocampal slices were prepared from 3- to 4-week-old mice. Slices were cut coronally in cold sucrose cutting buffer (72 mM sucrose, 22 mM glucose, 2.6 mM NaHCO3, 83 mM NaCl, 2.5 mM KCl, 3.3 mM MgSO4, and 0.5 mM CaCl2) at a thickness of 350 Îijm and transferred to a recovery chamber containing oxygenated artificial cerebrospinal fluid (ACSF) containing 11 mM glucose, 1 mM MgCl2, and 2 mM CaCl2. Slices were maintained at 34°C for 45 min and then at room temperature for 45 min.

Preparation of Aβ oligomers

Chinese hamster ovary (CHO) cells stably transfected with APP751(V717F) mutation, referred to as 7PA2 cells (Savonenko et al., 2005), were a gift from Dr. Edward Koo. 7PA2 cells or control CHO cells were cultured in Dulbecco's modified Eagle's medium (DMEM) containing 10% bovine fetal calf serum and grown to near confluence, then cultured in plain DMEM for 16 hr. The Aβ medium is collected, centrifuged at 200 g for 10 min and concentrated 10 fold using an Amicon Ultra 3k filtration device at 4000 $\times$ g for 30 min at 4°C. Levels of $A\beta_{40}$ and $A\beta_{42}$ oligomers were measured by enzyme-linked immunosorbent assay (ELISA). 7PA2 conditioned

medium was diluted to 1 nM total Aβ, and CHO conditioned medium from the same batch was diluted similarly. Western Blots were used to confirm the presence of Aβ oligomers.

Electrophysiology

Organotypic hippocampal slices were perfused with artificial CSF (ACSF, in mM: 118 NaCl, 2.5 KCl, 26 $NaHCO_3$, 1 NaH_2PO_4, 4 $MgCl_2$, 4 $CaCl_2$, 20 glucose) gassed with 95%O_2/5%CO_2). Whole-cell recordings were made with 3 - 5 MΩ pipettes, (Raccess < 20 MΩ, and R_{input} > 10 x R_{access}) filled with internal solution containing (in mM): 115 $CsMeSO_3$, 20 CsCl, 10 HEPES, 2.5 $MgCl_2$, 4 Na_2-ATP, 0.4 Na-GTP, 10 Na-Phosphocreatine, 0.6 EGTA. Miniature EPSCs were recorded at -60 mV with TTX (1 μM) and picrotoxin (50 μM) added to the bath. For evoked recordings, a cut was made between CA1 and CA3, and picrotoxin (50 μM) and 2-chloroadenosine (4 μM; Tocris) were added to the bath. Two stimulating electrodes, two-contact Pt/Ir cluster electrode (Frederick Haer, Bowdoin, USA), were placed between 100 and 300 μm down the apical dendrite, 100 μm apart, and 200 μm laterally in opposite directions. AMPAR-mediated EPSCs were measured as the peak inward current at -60 mV. NMDAR-mediated EPSCs were measured as the mean outward current between 40 and 90 ms after the stimulation at +40 mV, corrected by the current at 0 mV. EPSC amplitudes were obtained from an average of at least 40 sweeps at each holding potential. Data was acquired using a Multiclamp 700B amplifier (Molecular Devices, Sunnyvale, USA). Evoked recording were analyzed using custom software written in Igor Pro (Wavemetrics, Tigard, USA). Miniature EPSC recordings were analyzed with MiniAnalysis (Synaptosoft, Decatur, USA) with

an amplitude threshold of 5 pA. For LTP recordings, acute slices were transferred to a recording chamber, where it was submerged and received a continuous flow of ACSF supplemented with 11 mM glucose, 1 mM $MgCl_2$, 2 mM $CaCl_2$, and 100 μM picrotoxin (pH 7.4). Extracellular field potentials were recorded in the SR with glass electrodes (1.5-2.5 MΩ) containing ACSF. Field excitatory postsynaptic potentials (fEPSPs) were evoked by stimulating independent afferents by placing bipolar stimulation electrodes 150 μm down the apical dendrites, and 150-200 μm laterally in opposite directions. Aβ or control medium was added to the perfusion for 20 minutes during the acquisition of a stable baseline prior to LTP induction. LTP was induced by applying 4 trains of electrical stimulation at 100 Hz, lasting 100 ms each, every 20 s. After LTP induction, fEPSPs were recorded for an additional 60 min. Averaged normalized fEPSP for the last 10 minutes (50-60 minutes after LTP induction) of each recording was used to quantify the potentiation value. Experiments were conducted blind to experimental conditions.

Dendritic spine analysis in organotypic hippocampal slices

Three-dimensional images were collected by two-photon laser scanning microscopy (Femtonics Ltd. Hungary) with a Ti:sapphire laser (Chameleon, Coherent, Santa Clara, USA) tuned at 910 nm. Optical z-sections were captured every 0.75 μm of apical dendrites approximately 180 μm from the cell body. The density and diameter of spines protruding in the horizontal (x/y) plane were manually quantified from projections of stacked 3D images by an experimenter blind to experimental conditions and genotype using ImageJ software (http://fiji.sc).

Aβ plaque load and spine analysis in APP/PS1 mice

Mice were anesthetized with pentobarbital and perfused with 20 ml 0.1 M PBS followed by 80 ml of fixative (4% paraformaldehyde in 0.1 M PBS pH 7.2). Brains were removed, post-fixed for 1 hour in fixative, and washed in PBS.

For plaque load analysis: brains were kept in 20% sucrose overnight, snap-frozen in dry-ice and stored at -80°C. The brains were sliced into 10 μm sections on a Leica CM3050S cryostat and thaw-mounted onto microscope slides. Epitope retrieval was achieved by incubating the slides in a sodium citrate buffer (10mM sodium citrate, 0.05% Tween-20, pH 6.0) at 95°C. The sections were washed in PBS, incubated in blocking solution (10% normal donkey serum, 0.4% Triton X-100 in PBS) for 1 hour and subsequently incubated with the 6E10 antibody (1:15000 dilution, SIG-39320, Covance, Princeton, NJ, USA) overnight at room temperature in blocking solution, washed in PBS and incubated with Cy3-conjugated donkey anti-mouse IgG (1:1400, in PBS; Jackson ImmunoResearch, West Grove, PA, USA) for 2 hours at room temperature. Sections were washed in PBS and covered with VectaShield mounting medium with DAPI (Vector Labs, Burlingame, CA, USA). Images of the CA1 (10x magnified, 1392x1040, pixel size 0.65 μm^2 were obtained using a fluorescence microscope (Leica DM-RE, Wetzlar, Germany). Eight images per animals were acquired blind to experimental conditions, and analyzed with Image-Pro Plus software script (Media Cybernetics, Rockville, MD, USA). The level of plaque area was expressed as the percentage of positive pixels. Slices from wt and GluA3-KO littermates were included as negative controls (Fig. 2.10A).

For spine analysis: coronal 50 μm-thick slices were prepared from the fixed brains of Thy1-eYFP with a vibratome (Leica, Rijswijk, Netherlands) and mounted

with Vectashield medium (Vector Labs, Peterborough UK). Z-stack images of oblique apical dendrites were obtained with a Leica SP5 II confocal microscope. Laser power was adjusted to achieve similar fluorescence levels across images. Spine density and spine size was manually quantified by an experimenter blind to experimental conditions and genotype using ImageJ software (âĂŸhttp://fiji.sc'). Spine size was determined by measuring spine head diameters, since diameter measurements were largely independent on fluorescence intensity levels (Fig. 2.10C).

Contextual fear conditioning behavioral assay

Male mice ($GluA3^{-/Y}$) were placed in a box (29 cm high, 31.5 cm wide, 23 cm deep; Med Associates Inc., Georgia, VT) inside a sound-attenuating chamber for 4 min, in which a shock (0.45 mA, 2 s) was delivered after 2 min through a grid floor with stainless steel bars. Each trial took place between 1:00 and 4:00 pm during the light cycle. Freezing behavior and locomotion were quantified using custom-made Matlab script (Kopec et al., 2007). Absence of movement for at least 1 second was considered as freezing. Experiments were conducted blind to the genotype of the mice.

Statistical analysis

The Kolmogorov-Smirnov test (K-S) was used to test whether data sets were normally distributed. The F-test was used to test equal variance. Where necessary, data were log- or square root-transformed to obtain normal distributions and homogeneity of variance. Significance was determined using two-tailed Student *t* tests to compare 2 groups. Two-way ANOVA followed by post-hoc Sidak comparisons were

used when two independent variables (i.e. genotype and the expression/presence of Aβ) were measured. The K-S tests on the cumulative distributions were done on data normalized to its group mean. This allowed a comparison of distributions independent of a difference in mean. Mantel-Cox test with Bonferroni correction was used to compare mortality rates. *P* values below 0.05 were considered statistically significant.

Author Contributions

Author contributions: N.R.R., Y.P., M.C.R., C.M.d.S.-M., T.R.L. and H.W.K. performed experiments and analyzed data. N.R.R., Y.P., R.M. and H.W.K. wrote the manuscript.

2.6 Acknowledgments

We thank Prof. Dr. Ed Koo for providing AÎš-oligomer samples, and Prof. Elly Hol and Dr. Willem Kamphuis for their expert advice. This work was supported by the Netherlands Organization for Scientific Research (NWO-ALW), the Netherlands Organization for Health Research and Development (ZonMW), the AlzheimerâĂŹs Association and the Internationale Stichting Alzheimer Onderzoek. The authors declare no financial or non-financial competing interests.

Chapter 2, in full, is a reprint of the material as it occurs in *Proceedings of the National Academy of Sciences*, Reinders NR, Pao Y, Renner MC, da Silva-Matos CM, Malinow R, and Kessels HW, "AMPA-receptor subunit GluA3 makes synapses susceptible to amyloid-beta," *Proceedings of the National Academy of Science*,

113(42):e6526-6534, 2016. I was one of two primary authors, and I produced Figures 2.4 and 2.9.

2.7 Supplemental Information

2.7.1 Supplemental Figures

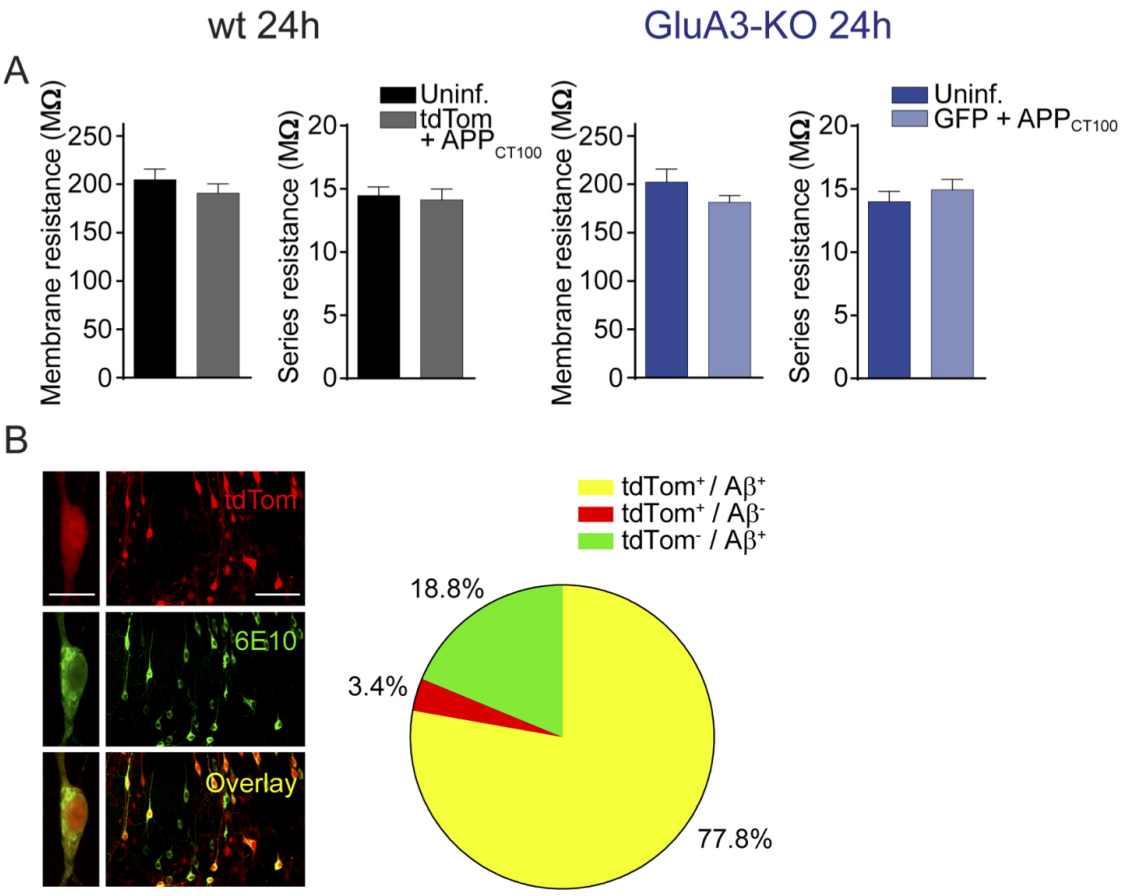

Figure 2.7: Sindbis virus expression does not affect membrane resistance of neurons and allows for dual APPCT100/tdTomato expression. (A) Average membrane (R_m) and series (R_s) resistance of whole-cell patch clamped CA1 neurons expressing tdTomato+APP_{CT100} (gray; n=24) and uninfected (black; n=24) wild-type neurons 24 hrs after infection, GFP+APP_{CT100} expressing (light blue; n=13) and uninfected (dark blue; n=15) GluA3-KO neurons 24 hrs after infection, and GFP+APP_{CT100} expressing (light blue; n=25) and uninfected (dark blue; n=11) neurons 48 hrs after infection. Mean R_m indicates that Sindbis-driven APP_{CT100} expression did not compromise neuronal health. Data are mean ±SEM. Statistics: 2-tailed unpaired t test. (B) Example images of an individual neuron (left panel; scale bar: 20μm) and a population of CA1 neurons in an organotypic slice (right panel; scale bar: 100μm) infected with Sindbis virus expressing APP_{CT100}/tdTomato and immunostained for Aβ (6E10 antibody). The majority of tdTomato-expressing CA1 neurons (total: n=144) showed positive staining for Aβ.

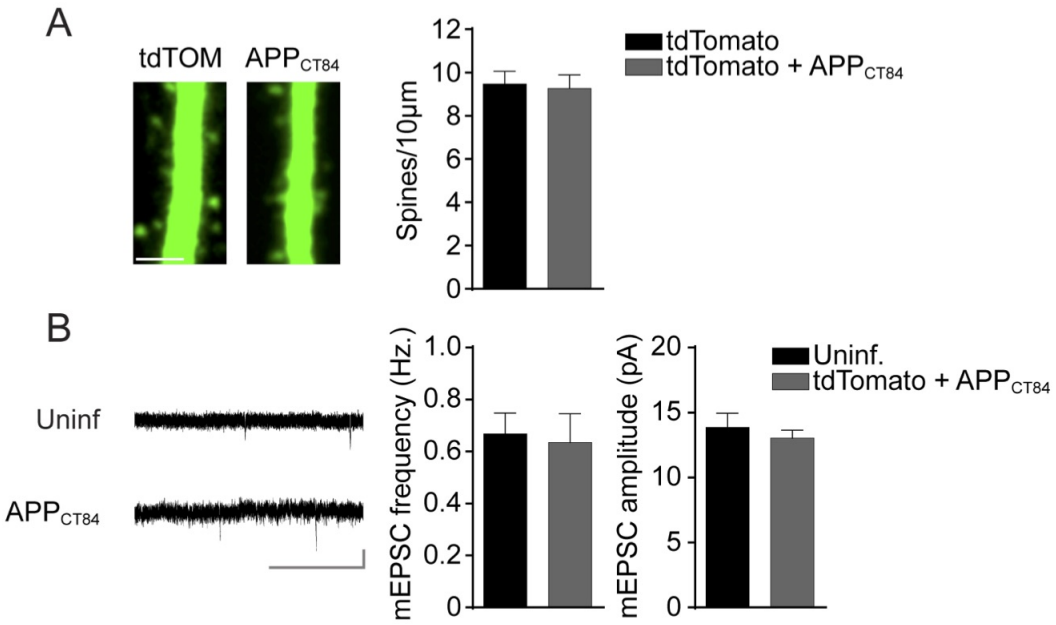

Figure 2.8: Expression of APP_{CT84} does not affect spine density or mEPSCs. (A) (left) Example of 2-photon images of apical CA1 dendrites infected with tdTomato or tdTomato+APP_{CT84}. Scale bar: 3μm. (right) The average spine density was not different between tdTomato (n=11) and tdTomato+APP_{CT84} (n=11) expressing CA1 pyramidal neurons. (B) (left) Example mEPSC traces of wt neurons with or without APP_{CT84}-expression. Scale bar: 3 sec, 10 pA. (right) APP_{CT84} expression did not affect mean mEPSC frequency or amplitude in wild-type neurons (uninf.: n=17 and CT84: n=14). Data are mean ±SEM. Statistics: 2-tailed unpaired t test.

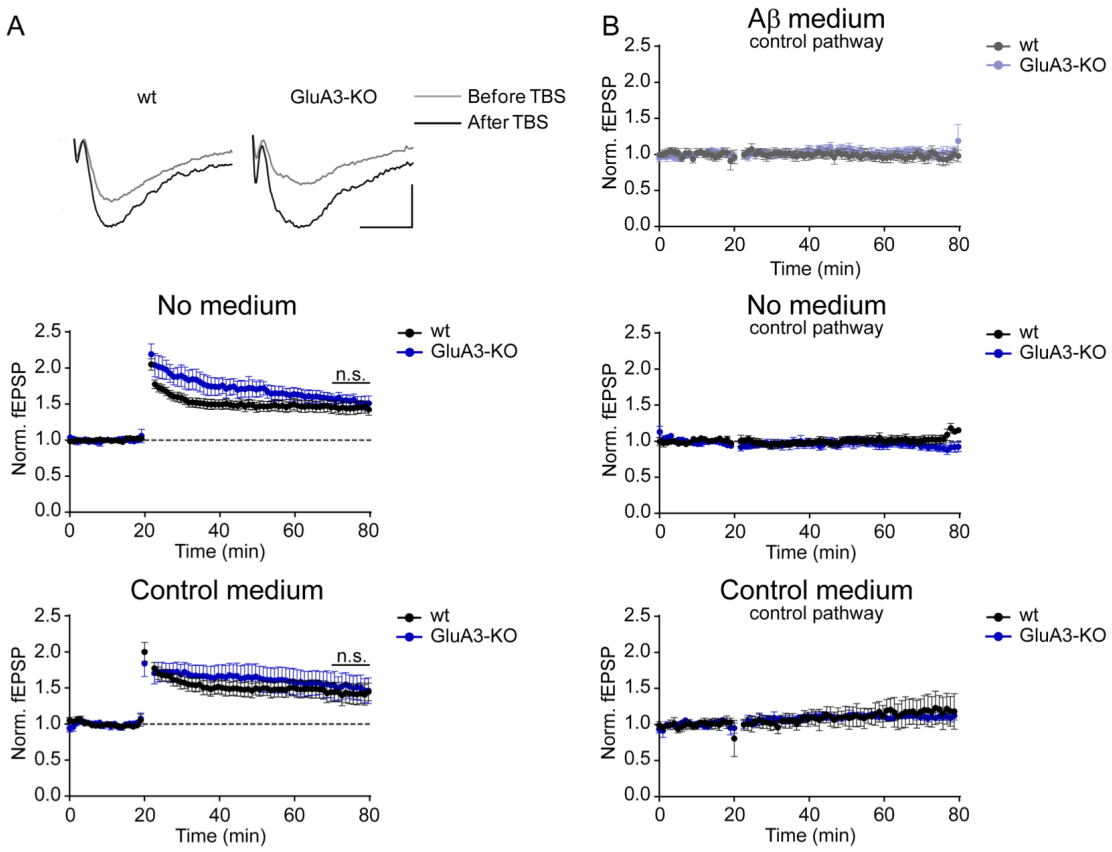

Figure 2.9: GluA3-KO slices show normal pathway-specific LTP. (A) LFP example traces (top; scale bar: 10 ms, 0.2 mV) and peak LFP responses show LTP with similar magnitude in the absence of medium (top panel; wt n=11; GluA3-KO n=6) and in the presence of control medium (bottom panel; wt n=6; GluA3-KO n=8) in wt and GluA3-KO slices. (B) Control pathways of LTP experiments in main Fig. 4 in Aβ medium (top panel: wt n=5, GluA3-KO n=8), in the absence of medium (middle panel: wt n=6, GluA3-KO n=6) and in control medium (bottom panel: wt n=3, GluA3-KO n=3) remained stable over time, demonstrating that the LTP was specific for the stimulated pathway. Data are mean ±SEM. Statistics: 2-tailed unpaired t test over the last 10 minutes of the recording.

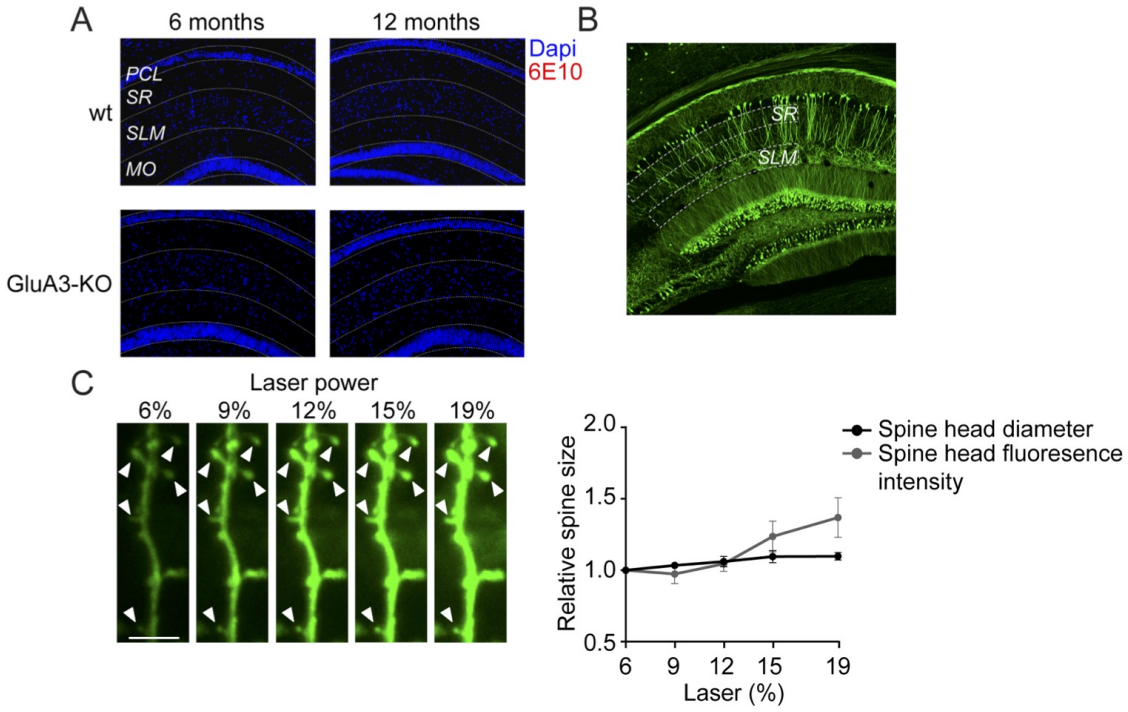

Figure 2.10: Control experiments for plaque load analysis and spine size analysis in the CA1 of aged mice. (A) 6E10 staining in 6 and 12 month old wt and GluA3-KO mice without the APP/PS1 transgenes confirmed an absence of plaque formation. (B) Confocal image of a hippocampal slice of a Thy1-eYFP mouse, depicting the regions where spine density was quantified. SR, stratum radiatum; SLM, stratum lacunosum-moleculare. (C) Comparison of two different spine size analyses showed that the average spine head diameter was less sensitive to variation in fluorescence intensity than spine volume reflected as the spine brightness (background-subtracted and corrected for fluorescence levels in dendritic shaft). Left: Confocal images of a CA1 dendrite obtained with different levels of laser intensity. Triangles indicate the spines analyzed. Scale bar: 2μm. Right: Spine head diameter en spine fluorescence (after background fluorescence subtraction) normalized to value at 6% laser intensity plotted against laser intensity (n=5 spines). Data are mean ±SEM.

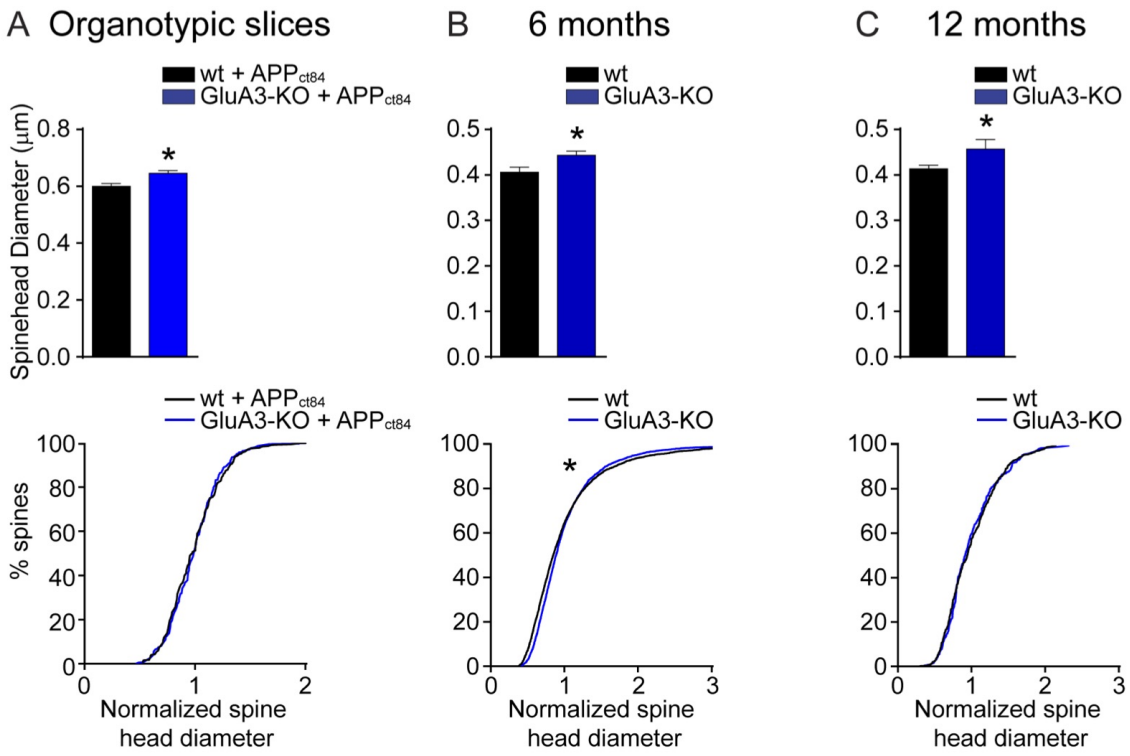

Figure 2.11: GluA3âĂŞdeficient CA1 neurons have increased spine head size in the stratum lacunosum-moleculare. (A-C) Average spine head diameter (top) and the normalized distribution of spine head sizes (bottom) of CA1 pyramidal neurons at wt (black) and GluA3-KO (blue) littermate mice. (A) SR dendrites in organotypic hippocampal slices as in Fig. 3 A, (B) SLM dendrites in 6-month old mice as in Fig. 6 G, and (C) 12-month old mice as in Fig. 5 H. Data are mean ÂśSEM. Statistics: 2-tailed unpaired t tests for spine diameter and K-S test on spine size distributions. * indicates $p < 0.05$.

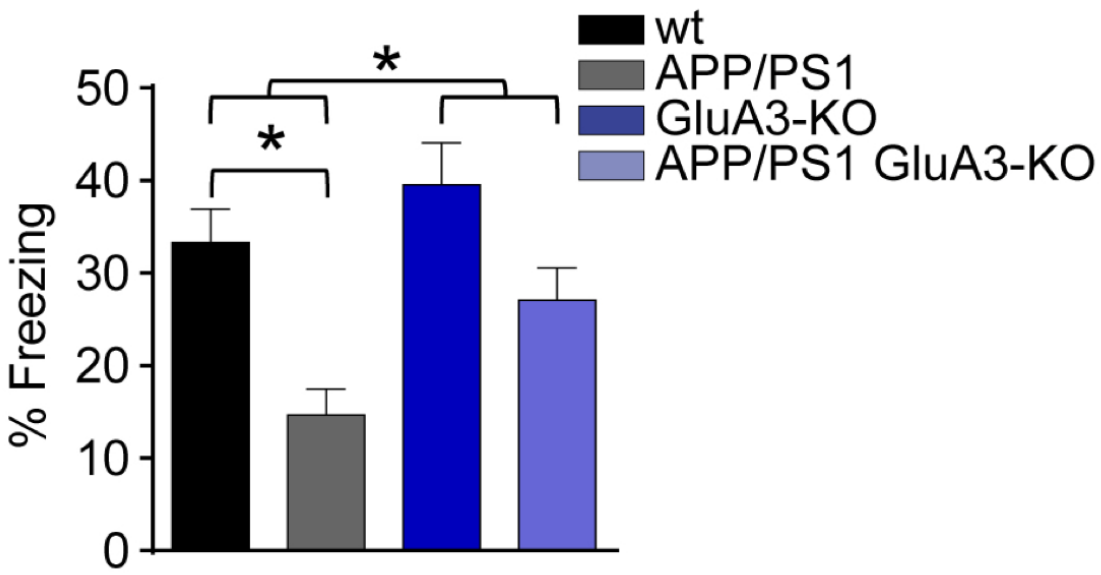

Figure 2.12: Freezing levels during fear-memory retrieval 24 hrs after conditioning in 3-month old littermates (D, wt n=11; APP/PS1 n=10; GluA3-KO n=7; APP/PS1/GluA3-KO n=11) shows a memory impairment of APP/PS1 mice that is not expressed in APP/PS1 GluA3-KO mice. Statistics: two-way ANOVA with post-hoc Sidak. * indicates $p<0.05$.

Chapter 3

Manipulating memories by modulating amyloid-β production

3.1 Abstract

The amyloid hypothesis suggests that the dysregulation of amyloid-beta (Aβ) leads to the neurodegeneration and, eventually, the loss of memories in Alzheimer's disease (AD). As a product of β- and γ-secretase cleavage of the amyloid precursor protein (APP), therapeutics have been aimed at blocking the production or accumulation of Aβ. However, many of these drugs have been studied in animal models chronically over-producing Aβ throughout their lifetimes, leaving many questions remaining. In this chapter, 1) a new method for acutely introducing Aβ *in vivo* will be introduced, 2) memory formation in the presence of the AD therapeutics known as γ-secretase modulators will be discussed, and 3) the acute effects of Aβ on memory inactivation will be described.

3.2 Introduction

Alzheimer's disease (AD) is initially characterized by mild memory loss and eventually progresses to general brain dysfunction. Pathological hallmarks of advanced AD consist of insoluble amyloid plaques, neurofibrillary tangles, and loss of neurons and synapses. The amyloid hypothesis suggests that the primary causative factor of AD is the accumulation of amyloid-β (Aβ), which exists in a 40- or 42-amino acid form when cleaved from the amyloid precursor protein (APP)(11). Aβ forms small, soluble oligomers in vitro and in vivo, and studies have shown that exogenous application of synthetic or cell-secreted Aβ oligomers blocks long-term potentiation (LTP) (Barghorn et al., 2005; Walsh et al., 2002)

Aβ has been shown to depress synapses by activating signaling pathways involved in long-term depression (LTD). For example, when CT100, the precursor to Aβ, is overexpressed in rodent hippocampal slices, it depresses synaptic transmission and leads to the endocytosis of AMPA receptors containing GluA2 (Hsieh et al., 2006; Kamenetz et al., 2003). In addition, sub-threshold LFS protocols are typically insufficient to induce LTD under normal conditions, but the presence of Aβ facilitates the induction of LTD with these protocols (Li et al., 2009), further indicating that Aβ acts through signaling pathways involved in LTD.

Because Aβ is thought to initiate the pathogenesis of AD, some therapeutics designed to slow the progression of the disease have been aimed at preventing the production of Aβ. APP is first cleaved by β-secretase, leading to the production of CT_{100}. CT100 is then cleaved by γ-secretase, leading to $A\beta_{40}$ or $A\beta_{42}$. γ-secretase inhibitors (GSIs) were initially promising because they blocked the effects of Aβ in vitro and improved deficits in APP transgenic mice (Wei et al., 2009; Comery, 2005),

but they ultimately failed in clinical trials because γ-secretase plays a critical role in Notch signaling (De Strooper, 2014). However, γ-secretase modulators (GSMs), do not inhibit γ-secretase. Rather, they modulate the function of γ-secretase such that $A\beta_{40}$ and $A\beta_{42}$ production are reduced, and the production of the nonpathogenic $A\beta_{38}$ increases (Kounnas et al., 2010). Furthermore, GSMs have been shown to improve cognitive function in APP transgenic mice, with both acute and long-term, chronic administration, unlike GSIs (Mitani et al., 2012).

A myriad of studies have demonstrated that Aβ dysregulates synaptic plasticity, and that preventing the accumulation of pathogenic Aβ species can prevent synaptic depression or rescue memory deficits in APP transgenic mice (Kounnas et al., 2010; Mitani et al., 2012). However, a few major questions remain: 1) Does Aβ production block the formation a new memory? 2) Does memory encoding "tag" synapses when LTP at those synapses is blocked by Aβ? Can this memory then be accessed if Aβ is removed during GSM treatment? 2) Does acute Aβ production lead to the inactivation of a memory?

Previous work in our lab demonstrated a direct relationship between plasticity and memory (Nabavi et al., 2014). In this experimental paradigm, an adeno-associated virus (AAV) expressing oChIEF, a variant of the light-activated ChR2, was injected into the medial geniculate nucleus (MGN) and the auditory cortex (AC) of Sprague-Dawley rats, which provide inputs into the lateral amygdala (LA). Once the viral expression of oChIEF reached axon terminals, cannulae containing optic fibers were placed in the dorsal tip of the LA; light delivery through these fibers activated terminals expressing oChIEF (optogenetically-driven input, ODI) (Figure 6B).

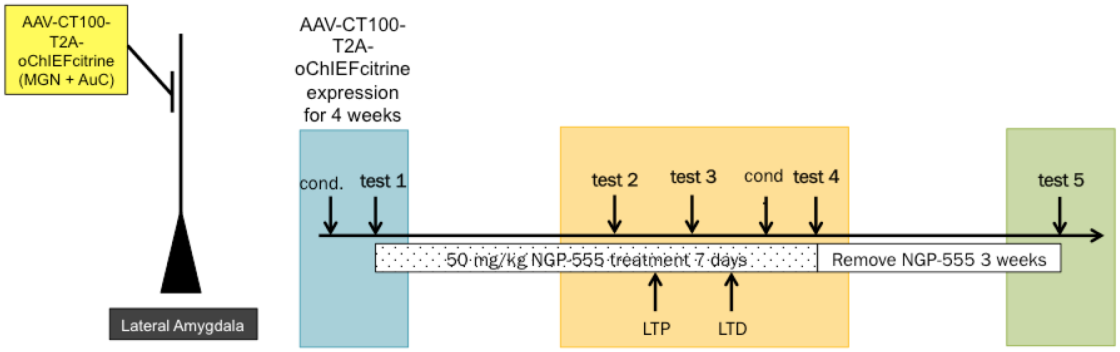

Figure 3.1: Schematic for injections and behavioral experiments for CT100-T2A-oChIEF rats.

Animals were trained to lever press for a sucrose reward in context A, and then received paired conditioning, using the ODI as the conditioned stimulus (CS), and a shock as the unconditioned stimulus (US) in another context, context B. Temporal pairing of an ODI and shock led to a conditioned response (CR) upon delivery of the CS during test sessions conducted 24 hours after training (Figure 6A and C). The CR was sensitive to extinction, thus indicating the formation of an associative memory. Application of an LTD protocol to the ODI (1 Hz for 15 min) inactivated the memory after 24 hours. These same animals were subsequently subjected to an LTP protocol through the ODI (light frequency: 100 Hz, 5 bursts). Testing the animals with a CS after 24 hours produced a CR, indicating that LTP reactivated the associative memory. Another round of LTD and LTP led to the inactivation and reactivation of the memory, with robust and long-lasting effects. These results showed that LTP and LTD could be used in vivo to manipulate memory.

Because Aβ-overproduction leads to synaptic depression resembling LTD, the next step was to investigate the effects of Aβ production on cued fear memory. To do so, I set up an experimental paradigm resembling that of Nabavi et al., 2014 (Fig. 3.1). An AAV expressing CT100 and oChIEF-tdTomato (AAV-CT100-T2A-oChIEF-

citrine) was injected into the auditory centers and cannulae were implanted dorsally to the lateral amygdala. Rats were subjected to the conditioning protocols described earlier, but in the presence or absence of the GSM NGP-555, which allowed us to manipulate the production of Aβ. If Aβ acts as LTD, then an animal that expresses CT100 in the auditory centers may not be able to form an associative memory, and would be able to form this associative memory when treated with NGP-555. Finally, when the NGP-555 is removed, we predict that Aβ would remove the memory.

3.3 Results

3.3.1 NGP-555 prevents the accumulation and synaptic depression of Aβ.

NGP-555 was kindly provided by NeuroGenetics Pharmaceuticals, and was injected intraperitoneally (i.p.) during the behavior experiments at a dosage of 50 mg/kg. With the help of Dr. Steve Wagner's lab, it was shown that this drug is effective at reducing $A\beta_{40}$ and $A\beta_{42}$ levels through I.P. injections in Sprague-Dawley rats (Fig. 3.2). Interestingly, although NGP-555 administration was sufficient to reduce plasma levels of $A\beta_{42}$, it was insufficient for decreasing brain levels of $A\beta_{42}$.

To determine the efficacy of NGP-555 in preventing Aβ-induced synaptic depression, cultured hippocampal slices infected with Sindbis-CT100 were incubated with 4 μM NGP-555 overnight. Whole-cell recordings on pairs of uninfected and infected cells were then performed to examine evoked synaptic transmission. Normally, excitatory synaptic transmission in CT100-expressing cells is reduced by approximately 40 percent (Fig. 3.2B and C). However, in the presence of NGP-555,

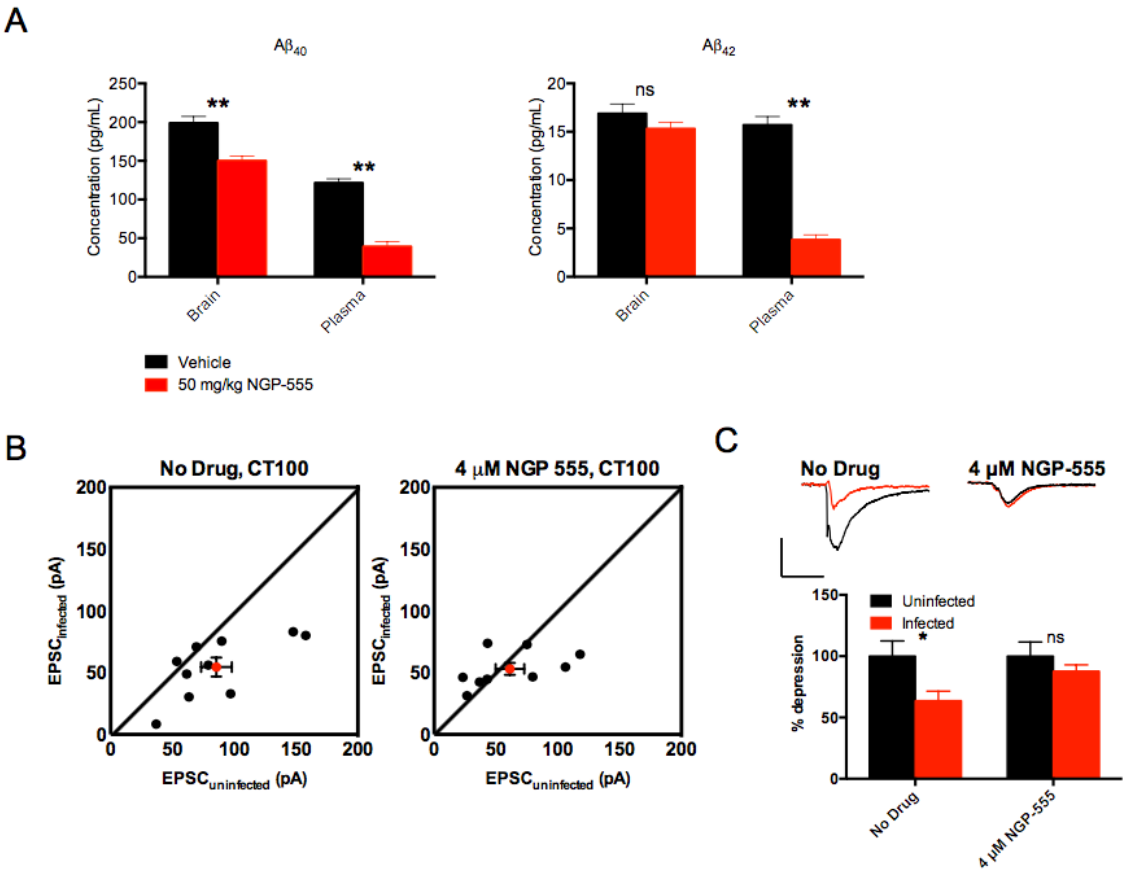

Figure 3.2: NGP-555 reduces Aβ levels *in vivo* and prevents Aβ-induced synaptic depression *in vitro*. (A) Intraperitoneal (i.p.) administration of NGP-555 at a dosage of 50 mg/kg for 7 consecutive days leads to a reduction in brain and plasma levels of $A\beta_{40}$ in Sprague-Dawley rats. NGP-555 administration was not sufficient to reduce brain levels of $A\beta_{42}$, but was sufficient to reduce plasma levels of $A\beta_{42}$. $A\beta_{38}$ levels were too low to detect in Sprague-Dawley rats. (Vehicle: n = 8, NGP-555: n = 8, ** indicates $p < 0.005$). (B) CT100 persistently leads to depression in $EPSC_{infected}$ compared with $EPSC_{uninfected}$ when treated with vehicle overnight. Treatment of slices with 4 μM NGP-555 prevents CT100-induced synaptic depression. (C) Top: Representative traces of paired whole-cell recordings. Bottom: Quantification of depression in vehicle- and NGP-555-treated slices. (No drug: n = 10, NGP-555: n = 9, * indicates $p < 0.05$)

excitatory transmission in CT100-expressing cells is reduced by approximately 10 percent (Fig. 3.2B and C). These results indicate that this GSM can prevent the depressive effects of Aβ.

3.3.2 Co-expression of Aβ and oChIEF using Sindbis and AAV

Several constructs were generated for these experiments. To ensure that infected cells expressing Aβ were also expressing oChIEF, an insert that linked CT100 with oChIEFcitrine with a T2A peptide sequence was generated. This sequence was subcloned into an AAV containing a human synapsin promoter (AAV-hSyn-CT100-T2A-oChIEFcitrine) and a Sindbis expression vector (pSR5-CT100-T2A-oChIEFcitrine) (Fig. 3.3B and C). Viruses were produced based on previously established protocols and titers were confirmed with the help of the Salk Gene Targeting, Transfer, and Therapeutics core.

To verify the efficacy of the “ribosomal skip” introduced by using the T2A peptide, organotypic slices were infected with Sindbis virus expressing CT100-T2A-oChIEFcitrine (Fig. 3.3B and C). Whole-cell recordings on pairs of uninfected and infected cells were then performed to examine evoked synaptic transmission. Transmission in cells expressing CT100-T2A-oChIEFcitrine was reduced by approximately 50 percent (Fig. 3.3C). To determine the functionality of oChIEFcitrine, pairs of uninfected and infected cells were exposed to an optical stimulus and the photostimulated current (PC) was recorded (Fig. 3.3D). Cells expressing oChIEFcitrine showed large responses to oChIEF activation, while uninfected cells showed no response. These results indicated that the ribosomal skip mechanism leads to the expression of functional Aβ and oChIEF.

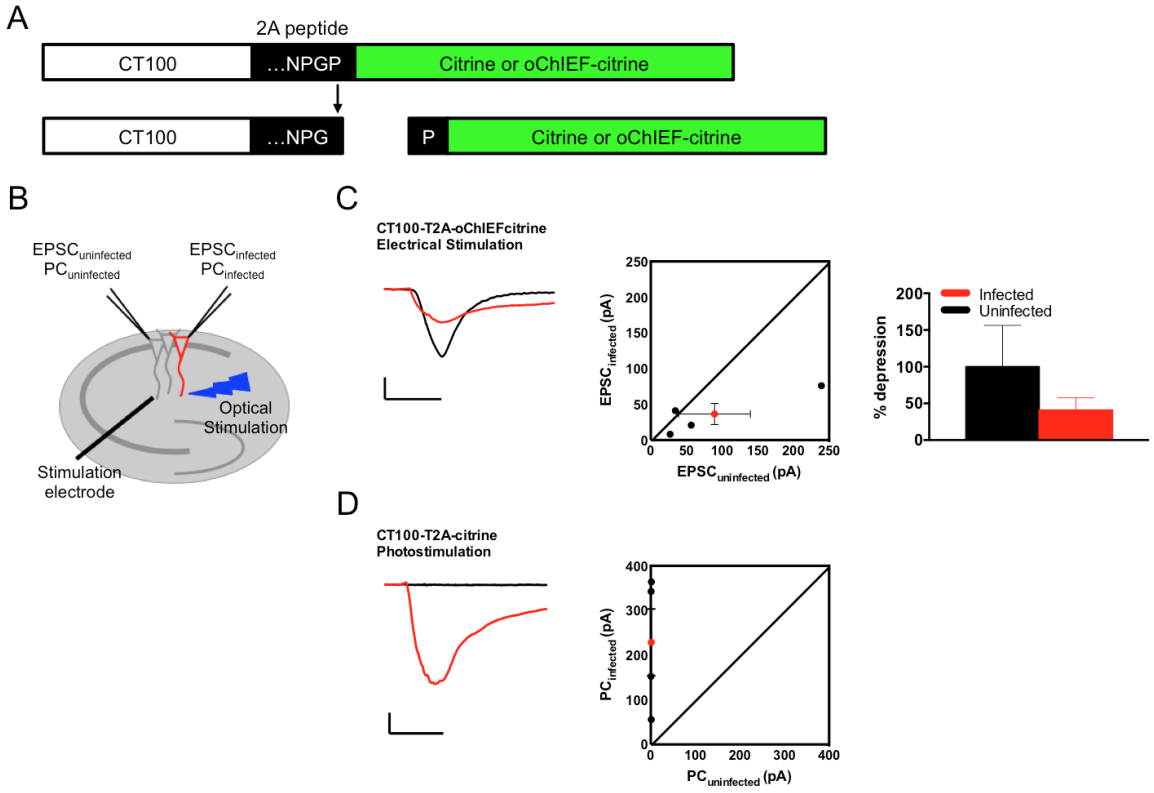

Figure 3.3: Validation of CT100-T2A-oChIEFcitrine expression and function. (A) Schematic of AAV and Sindbis design for CT100-T2A-oChIEFcitrine. (B) Schematic of recordings performed with one pathway for electrical stimulation and a second pathway for optical stimulation using 473 nm light. (EPSC: excitatory postsynaptic current; PC: photostimulated current.) (C) From left to right: representative trace of recordings in uninfected (black) and infected (red) cells; CT100-T2A-oChIEFcitrine causes synaptic depression, indicating that CT100-T2A-oChIEFcitrine still produces AÎš. (D) 473 nm light pulses for 2.5 ms generates a current in cells expressing CT100-T2A-oChIEFcitrine, indicating normal function of oChIEFcitrine.

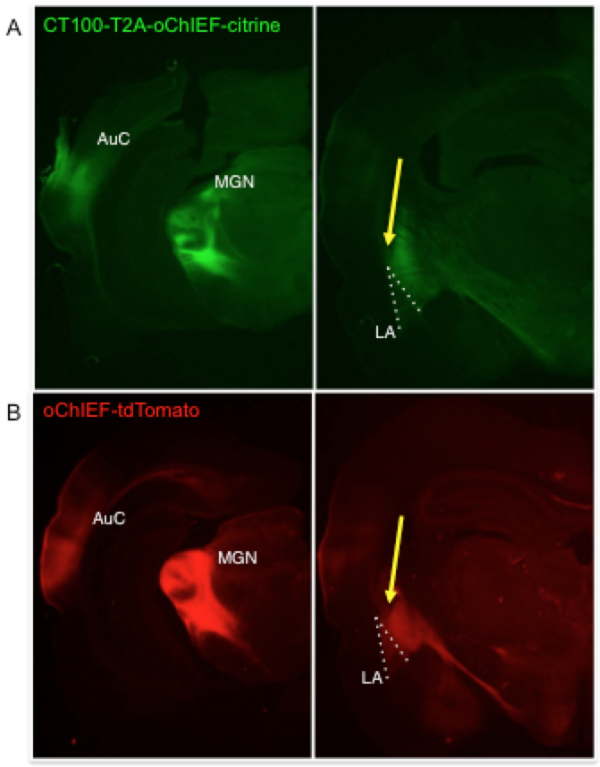

Figure 3.4: Histology on representative rats injected with AAV-CT100-T2A-oChIEFcitrine (A) and AAV-oChIEF-tdTomato (B). Yellow arrow represents cannula implantation.

3.3.3 Expression of Aβ *in vivo* leads to weak associative memories

Male Sprague-Dawley rats (age 6-8 weeks) were injected with AAV-hSyn-CT100-T2A-oChIEFcitrine in the auditory cortex (AuC) and the medial geniculate nucleus (MGN) (Fig. 3.4A). The rats recovered for 4-6 weeks, allowing time for the virus to express, and then cannula were implanted above the lateral amygdala one week prior to lever press training and conditioning. Once animals were trained to lever press for a 10% sucrose reward (Context A), they were subjected to a screening test (Test 0, Fig. 3.5A), in which the CS was presented to identify animals that had seizures or other responses to the CS in the absence of conditioning. Animals

whose lever press frequency decreased by 30% or more were removed from the experimental group.

Following Test 0, animals were subjected to a mild paired conditioning protocol where animals were subjected a new context (Context B), in which foot shocks (US) were delivered while paired with an ODI (CS) of 10 Hz, lasting 500 ms. After 24 hours, the animals underwent Test 1 in context A with the CS, and showed a mild CR of approximately 50% reduction in lever press frequency upon delivery of the CS (Fig. 3.5C)

The presence of a mild CR in Test 1 showed that the expression of CT100 in the auditory cortex and medial geniculate nucleus is not sufficient to entirely block the formation of new memories. However, when the rats underwent test 2 after several days of GSM treatment, the rats no longer showed a CR to the CS (Fig. 3.5D). This suggests that the initial memory that had formed in the presence of Aβ was weak, and was eventually removed after several days. Interestingly, upon GSM treatment, the application of an optical LTP protocol led to a stronger CR in Test 3 (Fig. 3.5E). These results imply that synapses in the associative memory were initially “tagged” during the mild conditioning protocol (Rogerson et al., 2014), but not fully potentiated because of Aβ overproduction. This synaptic tagging led to the formation of a weak fear memory that disappeared after several days.

Figure 3.5: Behavioral testing of animals expressing CT100-T2A-oChIEFcitrine. (A) Behavioral paradigm for tasks and GSM treatment of CT100-expressing rats. (B) Test 0, conducted before conditioning, showed that the CS has no effect before paired conditioning. (C) Test 1, conducted after the animal receives temporal pairing of light, the CS, and shock, the US. (D) Test 2, conducted several days after conditioning, shows the loss of the associative memory. (E) Test 3 shows that the application of the LTP protocol reactivates the memory during GSM treatment. (F) After LTD and a second conditioning protocol, test 4 demonstrates the formation of a robust memory at the end of the GSM treatment schedule. (G) Animals were tested after 3 weeks of Aβ production, showed a weakening of the associative memory. (H) Lever presses during the first minute of light were normalized to the baseline and compared to Test 0. Tests 1, 3, and 4 showed significant decreases in lever press frequency compared to Test 0. * indicates $p < 0.05$.

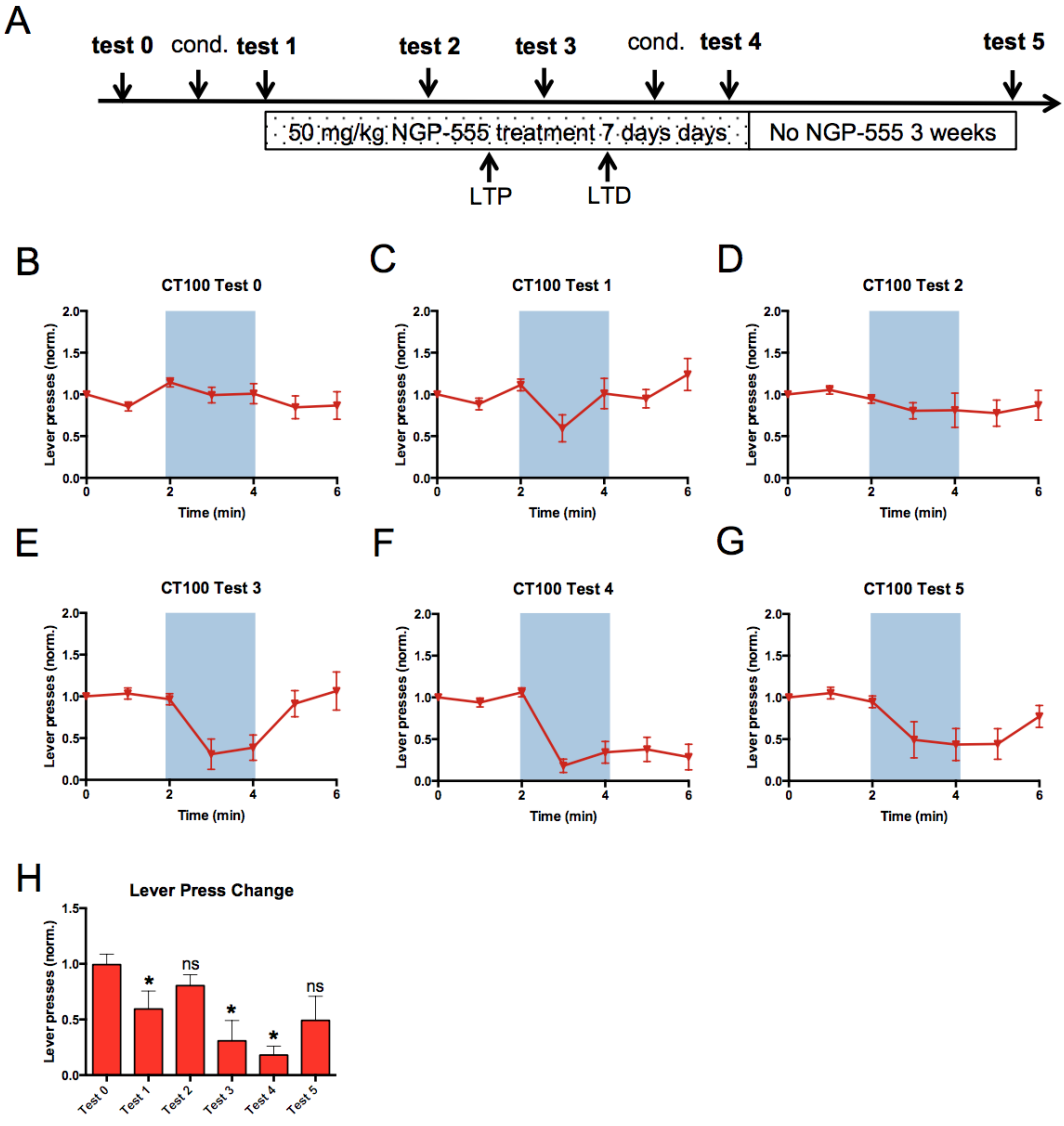
A
test 0
cond.
test 1
test 2
test 3
cond.
test 4
test 5
50 mg/kg NGP-555 treatment 7 days days
No NGP-555 3 weeks
LTP
LTD
B
CT100 Test 0
C
CT100 Test 1
D
CT100 Test 2
E
CT100 Test 3
F
CT100 Test 4
G
CT100 Test 5
Lever presses (norm.)
Time (min)
H
Lever Press Change
Lever presses (norm.)
ns
*
Test 0
Test 1
Test 2
Test 3
Test 4
Test 5

Following Test 3, the animals were subjected to an LTD protocol to inactivate the memory, and underwent a second mild fear conditioning session to ensure the formation of a strong fear memory in test 4 (Fig. 3.5F). NGP-555 was then removed for 3 weeks, and Aβ was allowed to accumulate at this synapse during that time. The animals then underwent Test 5, and still showed a CR (Fig. 3.5G). The associative memory was further quantified by normalizing the number of lever presses that occur during the first minute of light (2-3 min) is the baseline lever presses (0-2 min) (Fig. 3.5H). Lever press change in Tests 1 through 5 were compared to Test 0, and only Tests 1, 3, and 4 showed a statistically significant decrease in lever press frequency in CT100-expressing rats. While Test 5 showed that there was still a CR after 3 weeks of Aβ overexpression, the CR also appears to be weaker than it was in previous tests.

Based on the literature, we expected that CT100-overexpression *in vivo* would produce sufficient levels of Aβ to reproduce the memory deficits modeled in APP transgenic mice (Ashe and Zahs, 2010). So why did Aβ fail to inactivate the associative fear memory? One possibility is that 3 weeks of Aβ production did not lead to sufficient Aβ accumulation to act as LTD. This would be unsurprising because APP transgenic mouse strains demonstrate learning deficits when they are aged at least 10 months, while young mice show little or no cognitive deficits (Hsiao et al., 1996; Morgan, 2003). An alternative and more attractive possibility is that memories formed in the absence of Aβ are more robust and resistant to the deleterious effects of Aβ accumulation over a short time period.

3.3.4 Rats lacking Aβ form a strong associative memory

To determine whether the behavioral phenotypes witnessed in rats injected with CT100-T2A-oChIEF-citrine were actually the result of CT100 expression, a group of rats were injected with oChIEF-tdTomato in the MGN and AuC (Figure 10B). They were subjected to the same lever press training as the CT100-T2A-oChIEF-citrine rats, and were then screened prior to conditioning in Test 0 (Fig. 3.6B) such that only rats that did not have a decrease in lever press frequency in response to the CS were kept for behavioral experiments.

Following Test 0, the oChIEF-tdTomato rats were then subjected to the same mild conditioning protocol comprising 6 pairs of CS (ODI) and US (0.5 mA shock). As shown in ChR2 test 1, the rats formed a CR in response to the CS, indicating the presence of an associative memory (Fig. 3.6C). After several days, these rats were then subjected to a test approximately 1 week after they received conditioning, and they still exhibited a CR (Fig. 3.6D). It is important to note that test 3 occurred at the same number of days post-conditioning as test 3 for the CT100-T2A-oChIEF-citrine rats. The presence of a CR after a week indicates that the mild conditioning protocol allows the formation of a robust memory.

These control experiments demonstrated that the loss of memory in CT100-T2A-oChIEF-citrine rats by Test 2 (Fig. 3.5D) is likely because of the expression of CT100 in synapses involved in the associative memory. With these data, we can also rule out the possibility that a mild conditioning protocol undergoes extinction more rapidly than previously established protocols (Nabavi et al., 2014).

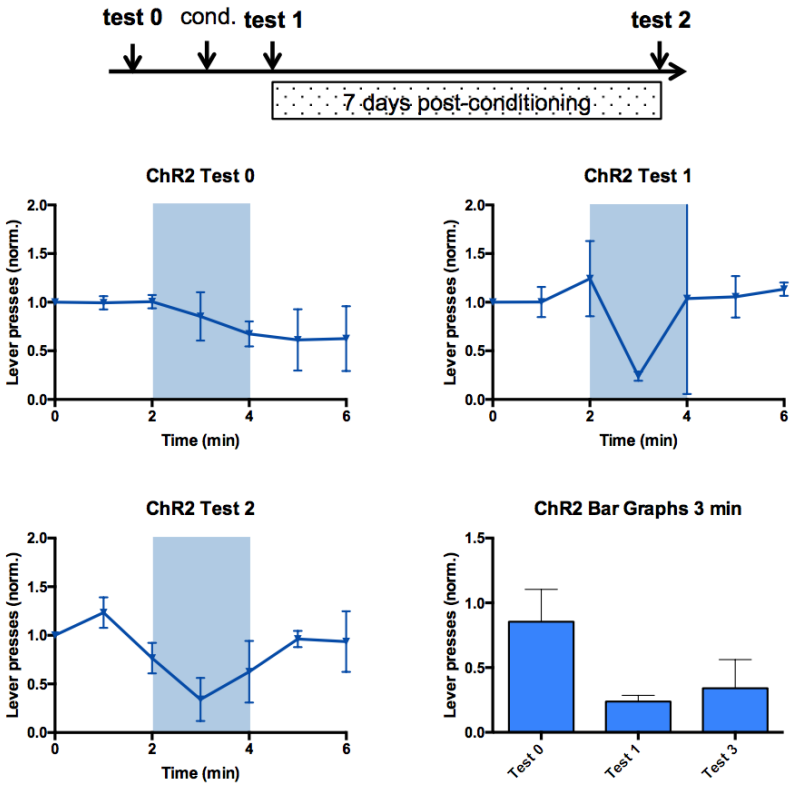

Figure 3.6: Behavioral testing of animals expressing oChIEF-tdTomato. (A) Schematic of experimental regimen for oChIEF-tdTomato injected rats. (B) Test 0 was used to screen for rats that had a response to light prior to conditioning. Rats with a reduction in lever press greater than 30% were excluded from experiments. (C) Test 1 was showed that oChIEF-tdTomato rats had a decrease in lever press frequency of approximately 80% after the mild conditioning protocol. (D) Test 2 showed that oChIEF-tdTomato rats had a decrease in lever press frequency of approximately 60% one week after conditioning. (n = 3 for all experiments.)

3.3.5 Discussion

Conclusions

In this chapter, I demonstrated that the GSM NGP-555 can reduce $A\beta_{40}$ and $A\beta_{42}$ levels *in vivo* through i.p. injections, demonstrating a new method for administering this drug. However, an increase in the non-pathogenic $A\beta_{38}$ was not observed, unlike previous studies (Kounnas et al., 2010). I also showed that NGP-555 blocks Aβ-induced synaptic depression electrophysiologically, indicating that this particular drug may be able to reverse the synaptic effects of Aβ overproduction. Furthermore, I generated a new method for simultaneously expressing Aβ and oChIEF within one virus to overcome the packaging limit of AAVs by using a T2A peptide.

Using this AAV, I found that CT100 overexpression in the auditory centers during conditioning was sufficient to cause a learning deficit in rats. After 7 days, these rats demonstrated a deficit in memory retrieval when subjected to the CS. However, during the GSM administration, an LTP protocol was sufficient to activate the associative memory. After undergoing LTD and then a second round of mild conditioning, these rats possessed a robust associative memory that persisted after 3 weeks of Aβ overproduction. These results suggest that 3 weeks of Aβ production resulting from AAV expression of CT100 is insufficient to inactivate an associative fear memory.

Although these results were inconsistent with our hypothesis that Aβ accumulation *in vivo* should behave as LTD, they are not entirely unexpected. Typically, rodent models of AD involve APP transgenic mice that over-express a familial AD mutation to overproduce Aβ during the course of their lifetime, and assays are conducted

in older animals (Hsiao et al., 1996; Morgan, 2003). AAV-mediated expression of Aβ appears to be more consistent with a recent study examining a transgenic APP strain, called the PDAPP strain, at younger ages (3-4 months). Young PDAPP mice have no learning deficits, but show deficits in memory retrieval several days after receiving training (Beglopoulos et al., 2016). The CT100-T2A-oChIEF rats show a similar phenotype in tests 1-3 (Fig. 3.5C-E), demonstrating that memory encoding but not memory retrieval is intact in the presence of Aβ. However, the persistence of a memory formed in the absence of Aβ, even after 3 weeks of Aβ overproduction, shown in test 5 (Fig. 3.5G), demonstrates that short periods of Aβ overproduction are not sufficient to act as LTD.

Further Work

Although the results described in this chapter are novel, some are preliminary and require repeated or control experiments. In this section, I will describe some of the necessary experiments.

In Figure 3.5, administration of GSM enables LTP to reactivate the memory after it has been lost in test 3. This is an interesting result because it suggests that during Aβ overproduction, synapses can be “tagged" even if a memory is not fully expressed. What remains to be seen, however, is whether this effect of LTP is dependent on GSM administration. Thus, another set of behavior experiments employing the same paradigm as described in Figure 3.5A is required. In these controls, NGP-555 administration should be replaced with vehicle administration. This would allow us to determine whether NGP-555 is required for the effect of LTP in test 3. We would also be able to observe whether NGP-555 is actually responsible

for the removal of memory in test 2, since GSM administration begins after the associative memory has formed, and the memory is lost during treatment. Although previous studies have shown the efficacy of other GSMs on improving spatial working memory in transgenic APP mice–specifically, the Tg2576 line–ours would be the first study to characterize the efficacy of NGP-555 on associative memory (Mitani et al., 2012), so careful control studies are necessary.

Finally, the experiments described in Figure 3.6 need to be repeated because of the small sample size (n = 3). In these experiments, no drug or vehicle was administered between tests 1 and 2, so it would also be interesting to examine the effect NGP-555 between tests 1 and 2 in rats expressing oChIEF-tdTomato. I expect that NGP-555 would have no impact on the memories formed in rats expressing oChIEF-tdTomato or CT100-T2A-oChIEFcitrine, but given the history of γ-secretase inhibitors (GSIs), it is necessary to determine that there is no negative impact of GSMs on associative memories.

3.3.6 Acknowledgments

I would like to acknowledge Dr. Maria Kounnas and Dr. Steven Wagner for graciously providing the GSM NGP-555 (Neurogenetics Pharmaceuticals). Phuong Nguyen, from Dr. Wagner's laboratory, contributed to Figure 3.2A and Stephanie Alfonso, from Dr. Roberto Malinow's laboratory, contributed to Figure 3.3B.

3.3.7 Experimental Procedures

Subject

Male Sprague-Dawley rats were used for all experiments. AAV was injected at age 6-8 weeks, and cannula were implanted at 10-12 weeks prior to behavioral experiments. Rats were housed two per cage and kept on a 12/12 h light-dark cycle (lights on/off at 7:00/19:00). Behavior experiments were performed during daylight. All procedures were approved by the Institutional Animal Care and Use Committees at the University of California, San Diego.

Viruses

AAV co-expressing wild-type CT100 and the citrine-tagged channelrhodopsin variant oChIEF-citrine was driven by the neuron-specific synapsin promoter. AAV expressing tdTomato-tagged oChIEF was driven by the neuron-specific synapsin promoter. Sindbis co-expressing wild-type CT100 and the oChIEF-citrine were made as described previously described (Malinow et al., 2010).

Training

Rats were trained to associate lever press for a reward (40 ml of 10% sucrose per lever press). During the training period rats were kept on a restricted water schedule (2 h daily of water ad libitum). Training context was a modular operant test chamber ($12.5 \times 3 \times 10 \times 3 \times 13$ inches) with a stainless grid floor and open roof located in a sound attenuating cubicle (Med Associates, St. Albans, VT). The test chamber was equipped with a retractable response lever, a liquid dispenser receptacle and a

light above the dispenser that signalled when liquid was injected into the dispenser. The consumption of liquid was detected by a head entry detector in the receptacle; each successive liquid reward was subsequently followed with a 15 s delay after head removal from the receptacle. The system was controlled and the data collected through a MED-SYST-16 interface, which was controlled by MED-PCR IV soft- ware running on a PC. Rats were initially trained to associate the reward with the light above the dispenser receptacle. In a 45 min session, rats with at least 60 head entries into the receptacle were selected for lever press training.

Lever-press training was conducted in the same context as above, but this time rats had to press a lever to receive the liquid. The level press turned the light above the receptacle on, which in the previous training session they had associated with liquid in the receptacle. Rats with a minimum of 6 responses per min in the first 10 min of the training session were selected for conditioning.

Optical conditioning

Rats were placed into the conditioning chamber and were attached to an optic fibre patch cord connected to a 473 nm solid-state laser diode (OEM Laser Systems) with 15âĂŞ20 mW of output from the 200 mm fibre. They were allowed to explore the chamber for 3 min before the conditioning. Optical conditioning was 6 trains of blue light (10 pulses of 10 Hz, 2 ms duration) applied at randomized intervals with an average of 3 min apart. For paired conditioning, the light stimulus co-terminated with 0.5 s of 0.5 mA footshock. Paired groups received a total of 6 pairs of light and shock. The delivery of shock and light was controlled by a pulse generator (Master-8; AMPI, Jerusalem, Israel). After the conditioning rats remained

in the box for additional three minutes before returning to their home cage.

Testing

After the conditioning, rats were water restricted for 24 h before they were tested for lever press. Testing was done in the same context as training except that the floor was a plastic sheet with white and red strips. Testing was a 7 min session in which rats had to press a lever to receive the liquid (10% sucrose). Rats were attached to the optic fiber patch cord, placed into the chamber, and allowed to explore the environment for 5 min before having access to the lever. The testing session, in which rats had free access to the lever, was a 3 min period of no light, followed by two minutes of light on (10 Hz of pulses with 2 ms duration), and 2 min of no light. At the end of the session rats were returned to their home cage. Only rats that in two consecutive days showed consistent reduction (20%) in the lever press during the light-on period were used for further behavioural phases. Those which failed the test were examined histologically to locate the position of cannula and viral injection.

LTD induction

Within one hour following testing, rats were placed in a separate context, a translucent plastic container (22.5$\times$3$\times$15$\times$3$\times$12 inches), attached to the optic fibre patch cord and allowed to explore the environment for 3 min before LTD induction. Optical LTD was induced with 900 pulses of light, each 2 ms, at 1 Hz. After the induction rats remained in the chamber for 3 additional minutes before returning to their home cage.

LTP induction

Within one hour following testing, rats were placed in a separate context, a cardboard box (20.5×3×15.5×3×14.5 inches), attached to the optic fibre patch cord and allowed to explore the environment for 3 min before LTP induction. Optical LTP was induced with 5 trains of light (each train 100 pulses, 100 Hz) at 3 min inter-train intervals. After the induction, rats remained in the chamber for 3 additional minutes before returning to their home cage. During all behavioural assays the light intensity remained the same for each animal. At the end of the experiment, animals were perfused and the location of the optic fibre was verified.

NGP-555 treatment

In vitro. NGP-555 (MW: 406 g/mol) was dissolved in DMSO to 25 mM and was serially diluted in hippocampal slice culture media to 4 μM. Slices were incubated with NGP-555 prior to Sindbis-CT100 infection overnight. After 18 h, slices were subjected to paired whole-cell recordings while 4 μM GSM was circulating in the perfusion. *In vivo*. NGP-555 was dissolved in 80% PEG-400, 20% H_2O, and 0.1% Tween-20. The drug mixture was sonicated in a bath sonicator for 60 minutes at 55°C and was kept warm prior to intraperitoneal administration. Animals were treated daily at the same time for 7 days, and were subjected to behavioral experiments during that time.

Chapter 4

SYNPLA: a new method for detecting recently potentiated synapses

4.1 Abstract

Changes in synaptic strength are widely accepted as the basis of memory and learning, but currently existing strategies for assessing learning-induced plasticity are unable to provide high-resolution information on newly potentiated synapses in a high-throughput manner. Here, we demonstrate a new technique for detecting synapses called the SYNaptic Proximity Ligation Assay (SYNPLA). SYNPLA applies the antibody-based methodology of PLA to the diversity of transsynaptic proteins to label synapses. Given the vast array of proteins at the postsynaptic density (PSD), and the changes that occur after plasticity, SYNPLA can be used to detect the proximity of various pairs of presynaptic and postsynaptic proteins. We show that

SYNPLA can be used to constitutively label all synapses or only recently potentiated synapses.

4.2 Introduction

Changes in synaptic strength are widely accepted as the basis of learning and memory (Kandel, 2001). Long-term potentiation (LTP) is a form of use-dependent synaptic plasticity and has been well characterized in *in vitro* and *in vivo* mammalian systems. Because long-term potentiation is an electrophysiological correlate of learning, researchers have studied this phenomenon intensively and have long sought various methods to identify synapses that have undergone LTP.

Currently, there are two main strategies used to assess learning-induced plasticity. The first method relies on physiology and imaging techniques both *in vivo* and *in vitro*. Under optimal conditions, imaging with two-photon excitation microscopy can provide data on changes in spine growth and density during plasticity, thereby allowing the characterization of changes in synaptic strength at a single synapse level. Although these techniques gather high-resolution data, they are limited by several factors. For one, the equipment is costly and the experiments require a great deal of technical expertise. Second, these techniques are labor-intensive and are thus low-throughput.

The second strategy for assessing learning-induced plasticity depends on the expression of immediate early genes (IEGs) such as *c-fos* or *arc*. Identifying brain regions expressing *c-fos* or *arc* is a relatively high-throughput technique for identifying areas that have undergone potentiation during a learning task. However,

relying on IEGs is limiting because IEG expression is largely limited to the cell soma, thus providing poor resolution of the synapses involved in plasticity. The correlation between IEGs and changes in synaptic strength is also poorly understood, thus complicating the interpretation of IEG screens (Madison et al., 1991).

An ideal technique for identifying changes in synaptic strength would combine a high throughput process that yields high-resolution information. In this chapter, I will describe a new technique, called the SYNaptic Proximity Ligation Assay, which combines the methodology of the proximity ligation assay (PLA) and AMPA receptor trafficking at excitatory synapses during LTP.

AMPA receptors comprise four different subunits: GluA1, GluA2, GluA3, and GluA4. In the adult rodent brain, AMPA receptors at glutamatergic synapses conduct basal synaptic transmission in primarily two heteromeric forms: GluA1/GluA2 and GluA2/GluA3 hetero-oligomers (Wenthold et al., 1996). Work in our lab has demonsrated that GluA2/GluA3 hetero-oligomers are continuously cycling between nonsynaptic and synaptic pools, while GluA1/GluA2 insertion into the synapse is activity-dependent (Shi et al., 2001; Hayashi, 2000). The insertion of GluA1 into the synapse is a major, if not the dominant, factor in the molecular changes underlying LTP (Huganir and Nicoll, 2013).

SYNPLA exploits the insertion of GluA1 to identify synapses that have undergone potentiation. PLA is an antibody-based method that can be used to detect protein complexes. Two primary antibodies are used to detect antigens that are in proximity (<40 nm), and each secondary antibody is conjugated to a complementary strand of DNA (Söderberg et al., 2006, 2008). If the antibodies are sufficiently close, then the complementary DNA strands will be ligated and amplified to create a “rolony”

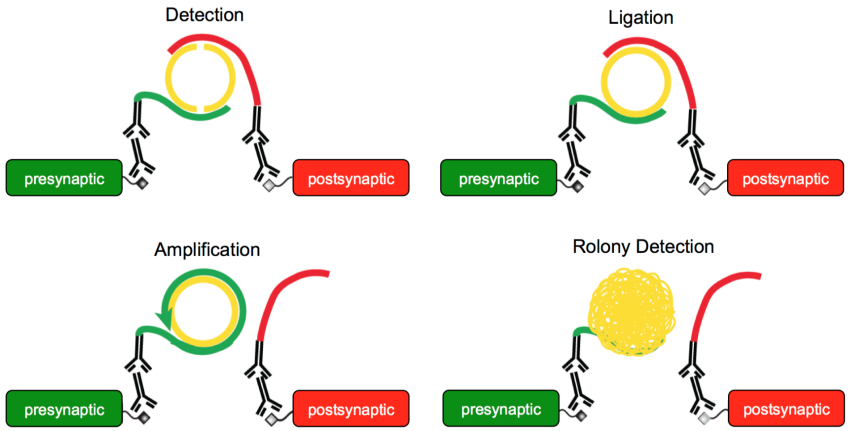

Figure 4.1: SYNPLA requires two trans-synaptic proteins to be in close proximity. Figure adapted from Justus Kebschull, CSHL.

(Fig. 4.1). Rolonies will then be detected with a fluorescent probe as dots. PLA has been used reliably to detect protein complexes in cultured cells and in the mouse striatum (Söderberg et al., 2006; Trifilieff et al., 2011).

Although there exist imaging techniques to identify protein interactions, they are limited. For example, although fluorescence resonance energy transfer (FRET) imaging enables the observation of protein interactions, the technique is low-throughput. Another technique often used to identify protein interactions is co-labeling using double immunofluorescence, which can lead to significant false-positives and provides low resolution. With PLA, the likelihood of false positives is greatly reduced because the proteins of interest must be less than 40 nm apart to form a rolony that can be detected by light microscopy. Although PLA has not previously been used to look at interactions between a pre- and postsynaptic protein, the size of the synaptic cleft (approximately 20 nm) makes this technique a potentially powerful tool for studying synapses.

In this chapter, I will show that while PLA is often applied to interacting

proteins, SYNPLA can be used to label synapses by detecting the proximity between non-interacting trans-synaptic proteins. Furthermore, SYNPLA can be used in a variety of systems, such as organotypic slice cultures and on *ex vivo* tissue collected from animals. SYNPLA appears to be a powerful technique that will enable high resolution detection of synapses that have undergone potentiation after learning tasks, such as cued fear conditioning.

4.3 Results

4.3.1 PLA labels trans-synaptic NRXN-NLGN interaction in primary cultured neurons

SYNPLA was first tested on primary cultured neurons to ensure that the interaction between neurexin-1B (NRXN) and neuroligin (NLGN) can be detected. Primary cultured neurons were electroporated to express mCherry-P2A-NRXN-MYC presynaptically or GFP-P2A-HA-NLGN postsynaptically. Neurons were then subjected to PLA using primary antibodies for MYC and HA to detect the interaction of NRXN and NLGN. As described in Fig. 4.1, PLA signal is detected as a “rolony,” which appears in our images as individual white dots, shown in Fig. 4.2B (right column). These results demonstrate that PLA is capable of detecting the interaction between trans-synaptic proteins and suggest that PLA for recombinant NRXN-MYC and HA-NLGN should constitutively label synapses.

Figure 4.2: PLA labels trans-synaptic NRXN-NLGN interaction in primary cultured neurons (A) Schematic for primary culture expression of recombinant NRXN and NLGN. Presynaptic neurons are electroporated to express GFP-P2A-MYC-NRXN and postsynaptic neurons are electroporated to expression mCherry-P2A-HA-NLGN. PLA will be conducted using primary antibodies for MYC and HA. (B) Expression of mCherry-P2A-HA-NLGN (left column), GFP-P2A-MYC-NRXN (middle column), and PLA rolonies (right column. PLA was conducted on neuronal cultures of various developmental stages from 2 days in vitro (DIV2) onward. PLA for recombinant NRXN and NLGN increases with culture maturation, indicating a correlation between synapse number and PLA rolonies. (C) Quantification of (B), right column. From J. Kebschull, CSHL.

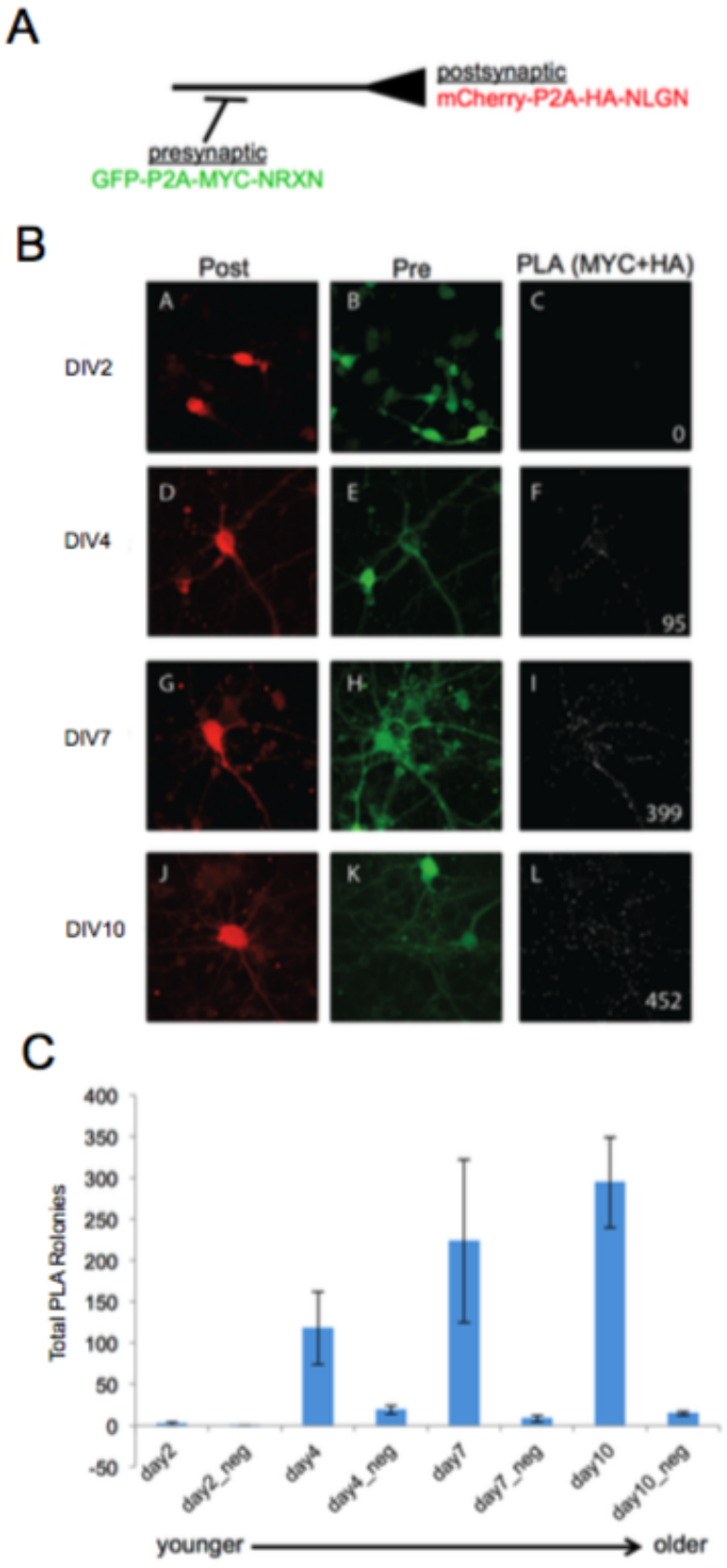
A
postsynaptic
mCherry-P2A-HA-NLGN
presynaptic
GFP-P2A-MYC-NRXN
B
Post
Pre
PLA (MYC+HA)
DIV2
DIV4
DIV7
DIV10
A
B
C
D
E
F
G
H
I
J
K
L
0
95
399
452
C
Total PLA Rolonies
400
350
300
250
200
150
100
50
0
-50
day2
day2_neg
day4
day4_neg
day7
day7_neg
day10
day10_neg
younger
older

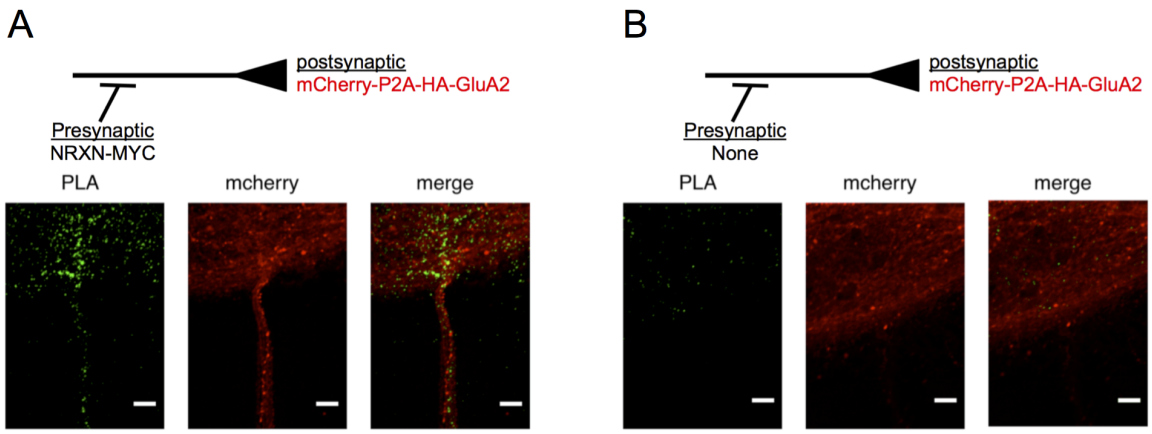

Figure 4.3: PLA labels trans-synaptic NRXN-GluA2 proximity in primary cultured neurons. (A) PLA rolonies (green) label NRXN-GluA2 proximity when both tags are present. (B) Few PLA rolonies when one tag is absent. From J. Kebschull.

Previous studies have shown that with progressive days in vitro (DIV), cultured neurons develop an increasing number of functional synapses (Basarsky et al., 1994). Thus, if PLA constitutively labels synapses primary neuronal cultures, then the total number of PLA dots, or "rolonies," should increase during the development of neuronal cultures. As expected, the total number of PLA rolonies increases with DIV (Fig. 4.2C), in a manner consistent with electrophysiological studies (Basarsky et al., 1994).

4.3.2 PLA labels trans-synaptic NRXN-GluA2 proximity in primary cultured neurons

After determining that PLA could constitutively label synapses in primary cultured neurons, we wanted to validate that PLA could label non-interacting trans-synaptic proteins, such as NRXN and GluA2. PLA for the pair of proteins should also label synapses, given GluA2 is constitutively trafficked to the synapse (Shi

et al., 2001).

To determine if PLA could label recombinant NRXN-MYC and HA-GluA2 proximity, primary cultured neurons were electroporated to express NRXN-MYC presynaptically and mCherry-P2A-HA-GluA2 postsynaptically (Fig. 4.3A). Using primary antibodies for HA and MYC, PLA rolonies could be detected in conditions where both the presynaptic and postsynaptic proteins are present. To ensure the specificity of the PLA signal, negative control experiments were performed in which the presynaptic NRXN-MYC was absent (Fig. 4.3B), while both the HA and MYC primary antibodies were used. The presence of PLA rolonies was greatly reduced, demonstrating the specificity of the NRXN-MYC and HA-GluA2 labeling in primary cultured neurons.

4.3.3 PLA labels trans-synaptic NRXN-GluA2 proximity in organotypic slices

Next, we sought to optimize SYNPLA in hippocampal slice cultures. In control "One Tag" experiments, slices were infected in the CA3 using a Sindbis expressing NRXN-MYC, and both HA and MYC primary antibodies were used (Fig. 4.4A, left). The first 10 μm of the slice cultures were imaged, and PLA rolony distribution was assessed (Fig. 4.4B, left). Control experiments showed some PLA rolonies, where none were expected, indicating that there was some background binding of primary antibodies in organotypic slices.

In "Both Tags" experiments, slices were expressed NRXN-MYC presynaptically, in the CA3, and HA-GluA2 postsynaptically, in the CA1 (Fig. 4.4A, right). Despite the presence of PLA rolonies in the control condition, the both tags experi-

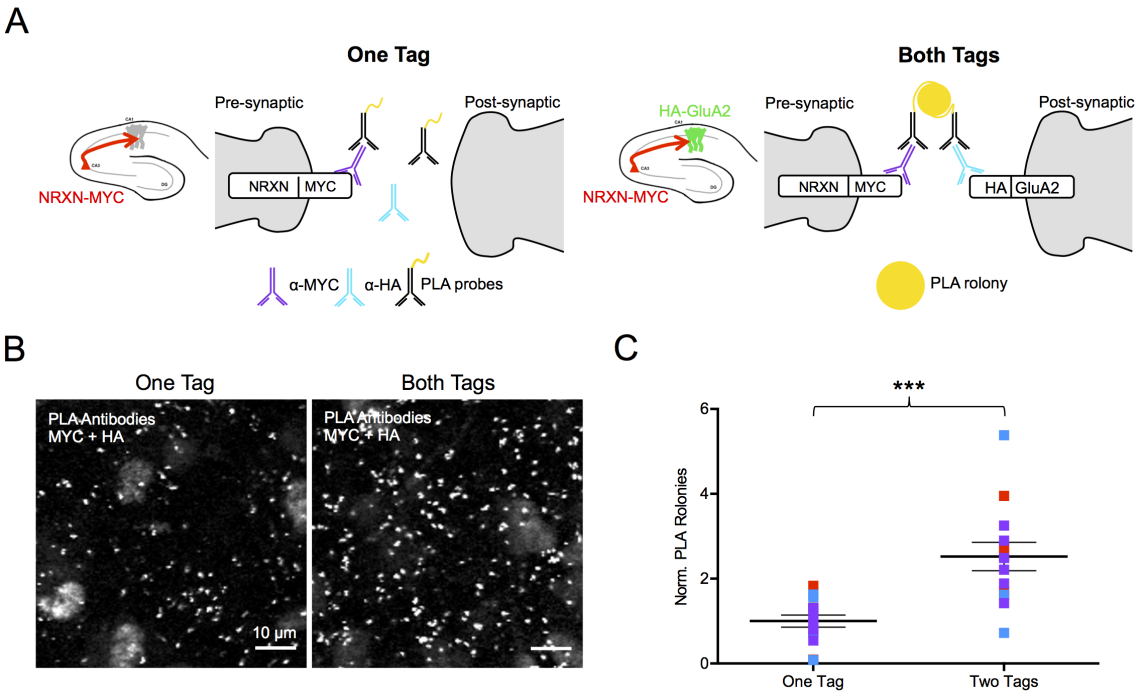

Figure 4.4: PLA labels trans-synaptic NRXN-GluA2 proximity in organotypic slices. (A) In "One Tag" experiments (left), organotypic slices are infected in the CA3 with Sindbis-NRXN-MYC, and HA and MYC primary antibodies are used for PLA. With no HA-tag present, there should be few to no PLA rolonies in ideal conditions because the PLA reaction requires the binding of both primary antibodies to their respective antigens. In "Both Tags" experiments, organotypic slices are infected in the CA3 with Sindbis-NRXN-MYC and in the CA1 with Sindbis-HA-GluA2, and HA and myc primary antibodies are used for PLA. PLA rolonies should be detected in these conditions. (B) One Tag experiments show some PLA rolonies. Both Tags experiments show an increase in detected PLA rolonies. (C) Quantification of data shown in B. Total PLA rolonies were counted for a $211.97\mu m \times 211.97\mu m$ image in both conditions. Total PLA rolony count was normalized to the mean total rolony count from the One Tag control for each experiment, providing a normalized PLA rolony value (Norm. PLA rolonies, y-axis). Each color represents an individual experiment; each dot represents a different image from that experiment. *** indicates $p < 0.005$.

ment shows an approximate 2.5-fold increase in the number of PLA rolonies (Fig. 4.4B). These data demonstrate that PLA for recombinant NRXN-GluA2 proximity successfully labels synapses in organotypic slices, albeit with higher background than in primary neuronal cultures.

4.3.4 Chemical LTP increases synaptic PLA signal in organotypic slices

After demonstrating the efficacy of PLA on labeling synapses in organotypic slices, our next goal was to label recently potentiated synapses. Because GluA1 insertion into the synapse is activity-dependent, we used PLA to label NRXN-GluA1 proximity at synapses. For these experiments, organotypic slices were infected in the CA3 with a Sindbis-NRXN-MYC (Fig. 4.5A, left). We first tested our cLTP protocol by performing extracellular local field potential recordings on organotypic slices (Kopec, 2006). Incubation of the slice with the cLTP solution led to stable potentiation approximately 40-60 minutes following the induction protocol (Fig. 4.5D).

After validating the cLTP protocol electrophysiologically, we performed PLA for recombinant NRXN and endogenous GluA1 on slices that received and did not receive cLTP concomitantly. In slices that received cLTP, it was expected that GluA1 would be trafficked to the synapse, and there would be a high number of PLA rolonies relative to slices that did not receive cLTP (Fig. 4.5A, right). As expected, slices receiving cLTP had much higher levels of PLA signal–approximately six-fold more than slices that did not receive chemical LTP (Fig. 4.5E).

Figure 4.5: cLTP increases PLA synaptic signal in organotypic slices. (A) Schematic for PLA on organotypic slices: slices are infected in the CA3 with a Sindbis-NRXN-MYC (left), and then subjected to cLTP. Following cLTP, GluA1 is inserted into the synapse, allowing NRXN-GluA1 proximity to be detected by PLA (right). (B) PLA signal in slices that receive cLTP (right) is much greater than in slices that do not receive cLTP (left). Individual z-slice is shown. (C) Z-stacks were acquired when imaging PLA in organotypic slices, and PLA rolonies were quantified on each z-slice. (D) cLTP protocol was applied to evoked field potential recordings in organotypic slices and led to robust potentiation. (E) Quantification of all PLA rolonies in a z-stack. Each dot represents a single z-stack, and each color represents a different experiment. * indicates $p < 0.05$.

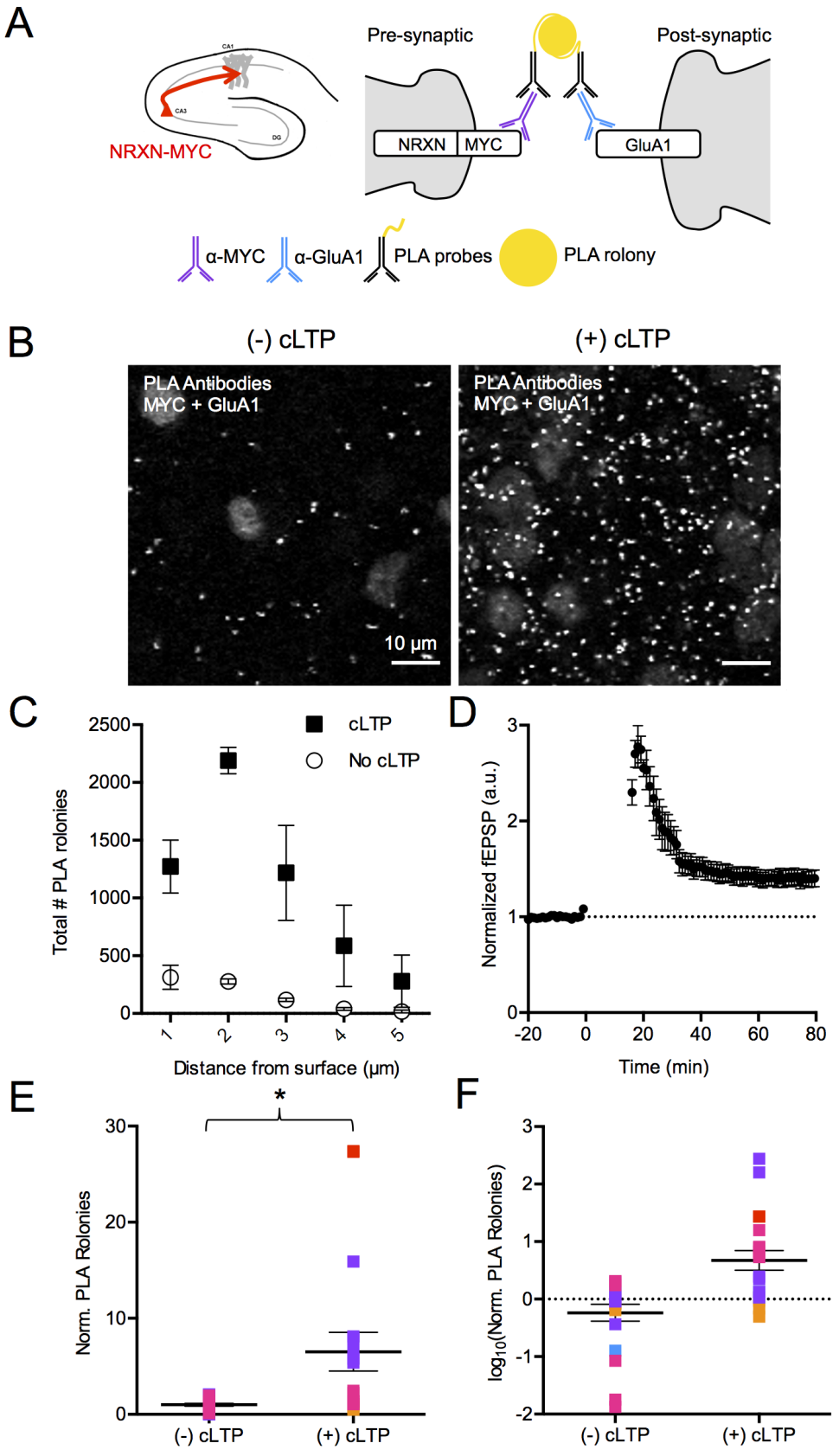
A
NRXN-MYC
Pre-synaptic
Post-synaptic
NRXN
MYC
GluA1
α-MYC
α-GluA1
PLA probes
PLA rolony
B
(-) cLTP
(+) cLTP
PLA Antibodies
MYC + GluA1
10 µm
C
cLTP
No cLTP
Total # PLA rolonies
Distance from surface (µm)
D
Normalized fEPSP (a.u.)
Time (min)
E
Norm. PLA Rolonies
(-) cLTP
(+) cLTP
F
log10(Norm. PLA Rolonies)
(-) cLTP
(+) cLTP

One concern with these results was that organotypic slices are relatively thick, which may prevent the PLA reaction from occurring effectively in deeper regions of the slice. To characterize whether the difference in PLA signal was limited to the top of the slice, or the first few z-slices in a z-stack, we quantified the total PLA rolonies in each individual z-slice at the first 5 μm of a slice (Fig. 4.5C). We found that slices receiving cLTP had more PLA rolonies than their no cLTP counterparts throughout the z-stack, demonstrating the efficacy of PLA in identifying recently potentiated synapses in thicker sections. These results demonstrate that cLTP leads to an increase in PLA signal, which is consistent with the model of increased synaptic GluA1 following activity.

We next wanted to ensure that cLTP was actually leading to increased GluA1 trafficking to the synapse, and therefore an increase in NRXN-GluA1 proximity. To do this, we performed control experiments in which organotypic slices expressed only endogenous GluA1 and subjected them to PLA following cLTP or no cLTP conditions (Fig. 4.6A, right). We expected that the absence of recombinant NRXN-MYC should lead to very few rolonies of PLA for recombinant NRXN-MYC and endogenous GluA1 is specifically detecting NRXN-GluA1 proximity. We observed that slices expressing only one tag had no PLA rolonies in the cLTP or no cLTP conditions (Fig. 4.6), demonstrating that PLA for MYC and GluA1 specifically detects a change in synaptic GluA1. Thus far, these data suggest that PLA for MYC and GluA1 in organotypic slices can detect recently potentiated synapses.

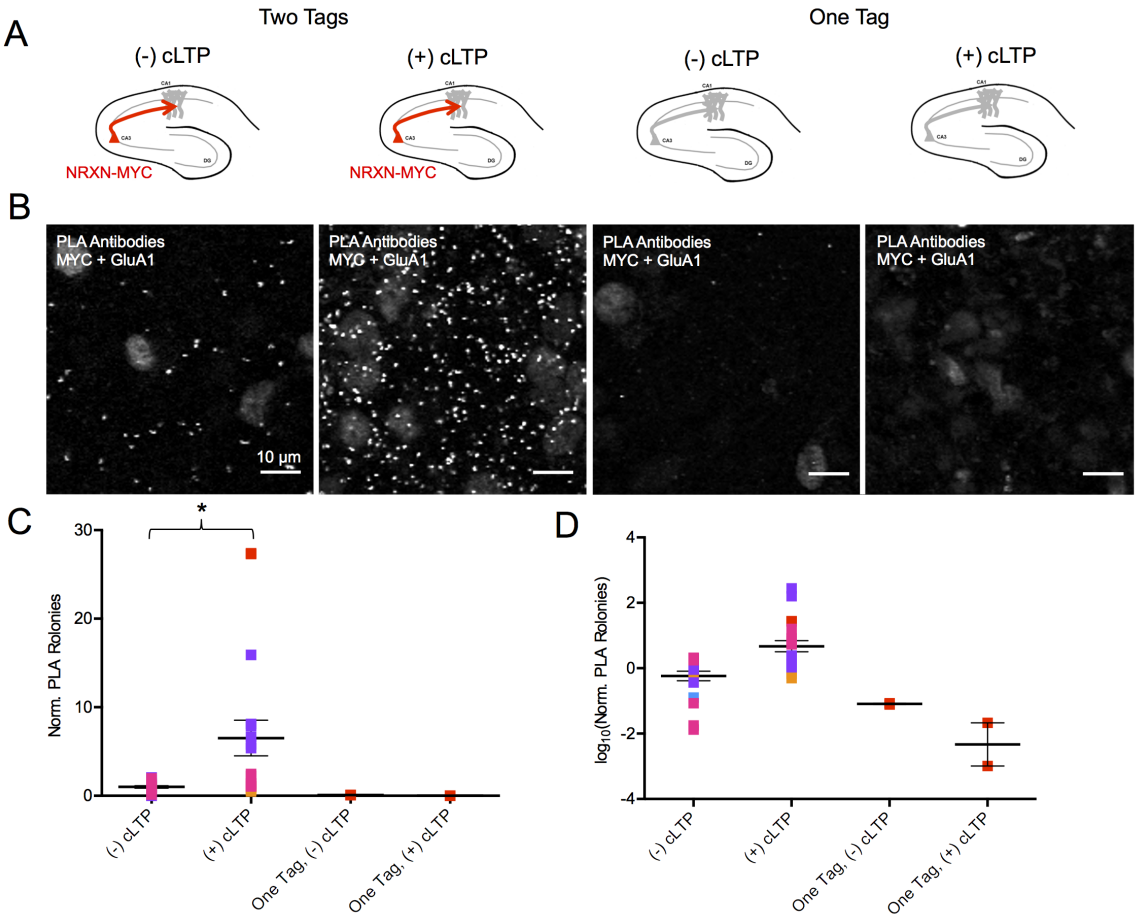

Figure 4.6: No PLA signal in cLTP control conditions. (A) Schematic for "Two Tags" and "One Tag" conditions. (B) PLA signal in the stratum radiatum for each condition. (C) Quantification of PLA rolonies per 211.97μm$\times$211.97μm images for each condition. Total PLA rolony count per image was normalized to the mean total rolony count of the (-) cLTP condition in every experiment. Each color indicates a different experiment; each dot represents the normalized PLA rolony (Norm. PLA Rolonies) count for a different image. * indicates $p < 0.05$. (D) Norm. PLA Rolonies were $\log_{10}$ normalized.

Figure 4.7: Inhibition of NMDA receptors with D-APV during cLTP reduces PLA rolonies. (A) cLTP with (right) or without (left) D-APV protocol was applied to evoked field potential recordings in organotypic slices. D-APV blocked LTP in organotypic slices. (B) Representative images of PLA signal in slices that receive D-APV have fewer rolonies than slices that do not receive D-APV. (C) Quantification of PLA rolonies shows that slices receiving cLTP without D-APV have 1.78$\times$ more rolonies than slices receiving cLTP with D-APV. * indicates $p < 0.05$.

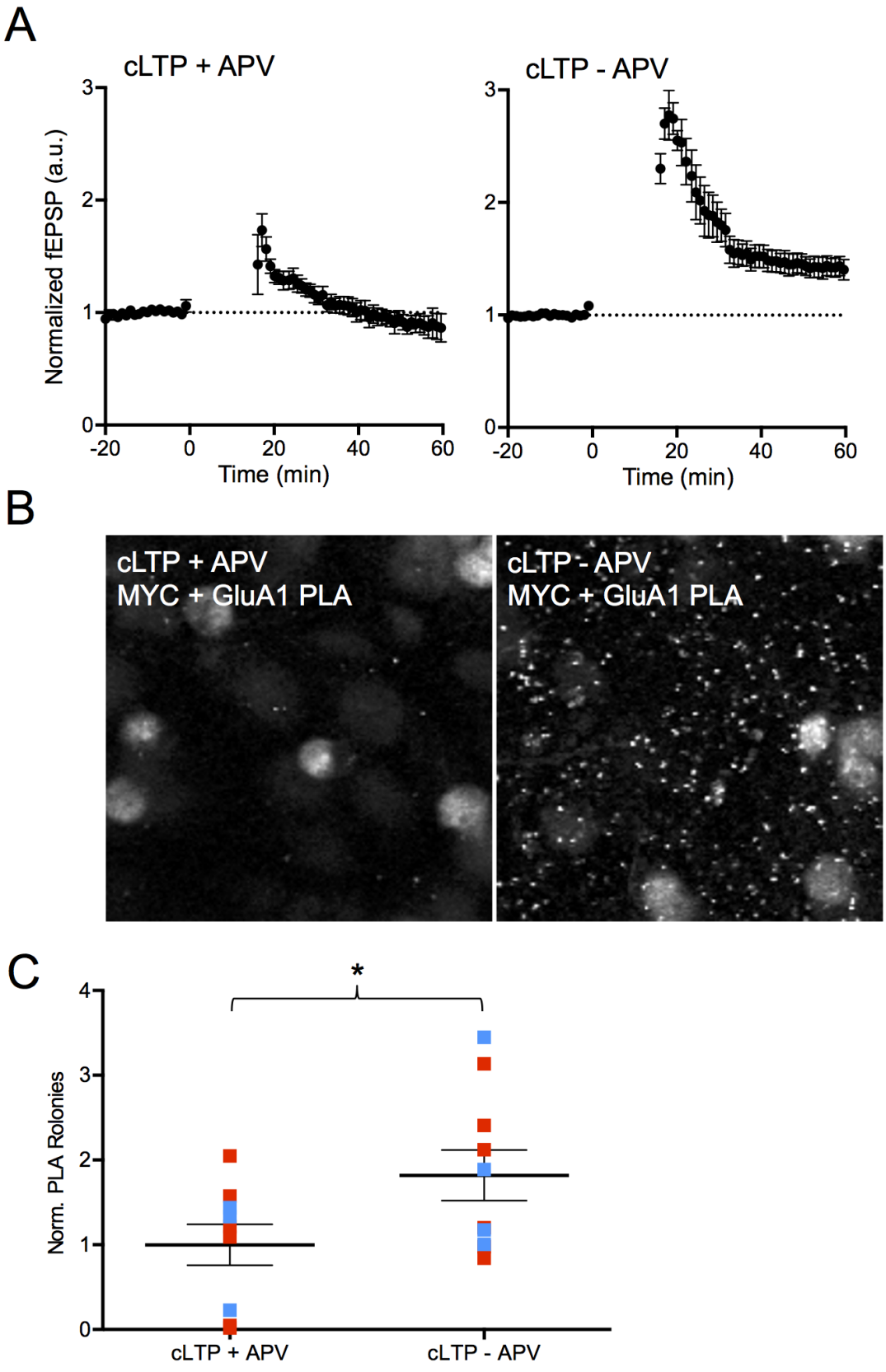
A
cLTP + APV
cLTP - APV
Normalized fEPSP (a.u.)
Time (min)
B
cLTP + APV
MYC + GluA1 PLA
cLTP - APV
MYC + GluA1 PLA
C
Norm. PLA Rolonies
cLTP + APV
cLTP - APV
*

We next addressed whether pharmacological inhibition of LTP would reduce the number of NRXN-GluA1 PLA rolonies in organotypic slices. The activation of NMDA receptors is required for LTP and LTD, and D-(-)-2-Amino-5-phosphonopentanoic acid (D-APV) is an antagonist of NMDA receptors (Madison et al., 1991). D-APV has been shown to block LTP (Fig. 4.7A, left), inhibit spine growth, and reduce GluA1 insertion into synapses (Kopec, 2006; Hou et al., 2011). Indeed, when organotypic slices expressing recombinant NRXN-MYC in the CA3 were subjected to a cLTP protocol in the presence of APV, PLA rolonies detecting NRXN-GluA1 proximity were significantly reduced compared to organotypic slices that received only the cLTP treatment (Fig. 4.7B and C). These results indicate that the application of SYNPLA to recombinant NRXN-MYC and endogenous GluA1 labels synapses that have undergone potentiation.

4.3.5 Increased endogenous GluA1 PLA in MGN and LA following cued fear conditioning

Thus far, SYNPLA has been characterized as a technique to label synapses in primary cultured neurons and organotypic hippocampal slices. Our next step was to apply SYNPLA to identify brain regions that have undergone potentiation after a learning task. For these experiments, the auditory cortical and thalamic projections to the lateral amygdala (LA) were examined because of their established role in cued fear conditioning (Rogan et al., 1997; Nabavi et al., 2013). Rats were injected in the auditory cortex (AuC) and medial geniculate nucleus (MGN) with an AAV co-expressing recombinant NRXN-MYC and GFP. Rats were then subjected to either paired or unpaired cued fear conditioning (Fig. 4.8A and B).

Figure 4.8: Increased endogenous GluA1 PLA in MGN and LA following cued fear conditioning. (A) Protocol for paired conditioning protocol. The tone (CS) lasts for 20 seconds and co-terminates with 1 second 0.5 mA foot-shock. The animal receives this pairing 10 times with an average interval of 3 min between tone and shock pairs. (B) Protocol for unpaired conditioning protocol. The CS and US are temporally unpaired. Shock and tone delivery was separated by a randomized interval between 1 and 4 min. (C-K) Rats expressed NRXN-MYC in the AuC and MGN and following perfusion, PLA for recombinant NRXN-MYC and endogenous GluA1 was conducted on coronal slices. Paired conditioning led to increased PLA rolonies in the MGN (D and E), LA (G and H) and caudate putamen (CPu) (J and K) compared with *ex vivo* tissue from rats receiving unpaired conditioning. Total PLA rolonies were quantified from a 211.97μm$\times$211.97μm image.

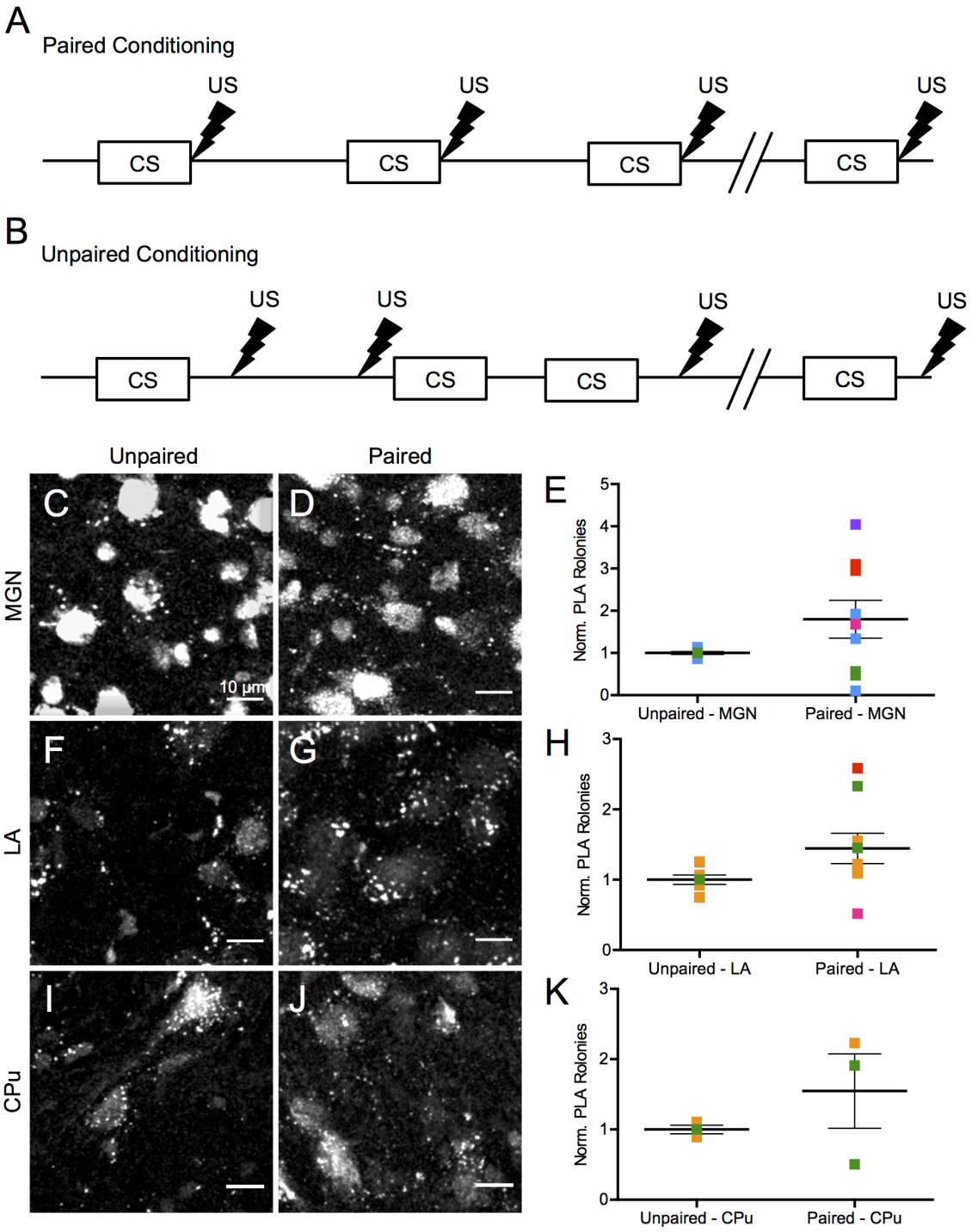
A
Paired Conditioning
US
CS
B
Unpaired Conditioning
Unpaired
Paired
MGN
LA
CPu
C
D
F
G
I
J
10 µm
E
H
K
Norm. PLA Rolonies
Unpaired - MGN
Paired - MGN
Unpaired - LA
Paired - LA
Unpaired - CPu
Paired - CPu

PLA for recombinant NRXN-MYC and endogenous GluA1 was conducted on coronal slices collected from these rats and pre- and postsynaptic brain regions were examined. Animals that received paired conditioning had, on average, more PLA rolonies in the LA (Fig. 4.8F-H) than those that received unpaired conditioning. Given that cued fear conditioning leads to LTP in the LA (Rogan et al., 1997), this is unsurprising. In addition, there were also more NRXN-GluA1 rolonies in the CPu of animals that received paired conditioning (Fig. 4.8I-K). This is unsurprising given that the CPu is receives cortical and thalamic inputs and is involved in auditory processing (Ledoux et al., 1991). More surprisingly, there were also more NRXN-GluA1 PLA rolonies in the MGN (Fig. 4.8C-E) of rats that underwent paired conditioning. Lastly, the AuC was also examined for NRXN-GluA1 proximity, but preliminary results indicate that there is little to no change in NRXN-GluA1 rolonies in the AuC of paired conditioned rats compared with the corresponding controls.

4.3.6 PLA and PSD-95 signals are significantly correlated

To ensure that PLA detecting NRXN-GluA1 proximity is synaptic, PLA for recombinant NRXN and endogenous GluA1 was performed simultaneously with immunofluorescence labeling for a synaptic marker, PSD-95 (Fig. 4.9A, left). PLA labeling for NRXN-GluA1 proximity and PSD-95 labeling both demonstrated high levels of signal distributed throughout a sample. To ensure that colocalization was not due to chance, the correlation coefficient was determined for individual z-slices in the PLA channel and the PSD-95 channel. Subsequent correlation coefficient analysis was performed in which images in the PLA channel were shifted by 2 pixels, while the PSD-95 channel remained unchanged, until an image was shifted by 50

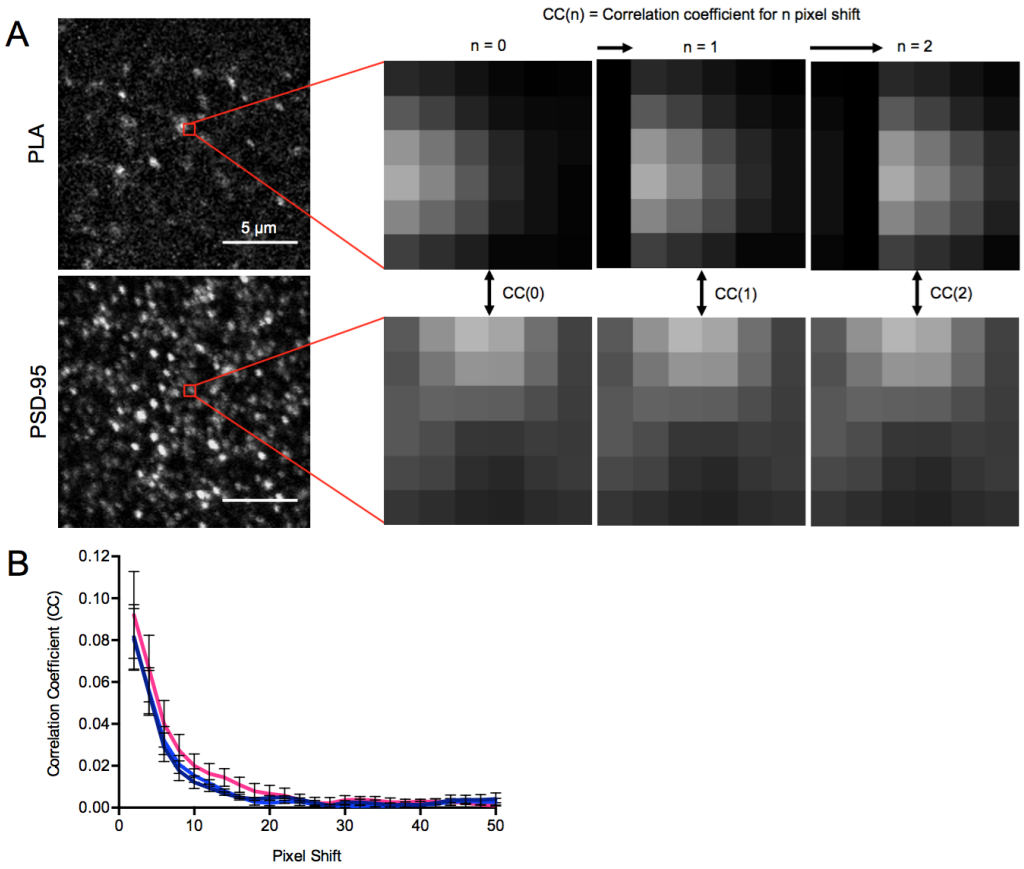

Figure 4.9: PLA and PSD-95 signals are significantly correlated. PLA and PSD-95 signals are significantly correlated. (A) PLA for NRXN-GluA1 proximity and PSD-95 labeling (left) and schematic for determining correlation coefficient by circular shift of the PLA image by n pixels, while the PSD-95 image remains constant (right). (B) Plot of the correlation coefficient versus pixel shift.

pixels (Fig. 4.9A, right). The correlation between the PLA and PSD-95 channels rapidly decreased upon pixel shifts (Fig. 4.9B), indicating that correlations observed between the PLA for NRXN-GluA1 proximity and PSD-95 was not due to chance. This analysis further bolsters the idea that SYNPLA for recombinant NRXN-MYC and endogenous GluA1 is labeling recently potentiated synapses.

4.3.7 Discussion

We characterized SYNPLA in three different systems: primary cultured neurons, organotypic hippocampal slices, and finally, on *ex vivo* brains from animals undergoing learning tasks. Across these three systems, SYNPLA has proven to be a reliable technique for identifying synapses that have recently undergone potentiation. SYNPLA for recombinant NRXN and endogenous GluA1 also showed that the MGN, CPu, and LA all undergo LTP after cued fear conditioning, providing some novel information about areas involved in plasticity following this particular learning task.

This study has focused mainly on optimizing SYNPLA for recombinant NRXN-MYC and endogenous GluA1, but PLA is an inherently flexible technique and not limited to the detection of these proteins. In fact, the ideal procedure for SYNPLA would involve the use of primary antibodies detecting only endogenous proteins, which would remove the need for expressing recombinant proteins, which can introduce a number of variables that can complicate a study. Another possibility would be to use SYNPLA for detecting NRXN-GluA3 or GluA2 proximity several days after an animal has undergone a learning task. One of the prevailing models for AMPA receptor trafficking suggests that GluA1 insertion into synapses occurs early in LTP, but when a new potentiated equilibrium has been reached, GluA1/GluA2

heteromers are replaced by GluA2/GluA3 receptors (Shi et al., 2001). This model suggests that it would be possible to view a change in the number of PLA rolonies for NRXN-GluA2 or GluA3.

In any case, we have established a new method for identifying recently potentiated synapses *in vitro* and *ex vivo*. The one caveat to using SYNPLA is that it limits studies to postfixation (*in vitro*) and postmortem (*ex vivo*) analyses, unlike *in vivo* TPLSM, but the advantages outweigh the disadvantages. One benefit of using SYNPLA over *in vivo* TPLSM is that with SYNPLA, higher resolution data on brain regions involved in plasticity can be acquired on whole-mount brain slices relatively quickly. Although conducting *in situ* hybridization or immunohistochemistry for IEGs such as *c-Fos* or *Arc* can also be performed with relative ease, these techniques are largely limited to the soma, and the correlation between expression and synaptic strength are unclear (Madison et al., 1991). Unlike IEG expression, trafficking of GluA1 to synapses is an important molecular mechanism of LTP (Hayashi, 2000; Shi et al., 2001; Li et al., 2011), making SYNPLA a technique that best assesses brain regions involved in learning a task.

4.3.8 Experimental Procedures

Organotypic hippocampal slices

Organotypic hippocampal slices were prepared from P7-8 mice as described previously (Stoppini et al., 1991) and used after 14-21 days in culture for electrophysiology and PLA. Constructs of myc-tagged neurexin-1B (NRXN-MYC), HA- and SEP-tagged GluA1 (HA-SEP-GluA1), and HA- and SEP-tagged GluA2 (HA-SEP-GluA2) were cloned into a pSinRep5 shuttle vector and infective Sindbis pseudo viruses were produced according to the manufacturer's protocol (Invitrogen/Thermo Fisher Scientific).

Electrophysiology

Organotypic hippocampal slices were perfused with artificial CSF (ACSF, in mM: 118 NaCl, 2.5 KCl, 26 $NaHCO_3$, 1 NaH_2PO_4, 1 $MgCl_2$, 2 $CaCl_2$, 20 glucose) gassed with 95%O_2/5%CO_2). For evoked recordings of extracellular field potentials, a cut was made between CA1 and CA3, and picrotoxin (50 μM) was added to the bath. Two stimulating electrodes, two-contact Pt/Ir cluster electrode (Frederick Haer, Bowdoin, USA), were placed between 100 and 300 μm down the apical dendrite, 100 μm apart, and 200 μm laterally in opposite directions. Extracellular field potentials were recorded in the SR with glass electrodes (1.5 MΩ-2.5 MΩ) containing ACSF. Field excitatory postsynaptic potentials (fEPSPs) were evoked by stimulating independent afferents.

Chemical LTP

For electrophysiology, fEPSPs were recorded until 20 minutes of a stable baseline was acquired. Following the stable baseline, ACSF was washed out and replaced with ACSF containing a drug cocktail to induce chemical LTP (cLTP: 0 mM $MgCl_2$, 2 mM $CaCl_2$, 100 nM rolipram, 50 μM forskolin, 100 μM picrotoxin) for 16 minutes, during which time no electrical stimulation was applied. The cLTP solution was subsequently washed out and replaced with ACSF as described in the previous section, and electrical stimulation was resumed at a frequency of 0.1 Hz per pathway. For experiments involving D-(-)-2-Amino-5-phosphonopentanoic acid (D-APV, Tocris), 100 μM D-APV was added to the ACSF containing the cLTP cocktail and to ACSF before and after cLTP induction.

For PLA, cLTP was conducted without electrophysiology by replacing slice culture media with ACSF containing the cLTP drug cocktail, incubating at 35°C for 16 minutes, and immediately fixing the slices with 4% paraformaldehyde (PFA) in phosphate-buffered saline (PBS: 100 mM Na_2HPO_4, 18 mM KH_2PO_4, 27 mM KCl, 1.37 M NaCl, pH 7.4). For D-APV experiments, D-APV was added to ACSF before and after cLTP induction, as well as the cLTP drug cocktail. Slices were first incubated with ACSF containing 1 mM $MgCl_2$, 2 mM $CaCl_2$, and 100 μM D-APV for 10 minutes at 35°C. Slices were then washed with ACSF containing cLTP drug cocktail, 100 μM D-APV, 0 $MgCl_2$, and 2 mM $CaCl_2$ for 16 min at 35°C. Following cLTP induction with D-APV, slices were washed with ACSF containing 1 mM $MgCl_2$, 2 mM $CaCl_2$, and 100 μM D-APV for 20 minutes at 35°C, and were subsequently fixed in 4% PFA.

Subject and Viruses

Male Sprague-Dawley rats were used for all experiments. Rats were housed two per cage and kept on a 12/12 h light-dark cycle (lights on/off at 7:00/19:00). Behavior experiments were performed during daylight. All procedures were approved by the Institutional Animal Care and Use Committees at the University of California, San Diego. AAV co-expressing GFP and recombinant NRXN-MYC was driven by a CAG promoter was injected at age 6-8 weeks, and expression was permitted for 8-12 weeks before subjects received cued fear conditioning. Viruses were provided by Anthony Zador at Cold Spring Harbor Laboratory.

Cued Fear Conditioning

After animals received the cued fear conditioning protocol in a chamber (12$\times$10.5$\times$13 inches) containing an electrified grid floor (Coulbourn Instruments, Allentown, PA) within a larger sound-attenuating box. The paired conditioning protocol comprised the delivery of a tone lasting 20 seconds that co-terminated with a 1 second 0.5 mA footshock. The temporally paired delivery of tone and shock occurred 10 times, with an average interval of 3 min between tone and shock pairs. The unpaired conditioning protocol comprised the delivery of tone and shock separated by a randomized interval between 1 and 4 min, with a total of 10 shocks and 10 tones being delivered at the end of the trial. Animals were perfused with 4% PFA in 1$\times$ PBS (pH 7.4) and tissue was collected after the experiment.

Preparation of Coronal Slices

Whole brains were fixed in 4% PFA at 4° overnight, and were transferred to 1× PBS. After transfer to 1× PBS, free-floating sections were made in 1× PBS in a vibratome at a thickness of 50μm. Sections were stored in 1× PBS containing 0.01% sodium azide until subjected to a PLA.

In situ PLA

PLA was performed on free floating sections. After fixation, a vibratome was used to make coronal sections at a thickness of 50 μm and slices were stored in PBS.

Primary Antibodies. For PLA, free floating sections were rinsed three times with PBS, followed by permeabilization with 0.5% v/v Triton X-100 in PBS for 1 hour at room temperature. Sections were then incubated with a blocking solution (Blocking One Histo, Nacalai Tesque) for 1 hour at room temperature. Subsequently, slices were incubated with primary antibodies in antibody diluent (5% v/v Blocking One Histo, 0.1% Tween-20 in PBS) at 4°C overnight.

PLA Secondary Probes. Following primary antibody incubation, slices were subjected to washes with Duolink wash buffer A (Sigma-Aldrich) for one hour at room temperature. Samples were then incubated with PLA secondary probes diluted 1:5 with antibody diluent and gently agitated for 2 hours at 37°C.

Ligation. Slices were then subjected to washes with Duolink wash buffer A for one hour at room temperature. Ligation steps were performed using a 1:40 dilution of ligase and 1:5 dilution of ligation buffer in MilliQ-H_2O. Slices were incubated with the ligation reaction for 2 hours at 37°C.

Amplification and Detection. After hybridization and ligation, slices were subjected to amplification and detection reaction containing a 1:60 dilution of polymerase and 1:5 dilution of detection reagents in MilliQ-H_2O. Slices were gently agitated for 2 hours at 37°C.

Mounting and Cover Slipping. Following amplification and detection, slices were subjected to 2$\times$10 min washes in Duolink wash buffer B, and 1$\times$1 min wash in 0.01x wash buffer B. Slices were then mounted on glass slides, allowed to dry, and then subjected to 1$\times$2 min in 96% ethanol, 1$\times$2 99% ethanol, and 1$\times$10 xylenes, and then coverslipped using Duolink In Situ Mounting Medium (Sigma-Aldrich).

4.4 Acknowledgments

"SYNPLA: a new method for detecting recently potentiated synapses" was produced in collaboration with Justus Kebschull and Dr. Anthony M. Zador, from Cold Spring Harbor Laboratory. Justus Kebschull and I were the primary researchers for this project. Justus Kebschull produced Figures 4.1, 4.2, and 4.3. I produced the remainder of the data described in this chapter.

4.5 Supplemental Information

4.5.1 Supplemental Figures

Figure 4.10: cLTP leads to increased recombinant NRXN-MYC and HA-GluA1 PLA labeling. (A) Schematic for infection of organotypic slices. “One Tag” (left) condition comprises only CA3 infection with Sindbis-NRXN-MYC-tdTomato. “Both Tags” (middle and right) conditions involve CA3 infection with Sindbis-NRXN-MYC and CA1 infection with Sindbis-HA-GluA1. Slices in “Both Tags” are subjected to no cLTP or cLTP protocol (middle and right). (B) Representative images of PLA rolonies in “One Tag’ (left), ’ “Both Tags, (-) cLTP” (middle), and “Both Tags, (+) cLTP” (right) conditions. (C) Quantification of PLA rolonies, with rolony count from each experiment normalized to the mean of “Both Tags, (-) cLTP)” from each experiment. Note that PLA signal in “Both Tags, (+) cLTP” is roughly $2\times$ that of the PLA signal in the “Both Tags, (-) cLTP” condition. * indicates $p < 0.05$.

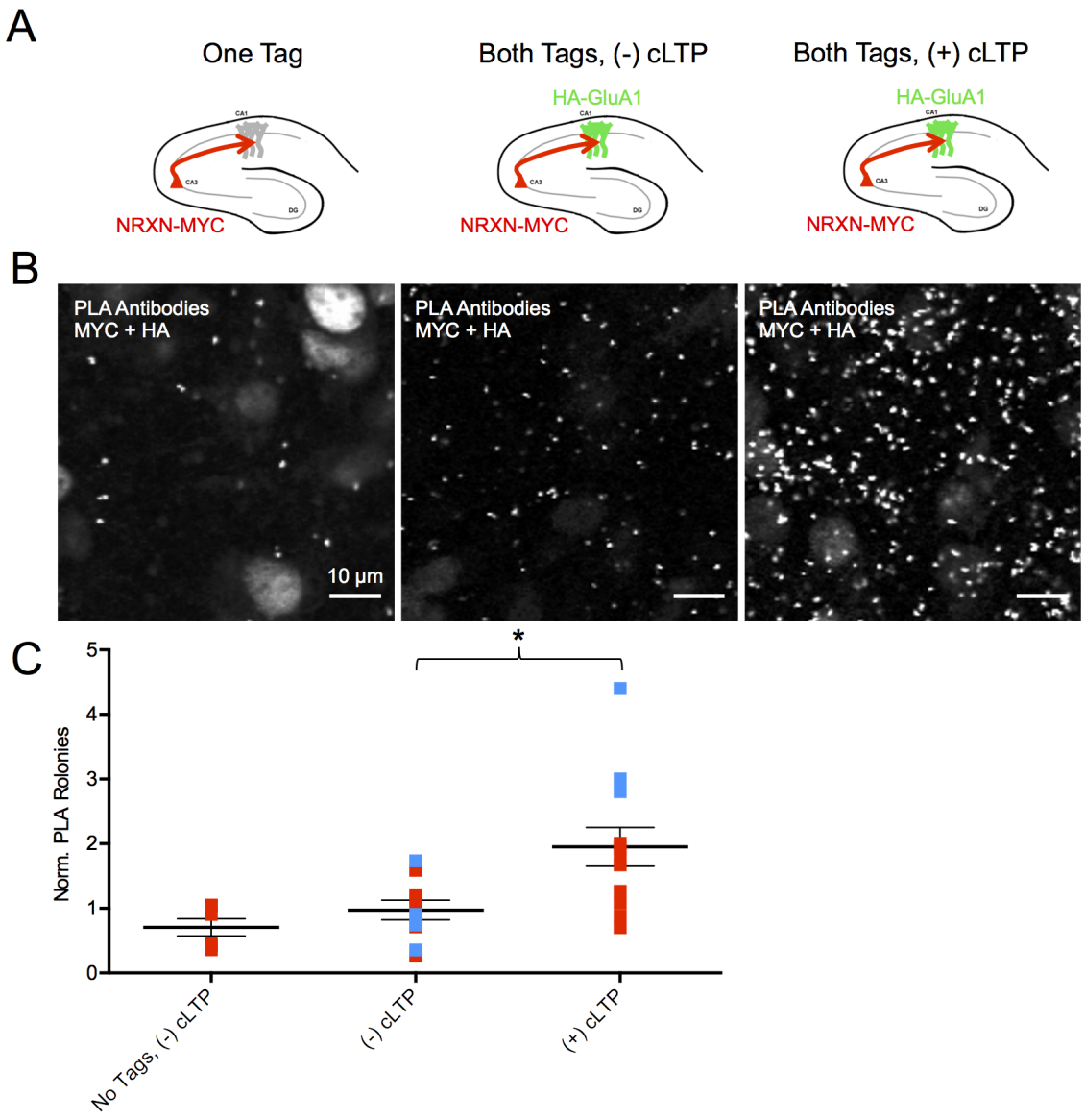
A
One Tag
Both Tags, (-) cLTP
Both Tags, (+) cLTP
HA-GluA1
HA-GluA1
NRXN-MYC
NRXN-MYC
NRXN-MYC
B
PLA Antibodies
MYC + HA
PLA Antibodies
MYC + HA
PLA Antibodies
MYC + HA
10 µm
C
Norm. PLA Rolonies
0
1
2
3
4
5
*
No Tags, (-) cLTP
(-) cLTP
(+) cLTP

Chapter 5

Conclusion

5.1 AMPA receptor subunit GluA3 is required for Aβ-induced synaptic depression

In Chapter 2, the importance of the AMPA receptor subunit GluA3 in the synaptic dysregulation caused by Aβ was described. GluA3 has been a largely ignored AMPA receptor subunit, given its role in constitutively replacing synaptic AMPA receptors and that GluA3 knockout mice have appeared phenotypically normal in behavioral tasks before our study (Shi et al., 2001; Meng et al., 2003). Chapter 2 described the importance of GluA3 in the molecular mechanism of Alzheimer's disease in three parts. First, we demonstrated that APP_{CT100}-overexpressing cells are vulnerable to synaptic depression in wild-type but not $GluA3^{-/-}$ mice. Second, Aβ oligomers block LTP in the hippocampus of acutely isolated slices from wild-type mice but not from $GluA3^{-/-}$ mice. Finally, we showed that GluA3-lacking APP/PS1 transgenic mice lack mortality, contextual fear memory deficits, and spine loss that

are normally present.

Previous work has demonstrated that Aβ leads to the activation of signaling pathways involved in LTD (Wang, 2004; Hsieh et al., 2006; Li et al., 2009). Aβ is also known to cause the endocytosis of AMPA receptors, particularly GluA2-containing receptors (Hsieh et al., 2006). Our study suggests that Aβ triggers a signaling cascade that resembles LTD, leading to the preferential endocytosis of GluA3-containing AMPA receptors. It would be interesting to determine whether mutations affecting GluA3 trafficking are present in Alzheimer's disease patients and their healthy counterparts. Given the large-scale genomic studies that have been carried out for Alzheimer's disease, it would be interesting to examine these available data sets for mutations correlated with disease prevention or onset (Suh et al., 2013).

5.2 GSMs prevent Aβ-induced synaptic depression

In Chapter 3, the efficacy of new Alzheimer's disease therapies was assessed and a new method of overproducing Aβ *in vivo* was described. Previous studies have evaluated the pharmacokinetics and effect of GSMs on Aβ levels and behavioral tasks, but our lab was the first to demonstrate that GSMs can prevent Aβ-induced synaptic depression in organotypic hippocampal slices (Kounnas et al., 2010; Mitani et al., 2012). Based largely on the method developed by Nabavi et al. (2014), it was shown that AAV-mediated overexpression of CT100 and oChIEF-citrine leads to behavioral phenotypes resembling young APP transgenic mice (Beglopoulos et al., 2016). Rats expressing CT100 in the AuC and MGN have initial deficits in memory

formation and retrieval, but it seems that once a robust memory has been formed, Aβ expression for a few weeks is insufficient to inactivate memories like LTD.

It should be noted that our study utilized a wild-type form of CT100, and that a familial APP or CT100 mutation would produce higher levels of Aβ and affect memory. To truly engineer and modulate a memory in this system would require further characterization of using AAV to introduce excessive Aβ production *in vivo*. Careful time points would need to be carried out to examine the impact of Aβ on learning tasks and memory deficits throughout an animal subject's lifetime. Furthermore, the effect of GSMs in rats producing Aβ in the AuC and MGN also needs to be assessed to ensure that acute treatment with GSMs does not exacerbate memory deficits.

5.3 SYNPLA labels recently potentiated synapses

In Chapter 4, a new method for labeling recently potentiated synapses was described. SYNPLA was characterized in dissociated cultured neurons, organotypic hippocampal slices, and *ex vivo* slices prepared from animals that underwent learning tasks. Across these three systems, SYNPLA has proven to be a reliable technique for identifying synapses.

SYNPLA is particularly powerful because of the inherent flexibility of the technique. The results described in Chapter 4 were collected using antibodies for recombinant NRXN-MYC and endogenous GluA1. If this technique were to be optimized to label synapses using only endogenous proteins, it would remove the complicating–and often variable–factor of injecting AAVs in brain regions of interest.

Another way this technique could be used is to examine NRXN-GluA2 proximity in animals that have received longer, more complex behavioral tasks. The cued fear conditioning paradigm in Chapter 4 are fairly straightforward, and PLA for NRXN-GluA1 proximity was performed on tissue fixed shortly after conditioning (approximately 30 min). This procedure allowed us to determine very recently potentiated synapses, which would have high levels of newly inserted GluA1. However, GluA2/3 heteromers are constitutively cycling, and are thought to replace GluA1/2 heteromers once a new, potentiated equilibrium has been established. Thus, if one wanted to examine the change in the overall number of synapses after a long-term behavior task, one could do so by performing PLA for NRXN-GluA2 proximity.

SYNPLA will provide a new way of identifying brain regions that have undergone plasticity after behavior tasks, but it is not meant to be the only approach. It would be interesting to determine whether the information provided by SYNPLA would differ much from data provided by immunolabeling IEGs. Furthermore, given that PLA is performed entirely on fixed tissue, it does not provide us with the temporal resolution offered by *in vivo* TPLSM.

Bibliography

Adamczyk, A., Mejias, R., Takamiya, K., Yocum, J., Krasnova, I. N., Calderon, J., Cadet, J. L., Huganir, R. L., Pletnikov, M. V., and Wang, T. (2012). GluA3-deficiency in mice is associated with increased social and aggressive behavior and elevated dopamine in striatum. *Behavioural Brain Research*, 229(1):265–272.

Alfonso, S., Kessels, H. W., Banos, C. C., Chan, T. R., Lin, E. T., Kumaravel, G., Scannevin, R. H., Rhodes, K. J., Huganir, R., Guckian, K. M., Dunah, A. W., and Malinow, R. (2014). Synapto-depressive effects of amyloid beta require PICK1. *European Journal of Neuroscience*, 39(7):1225–1233.

Alfonso, S. I., Callender, J. A., Hooli, B., Antal, C. E., Mullin, K., Sherman, M. A., Lesné, S. E., Leitges, M., Newton, A. C., Tanzi, R. E., and Malinow, R. (2016). Gain-of-function mutations in protein kinase Cα (PKCα) may promote synaptic defects in Alzheimer's disease. *Science Signaling*, 9(427):ra47.

Aow, J., Dore, K., and Malinow, R. (2015). Conformational signaling required for synaptic plasticity by the nmda receptor complex. *Proceedings of the National Academy of Sciences*, 112(47):14711–14716.

Ashe, K. H. and Zahs, K. R. (2010). Probing the Biology of Alzheimer*s Disease in Mice. *Neuron*, 66(5):631–645.

Balducci, C., Beeg, M., Stravalaci, M., Bastone, A., Sclip, A., Biasini, E., Tapella, L., Colombo, L., Manzoni, C., Borsello, T., Chiesa, R., Gobbi, M., Salmona, M., and Forloni, G. (2010). Synthetic amyloid- oligomers impair long-term memory independently of cellular prion protein. *Proceedings of the National Academy of Sciences*, 107(5):2295–2300.

Barghorn, S., Nimmrich, V., Striebinger, A., Krantz, C., Keller, P., Janson, B., Bahr, M., Schmidt, M., Bitner, R. S., Harlan, J., Barlow, E., Ebert, U., and Hillen, H. (2005). Globular amyloid beta-peptide1-42 oligomer - a homogenous and stable neuropathological protein in Alzheimer's disease. *Journal of Neurochemistry*, 95(3):834–847.

Basarsky, T., Parpura, V., and Haydon, P. (1994). Hippocampal synaptogenesis in cell culture: developmental time course of synapse formation, calcium influx, and synaptic protein distribution. *The Journal of Neuroscience*, 14(11):6402–6411.

Beglopoulos, V., Tulloch, J., Roe, A. D., Daumas, S., Ferrington, L., Watson, R., Fan, Z., Hyman, B. T., Kelly, P. A. T., Bard, F., and Morris, R. G. M. (2016). Early detection of cryptic memory and glucose uptake deficits in pre-pathological APP mice. *Nature Communications*, 7:1–10.

Benilova, I., Karran, E., and De Strooper, B. (2012). The toxic A. *Nature Publishing Group*, 15(3):349–357.

Berchtold, N. C., Sabbagh, M. N., Beach, T. G., Kim, R. C., Cribbs, D. H., and Cotman, C. W. (2014). Neurobiology of Aging. *Neurobiology of Aging*, 35(9):1961–1972.

Boyle, P. A., Wilson, R. S., Aggarwal, N. T., Tang, Y., and Bennett, D. A. (2006). Mild cognitive impairment Risk of Alzheimer disease and rate of cognitive decline. *Neurology*, 67(3):441–445.

Brookmeyer, R., Johnson, E., Ziegler-Graham, K., and Arrighi, H. M. (2007). Forecasting the global burden of Alzheimer's disease. *Alzheimer's & Dementia*, 3(3):186–191.

Brown, D. F., Risser, R. C., Bigio, E. H., Tripp, P., Stiegler, A., Welch, E., Eagan, K. P., Hladik, C. L., and White, III, C. L. (1998). Neocortical Synapse Density and Braak Stage in the Lewy Body Variant of Alzheimer Disease: A Comparison with Classic Alzheimer Disease and Normal Aging. *Journal of Neuropathology and Experimental Neurology*, 57(10):955–960.

Cissé, M., Halabisky, B., Harris, J., Devidze, N., Dubal, D. B., Sun, B., Orr, A., Lotz, G., Kim, D. H., Hamto, P., Ho, K., Yu, G.-Q., and Mucke, L. (2010). Reversing EphB2 depletion rescues cognitive functions in Alzheimer model. *Nature*, 469(7328):47–52.

Collingridge, G. L. (2012). A pivotal role of GSK-3 in synaptic plasticity. pages 1–11.

Comery, T. A. (2005). Acute -Secretase Inhibition Improves Contextual Fear Conditioning in the Tg2576 Mouse Model of Alzheimer's Disease. *Journal of Neuroscience*, 25(39):8898–8902.

De Strooper, B. (2014). Lessons from a Failed g-Secretase Alzheimer Trial. *Cell*, 159(4):721–726.

Doody, R. S., Raman, R., Farlow, M., Iwatsubo, T., Vellas, B., Joffe, S., Kieburtz, K., He, F., Sun, X., Thomas, R. G., Aisen, P. S., Siemers, E., Sethuraman, G., and Mohs, R. (2013). A Phase 3 Trial of Semagacestat for Treatment of Alzheimer's Disease. *New England Journal of Medicine*, 369(4):341–350.

Dore, K., Aow, J., and Malinow, R. (2015). Agonist binding to the nmda receptor drives movement of its cytoplasmic domain without ion flow. *Proceedings of the National Academy of Sciences*, 112(47):14705–14710.

Du Yan, S., Zhu, H., Fu, J., Yan, S. F., Roher, A., Tourtellotte, W. W., Rajavashisth, T., Chen, X., Godman, G. C., and Stern, D. (1997). Amyloid-β peptide–Receptor for Advanced Glycation Endproduct interaction elicits neuronal expression of macrophage-colony stimulating factor: A proinflammatory pathway in Alzheimer disease. *Proceedings of the National Academy of Sciences of the United States of America*, 94(10):5296–5301.

Grutzendler, J. and Gan, W.-B. (2006). Two-photon imaging of synaptic plasticity and pathology in the living mouse brain. *NeuroRx : the journal of the American Society for Experimental NeuroTherapeutics*, 3(4):489–496.

Haass, C. and Selkoe, D. J. (2007). Soluble protein oligomers in neurodegeneration: lessons from the Alzheimer's amyloid β-peptide. *Nature Reviews Molecular Cell Biology*, 8(2):101–112.

Hayashi, Y. (2000). Driving AMPA Receptors into Synapses by LTP and CaMKII: Requirement for GluR1 and PDZ Domain Interaction. *Science*, 287(5461):2262–2267.

Hou, Q., Gilbert, J., and Man, H.-Y. (2011). Homeostatic Regulation of AMPA Receptor Trafficking and Degradationby Light-Controlled Single-Synaptic Activation. *Neuron*, 72(5):806–818.

Hsiao, K., Chapman, P., Nilsen, S., Eckman, C., Harigaya, Y., Younkin, S., Yang, F., and Cole, G. (1996). Correlative Memory Deficits, A Elevation, and Amyloid Plaques in Transgenic Mice. *Science*, 274(5284):99–103.

Hsieh, H., Boehm, J., Sato, C., Iwatsubo, T., Tomita, T., Sisodia, S., and Malinow, R. (2006). AMPAR Removal Underlies Aβ-Induced Synaptic Depression and Dendritic Spine Loss. *Neuron*, 52(5):831–843.

Hu, N.-W., Klyubin, I., Anwyl, R., and Rowan, M. J. (2009). GluN2B subunit-containing NMDA receptor antagonists prevent A beta-mediated synaptic plasticity disruption in vivo. *Science Signaling*, 106(48):20504.

Hu, X., He, W., Diaconu, C., Tang, X., Kidd, G. J., Macklin, W. B., Trapp, B. D., and Yan, R. (2008). Genetic deletion of BACE1 in mice affects remyelination of sciatic nerves. *The FASEB Journal*, 22(8):2970–2980.

Huganir, R. L. and Nicoll, R. A. (2013). Perspective. *Neuron*, 80(3):704–717.

Humeau, Y., Reisel, D., Johnson, A. W., Borchardt, T., Jensen, V., Gebhardt, C., Bosch, V., Gass, P., Bannerman, D. M., Good, M. A., Hvalby, O., Sprengel, R., and Luthi, A. (2007). A Pathway-Specific Function for Different AMPA Receptor Subunits in Amygdala Long-Term Potentiation and Fear Conditioning. *Journal of Neuroscience*, 27(41):10947–10956.

Jang, S.-S. and Chung, H. J. (2016). Emerging Link between Alzheimer's Disease and Homeostatic Synaptic Plasticity. *Neural Plasticity*, 2016(13):1–19.

Jo, J., Whitcomb, D. J., Olsen, K. M., Kerrigan, T. L., Lo, S.-C., Bru-Mercier, G., Dickinson, B., Scullion, S., Sheng, M., Collingridge, G., and Cho, K. (2011). Aβ1–42 inhibition of LTP is mediated by a signaling pathway involving caspase-3, Akt1 and GSK-3β. *Nature Neuroscience*, 14(5):545–547.

Kaether, C., Haass, C., and Steiner, H. (2006). Assembly, Trafficking and Function of γ-Secretase. *Neurodegenerative Diseases*, 3(4-5):275–283.

Kamenetz, F., Tomita, T., Hsieh, H., Seabrook, G., Borchelt, D., Iwatsubo, T., Sisodia, S., and Malinow, R. (2003). APP processing and synaptic function. *Neuron*, 37(6):925–937.

Kandel, E. R. (2001). The molecular biology of memory storage: a dialogue between genes and synapses. *Science*, 294(5544):1030–1038.

Karran, E., Mercken, M., and De Strooper, B. (2011). The amyloid cascade hypothesis for Alzheimer's disease: an appraisal for the development of therapeutics. *Nature Reviews Drug Discovery*, pages 1–15.

Kessels, H. W., Kopec, C. D., Klein, M. E., and Malinow, R. (2009). Roles of stargazin and phosphorylation in the control of AMPA receptor subcellular distribution. *Nature Neuroscience*, 12(7):888–896.

Kessels, H. W., Nabavi, S., and Malinow, R. (2013). Metabotropic NMDA receptor function is required for β-amyloid-induced synaptic depression. *Proceedings of the National Academy of Sciences*, 110(10):4033–4038.

Kessels, H. W., Nguyen, L. N., Nabavi, S., and Malinow, R. (2010). The prion protein as a receptor for amyloid-β. *Nature*, 466(7308):E1–E1.

Kim, C. H., Chung, H. J., and Lee, H. K. (2001). Interaction of the AMPA receptor subunit GluR2/3 with PDZ domains regulates hippocampal long-term depression. *Proceedings of the National Academy of Sciences of the United States of America*.

Kim, C.-H., Takamiya, K., Petralia, R. S., Sattler, R., Yu, S., Zhou, W., Kalb, R., Wenthold, R., and Huganir, R. (2005). Persistent hippocampal CA1 LTP in mice lacking the C-terminal PDZ ligand of GluR1. *Nature Neuroscience*, 8(8):985–987.

Kopec, C. D. (2006). Glutamate Receptor Exocytosis and Spine Enlargement during Chemically Induced Long-Term Potentiation. *Journal of Neuroscience*, 26(7):2000–2009.

Kopec, C. D., Kessels, H. W. H. G., Bush, D. E. A., Cain, C. K., LeDoux, J. E., and Malinow, R. (2007). A robust automated method to analyze rodent motion during fear conditioning. *Neuropharmacology*, 52(1):228–233.

Kounnas, M. Z., Danks, A. M., Cheng, S., Tyree, C., Ackerman, E., Zhang, X., Ahn, K., Nguyen, P., Comer, D., Mao, L., Yu, C., Pleynet, D., Digregorio, P. J., Velicelebi, G., Stauderman, K. A., Comer, W. T., Mobley, W. C., Li, Y.-M., Sisodia, S. S., Tanzi, R. E., and Wagner, S. L. (2010). Modulation of g-Secretase Reduces b-Amyloid Deposition in a Transgenic Mouse Model of Alzheimer's Disease. *Neuron*, 67(5):769–780.

Lacor, P. N., Buniel, M. C., Furlow, P. W., Sanz Clemente, A., Velasco, P. T., Wood, M., Viola, K. L., and Klein, W. L. (2007). A Oligomer-Induced Aberrations in Synapse Composition, Shape, and Density Provide a Molecular Basis for Loss of Connectivity in Alzheimer's Disease. *Journal of Neuroscience*, 27(4):796–807.

Lambert, M. P., Barlow, A. K., Chromy, B. A., Edwards, C., Freed, R., Liosatos, M., Morgan, T. E., Rozovsky, I., Trommer, B., Viola, K. L., Wals, P., Zhang, C., Finch, C. E., Krafft, G. A., and Klein, W. L. (1998). Diffusible, nonfibrillar ligands derived from Abeta1-42 are potent central nervous system neurotoxins. *Proceedings of the National Academy of Sciences of the United States of America*, 95(11):6448–6453.

Laurén, J., Gimbel, D. A., Nygaard, H. B., Gilbert, J. W., and Strittmatter, S. M. (2009). Cellular prion protein mediates impairment of synaptic plasticity by amyloid-β oligomers. *Nature*, 457(7233):1128–1132.

Ledoux, J. E., Farb, C. R., and Romanski, L. M. (1991). Overlapping projections to the amygdala and striatum from auditory processing areas of the thalamus and cortex. *Neuroscience Letters*, 134(1):139–144.

Lesné, S., Koh, M. T., Kotilinek, L., Kayed, R., Glabe, C. G., Yang, A., Gallagher, M., and Ashe, K. H. (2006). A specific amyloid-β protein assembly in the brain impairs memory. *Nature Cell Biology*, 440(7082):352–357.

Li, B., Piriz, J., Mirrione, M., Chung, C., Proulx, C. D., Schulz, D., Henn, F., and Malinow, R. (2011). Synaptic potentiation onto habenula neurons in the learned helplessness model of depression. *Nature*, 470(7335):535–539.

Li, S., Hong, S., Shepardson, N. E., Walsh, D. M., Shankar, G. M., and Selkoe, D. (2009). Soluble Oligomers of Amyloid β Protein Facilitate Hippocampal Long-Term Depression by Disrupting Neuronal Glutamate Uptake. *Neuron*, 62(6):788–801.

Liu, Q., Xie, X., Lukas, R. J., St John, P. A., and Wu, J. (2013). A Novel Nicotinic Mechanism Underlies -Amyloid-Induced Neuronal Hyperexcitation. *Journal of Neuroscience*, 33(17):7253–7263.

Liu, Q.-s., Kawai, H., and Berg, D. K. (2001). β-Amyloid peptide blocks the response of α7-containing nicotinic receptors on hippocampal neurons. *Proceedings of the National Academy of Sciences of the United States of America*, 98(8):4734–4739.

Lorenzo, A., Yuan, M., Zhang, Z., Paganetti, P. A., Sturchler-Pierrat, C., Staufenbiel, M., Mautino, J., Vigo, F. S., Sommer, B., and Yankner, B. A. (2000). Amyloid β interacts with the amyloid precursor protein: a potential toxic mechanism in Alzheimer's disease. *Nature Neuroscience*, 3(5):460–464.

Luo, Y., Bolon, B., Kahn, S., and Bennett, B. D. (2001). Mice deficient in BACE1, the Alzheimer's β-secretase, have normal phenotype and abolished β-amyloid generation. *Nature*.

Madison, D. V., Malenka, R., and Nicoll, R. A. (1991). Mechanisms underlying long-term potentiation of synaptic transmission. *Annual Review of Neuroscience*, 14:379–397.

Makino, H. and Malinow, R. (2011). Compartmentalized versus Global Synaptic Plasticity on Dendrites Controlled by Experience. *Neuron*, 72(6):1001–1011.

Malenka, R. (2003). The long-term potential of LTP. *Nature Reviews Neuroscience*.

Malenka, R. C. and Bear, M. F. (2004). LTP and LTD: an embarrassment of riches. *Neuron*, 44(1):5–21.

Malinow, R., Hayashi, Y., Maletic-Savatic, M., Zaman, S. H., Poncer, J.-C., Shi, S.-H., Esteban, J. A., Osten, P., and Seidenman, K. (2010). Introduction of green fluorescent protein (gfp) into hippocampal neurons through viral infection. *Cold Spring Harbor Protocols*, 2010(4):pdb.prot5406.

Malinow, R., Mainen, Z., and Hayashi, Y. (2000). LTP mechanisms: from silence to four-lane traffic. *Current Opinion in Neurobiology*, 10(3):352–357.

Matsuzaki, M., Ellis-Davies, G. C., Nemoto, T., Miyashita, Y., Iino, M., and Kasai, H. (2001). Dendritic spine geometry is critical for AMPA receptor expression in hippocampal CA1 pyramidal neurons. *Nature Neuroscience*, 4(11):1086–1092.

Mayer, M. L. and Armstrong, N. (2004). Structure and Function of Glutamate Receptor Ion Channels 1. *Annual Review of Physiology*, 66(1):161–181.

McLean, C. A., Cherny, R. A., Fraser, F. W., Fuller, S. J., Smith, M. J., Beyreuther, K., Bush, A. I., and Masters, C. L. (1999). Soluble pool of Abeta amyloid as a determinant of severity of neurodegeneration in Alzheimer's disease. *Annals of Neurology*, 46(6):860–866.

Megill, A., Tran, T., Eldred, K., Lee, N. J., Wong, P.C., Hoe, H. S., Kirkwood, A., and Lee, H. K. (2015). Defective Age-Dependent Metaplasticity in a Mouse Model of Alzheimer's Disease. *Journal of Neuroscience*, 35(32):11346–11357.

Meng, Y. Y., Zhang, Y. Y., and Jia, Z. Z. (2003). Synaptic transmission and plasticity in the absence of AMPA glutamate receptor GluR2 and GluR3. *Neuron*, 39(1):163–176.

Mitani, Y., Yarimizu, J., Saita, K., Uchino, H., Akashiba, H., Shitaka, Y., Ni, K., and Matsuoka, N. (2012). Differential Effects between -Secretase Inhibitors and Modulators on Cognitive Function in Amyloid Precursor Protein-Transgenic and Nontransgenic Mice. *Journal of Neuroscience*, 32(6):2037–2050.

Mitsushima, D., Ishihara, K., Sano, A., Kessels, H. W., and Takahashi, T. (2011). Contextual learning requires synaptic AMPA receptor delivery in the hippocampus. *Proceedings of the National Academy of Sciences*, 108(30):12503–12508.

Miyamoto, T., Kim, D., Knox, J. A., Johnson, E., and Mucke, L. (2016). Increasing the Receptor Tyrosine Kinase EphB2 Prevents Amyloid-β-induced Depletion of Cell Surface Glutamate Receptors by a Mechanism That Requires the PDZ-binding Motif of EphB2 and Neuronal Activity. *Journal of Biological Chemistry*, 291(4):1719–1734.

Morgan, D. (2003). Learning and memory deficits in APP transgenic mouse models of amyloid deposition. *Neurochemical Research*, 28(7):1029–1034.

Mucke, L. and Selkoe, D. J. (2012). Neurotoxicity of Amyloid -Protein: Synaptic and Network Dysfunction. *Cold Spring Harbor Perspectives in Medicine*, 2(7):a006338–a006338.

Nabavi, S., Fox, R., Proulx, C. D., Lin, J. Y., Tsien, R. Y., and Malinow, R. (2014). Engineering a memory with LTD and LTP. *Nature*, pages 1–17.

Nabavi, S., Kessels, H. W., Alfonso, S., Aow, J., Fox, R., and Malinow, R. (2013). Metabotropic NMDA receptor function is required for NMDA receptor-dependent long-term depression. *Proceedings of the National Academy of Sciences*, 110(10):4027–4032.

Okuno, H. (2011). Neuroscience Research. *Neuroscience research*, 69(3):175–186.

Podlisny, M. B., Ostaszewski, B. L., Squazzo, S. L., Koo, E. H., Rydell, R. E., Teplow, D. B., and Selkoe, D. J. (1995). Aggregation of secreted amyloid-protein into sodium dodecyl sulfate-stable oligomers in cell culture. *Journal of Biological Chemistry*, 270(16):9564–9570.

Rahman, M. M., Zetterberg, H., Lendel, C., and Härd, T. (2015). Binding of Human Proteins to Amyloid-β Protofibrils. *ACS Chemical Biology*, 10(3):766–774.

Rial Verde, E. M., Lee-Osbourne, J., Worley, P. F., Malinow, R., and Cline, H. T. (2006). Increased Expression of the Immediate-Early Gene Arc/Arg3.1 Reduces AMPA Receptor-Mediated Synaptic Transmission. *Neuron*, 52(3):461–474.

Roberds, S. L., Anderson, J., Basi, G., Bienkowski, M. J., Branstetter, D. G., Chen, K. S., Freedman, S. B., Frigon, N. L., Games, D., Hu, K., Johnson-Wood, K., Kappenman, K. E., Kawabe, T. T., Kola, I., Kuehn, R., Lee, M., Liu, W., Motter, R.,

Nichols, N. F., Power, M., Robertson, D. W., Schenk, D., Schoor, M., Shopp, G. M., Shuck, M. E., Sinha, S., Svensson, K. A., Tatsuno, G., Tintrup, H., Wijsman, J., Wright, S., and McConlogue, L. (2001). BACE knockout mice are healthy despite lacking the primary beta-secretase activity in brain: implications for Alzheimer's disease therapeutics. *Human Molecular Genetics*, 10(12):1317–1324.

Rogan, M. T., Stäubli, U. V., and Ledoux, J. E. (1997). Fear conditioning induces associative long-term potentiation in the amygdala. *Nature*, 390(6660):604–607.

Rogerson, T., Cai, D. J., Frank, A., Sano, Y., Shobe, J., Lopez-Aranda, M. F., and Silva, A. J. (2014). Synaptic tagging during memoryallocation. *Nature Reviews Neuroscience*, 15(3):157–169.

Rumpel, S. (2005). Postsynaptic Receptor Trafficking Underlying a Form of Associative Learning. *Science*, 308(5718):83–88.

Saglietti, L., Dequidt, C., Kamieniarz, K., Rousset, M.-C., Valnegri, P., Thoumine, O., Beretta, F., Fagni, L., Choquet, D., Sala, C., Sheng, M., and Passafaro, M. (2007). Extracellular Interactions between GluR2 and N-Cadherin in Spine Regulation. *Neuron*, 54(3):461–477.

Savonenko, A., Xu, G. M., Melnikova, T., Morton, J. L., Gonzales, V., Wong, M. P. F., Price, D. L., Tang, F., Markowska, A. L., and Borchelt, D. R. (2005). Episodic-like memory deficits in the APPswe/PS1dE9 mouse model of Alzheimer's disease: Relationships to β-amyloid deposition and neurotransmitter abnormalities. *Neurobiology of Disease*, 18(3):602–617.

Savonenko, A. V., Melnikova, T., Laird, F. M., Stewart, K.-A., Price, D., and Wong, P.C. (2008). Alteration of BACE1-dependent NRG1/ErbB4 signaling and schizophrenia-like phenotypes in BACE1-null mice. *Proceedings of the National Academy of Sciences*, 105(14):5585–5590.

Scharfman, H. E. (2012). "Untangling" Alzheimer's disease and epilepsy. *Epilepsy Currents*.

Scheff, S. W., Price, D. A., Schmitt, F. A., and Mufson, E. J. (2006). Hippocampal synaptic loss in early Alzheimer's disease and mild cognitive impairment. *Neurobiology of Aging*, 27(10):1372–1384.

Selkoe, D. J. and Schenk, D. (2003). A LZHEIMER'SD ISEASE: Molecular Understanding Predicts Amyloid-Based Therapeutics. *Annual Review of Pharmacology and Toxicology*, 43(1):545–584.

Shankar, G. M., Bloodgood, B. L., Townsend, M., Walsh, D. M., Selkoe, D. J., and Sabatini, B. L. (2007). Natural Oligomers of the Alzheimer Amyloid- Protein Induce Reversible Synapse Loss by Modulating an NMDA-Type Glutamate Receptor-Dependent Signaling Pathway. *Journal of Neuroscience*, 27(11):2866–2875.

Shankar, G. M., Li, S., Mehta, T. H., Garcia-Munoz, A., Shepardson, N. E., Smith, I., Brett, F. M., Farrell, M. A., Rowan, M. J., Lemere, C. A., Regan, C. M., Walsh, D. M., Sabatini, B. L., and Selkoe, D. J. (2008). Amyloid-β protein dimers isolated directly from Alzheimer's brains impair synaptic plasticity and memory. *Nature Medicine*, 14(8):837–842.

Shi, S. (1999). Rapid Spine Delivery and Redistribution of AMPA Receptors After Synaptic NMDA Receptor Activation. *Science*, 284(5421):1811–1816.

Shi, S., Hayashi, Y., Esteban, J., and Malinow, R. (2001). Subunit-specific rules governing AMPA receptor trafficking to synapses in hippocampal pyramidal neurons. *Cell*, 105(3):331–343.

Silverman, J. B., Restituito, S., Lu, W., Lee-Edwards, L., Khatri, L., and Ziff, E. B. (2007). Synaptic Anchorage of AMPA Receptors by Cadherins through Neural Plakophilin-Related Arm Protein AMPA Receptor-Binding Protein Complexes. *Journal of Neuroscience*, 27(32):8505–8516.

Šišková, Z., Justus, D., Kaneko, H., Friedrichs, D., Henneberg, N., Beutel, T., Pitsch, J., Schoch, S., Becker, A., von der Kammer, H., and Remy, S. (2014). Dendritic Structural Degeneration Is Functionally Linked to Cellular Hyperexcitability in a Mouse Model of Alzheimer's Disease. *Neuron*, 84(5):1023–1033.

Snyder, E. M., Nong, Y., Almeida, C. G., Paul, S., Moran, T., Choi, E. Y., Nairn, A. C., Salter, M. W., Lombroso, P. J., Gouras, G. K., and Greengard, P. (2005). Regulation of NMDA receptor trafficking by amyloid-β. *Nature Neuroscience*, 8(8):1051–1058.

Söderberg, O., Gullberg, M., Jarvius, M., Ridderstråle, K., Leuchowius, K.-J., Jarvius, J., Wester, K., Hydbring, P., Bahram, F., Larsson, L.-G., and Landegren, U. (2006). Direct observation of individual endogenous protein complexes in situ by proximity ligation. *Nature Methods*, 3(12):995–1000.

Söderberg, O., Leuchowius, K.-J., Gullberg, M., Jarvius, M., Weibrecht, I., Larsson, L.-G., and Landegren, U. (2008). Characterizing proteins and their interactions in cells and tissues using the in situ proximity ligation assay. *Methods*, 45(3):227–232.

Stoppini, L., Buchs, P. A., and Muller, D. (1991). A simple method for organotypic cultures of nervous tissue. *Journal of Neuroscience Methods*.

Sturchler, E., Galichet, A., Weibel, M., Leclerc, E., and Heizmann, C. W. (2008). Site-Specific Blockade of RAGE-Vd Prevents Amyloid- Oligomer Neurotoxicity. *Journal of Neuroscience*, 28(20):5149–5158.

Suh, J., Choi, S. H., Romano, D. M., Gannon, M. A., Lesinski, A. N., Kim, D. Y., and Tanzi, R. E. (2013). ADAM10 Missense Mutations Potentiate b-Amyloid Accumulation by Impairing Prodomain Chaperone Function. *Neuron*, 80(2):385–401.

Terashima, A., Pelkey, K. A., Rah, J.-C., Suh, Y. H., Roche, K. W., Collingridge, G. L., McBain, C. J., and Isaac, J. T. R. (2008). An Essential Role for PICK1 in NMDA Receptor-Dependent Bidirectional Synaptic Plasticity. *Neuron*, 57(6):872–882.

Trifilieff, P., Rives, M.-L., Urizar, E., Piskorowski, R., Vishwasrao, H., Castrillon, J., Schmauss, C., Slättman, M., Gullberg, M., and Javitch, J. (2011). Detection of antigen interactions ex vivo by proximity ligation assay: endogenous dopamine D2-adenosine A2A receptor complexes in the striatum. *BioTechniques*.

Tsai, J., Grutzendler, J., Duff, K., and Gan, W.-B. (2004). Fibrillar amyloid deposition leads to local synaptic abnormalities and breakage of neuronal branches. *Nature Neuroscience*, 7(11):1181–1183.

Vassar, R. (1999). Beta-Secretase Cleavage of Alzheimer's Amyloid Precursor Protein by the Transmembrane Aspartic Protease BACE. *Science*, 286(5440):735–741.

Vassar, R. (2014). BACE1 inhibitor drugs in clinical trials for Alzheimer's disease. *Alzheimer's Research & Therapy*, 6(9):353.

Verret, L., Mann, E. O., Hang, G. B., Barth, A. M. I., Cobos, I., Ho, K., Devidze, N., Masliah, E., Kreitzer, A. C., Mody, I., Mucke, L., and Palop, J. J. (2012). Inhibitory Interneuron Deficit Links Altered Network Activity and Cognitive Dysfunction in Alzheimer Model. *Cell*, 149(3):708–721.

Walsh, D. M. D., Klyubin, I. I., Fadeeva, J. V. J., Cullen, W. K. W., Anwyl, R. R., Wolfe, M. S. M., Rowan, M. J. M., and Selkoe, D. J. D. (2002). Naturally secreted oligomers of amyloid beta protein potently inhibit hippocampal long-term potentiation in vivo. *Nature*, 416(6880):535–539.

Wang, H.-Y., Lee, D. H., D'Andrea, M. R., Peterson, P. A., Shank, R. P., and Reitz, A. B. (2000). β-Amyloid1–42 Binds to α7 Nicotinic Acetylcholine Receptor with High Affinity Implications for Alzheimer's Disease Pathology. *Journal of Biological Chemistry*, 275(8):5626–5632.

Wang, Q. (2004). Block of Long-Term Potentiation by Naturally Secreted and Synthetic Amyloid -Peptide in Hippocampal Slices Is Mediated via Activation of the Kinases c-Jun N-Terminal Kinase, Cyclin-Dependent Kinase 5, and p38 Mitogen-Activated Protein Kinase as well as Metabotropic Glutamate Receptor Type 5. *Journal of Neuroscience*, 24(13):3370–3378.

Wei, W., Nguyen, L. N., Kessels, H. W., Hagiwara, H., Sisodia, S., and Malinow, R. (2009). Amyloid beta from axons and dendrites reduces local spine number and plasticity. *Nature Publishing Group*, 13(2):190–196.

Wenthold, R. J., Petralia, R. S., and Niedzielski, A. S. (1996). Evidence for multiple AMPA receptor complexes in hippocampal CA1/CA2 neurons. *The Journal of*

neuroscience : the official journal of the Society for Neuroscience, 16(6):1982–1989.

Willem, M., Garratt, A. N., Novak, B., Citron, M., Kaufmann, S., Rittger, A., DeStrooper, B., Saftig, P., Birchmeier, C., and Haass, C. (2006). Control of peripheral nerve myelination by the ß-secretase bace1. *Science*, 314(5799):664–666.

Zamanillo, D. (1999). Importance of AMPA Receptors for Hippocampal Synaptic Plasticity But Not for Spatial Learning. *Science*, 284(5421):1805–1811.